論文 / 著書情報
Article / Book Information

題目(和文)	合成手法の異なるアルミノシリケートゼオライトの構造、酸特性ならびに触媒特性に関する研究
Title(English)	Study on the structural, acidic and catalytic properties of aluminosilicate zeolites synthesized by different methods
著者(和文)	劉明
Author(English)	Ming Liu
出典(和文)	学位:博士(工学), 学位授与機関:東京工業大学, 報告番号:甲第9501号, 授与年月日:2014年3月26日, 学位の種別:課程博士, 審査員:野村　淳子,小泉　武昭,林　智広,松下　伸広,冨田　育義
Citation(English)	Degree:Doctor (Engineering), Conferring organization: Tokyo Institute of Technology, Report number:甲第9501号, Conferred date:2014/3/26, Degree Type:Course doctor, Examiner:,,,,
学位種別(和文)	博士論文
Type(English)	Doctoral Thesis

Doctor thesis

Study on the structural, acidic and catalytic properties of aluminosilicate zeolites synthesized by different methods

（和訳: 合成手法の異なるアルミノシリケートゼオライトの構造、酸特性ならびに触媒特性に関する研究）

This thesis was submitted to Tokyo Institute of Technology for the degree of Doctor of Science.

Ming Liu (11D27110)

Department of Electronic Chemistry

Interdisciplinary Graduate School of Science and Engineering

Tokyo Institute of Technology

Contents

Chapter 1

General Introduction

1.1 Zeolites

Zeolite materials are very important crystalline inorganic microporous solids containing channel and cavities. Zeolite materials formed by TO_4 tetrahedra (T = Si, P, Al, B, Fe, Ga, etc) with a well defined regular pore system [1]. The general formula of aluminosilicate zeolites is $M_{2/n}•Al_2O_3•ySiO_2•wH_2O$, where y is 2 to 10, n is cation valence, and w represents the water contained in the voids of the zeolite [2].

The history of zeolites began in 1756 when the Swedish mineralogist Crönstedt discovered the first zeolite mineral, stilbite [3]. He recognized zeolites as a new class of minerals consisting of hydrated aluminosilicates of the alkali and alkaline earths. This new family of minerals (hydrated aluminosilicates) was called zeolite from the Greek words “zeo” and “lithos” meaning “to boil” and “stone”. For nearly 200 years, the beautiful and large natural zeolite crystals were only attractions displayed in museum collections [4]. In 1845 Schafhautle reported the hydrothermal synthesis of quartz by heating a gel silica with water in an autoclave [5]. In 1862 St. Claire Deville reported the first hydrothermal synthesis of a zeolite, levynite [6].

While some 40 different zeolites were discovered in nature, approximately 130 zeolites were synthesized. The first synthetic zeolites (X, Y, A) have rapidly found applications in three main areas:

· **Adsorption**: first in the drying of refrigerant gas and natural gas (1955), followed by the n-/iso-butane separation on the A zeolite (ISOSIV process, 1959)

· **Catalysis**: with the use of X and Y zeolites in isomerization (1959) and cracking (1962)

· **Ion-exchange**: in detergents, A zeolites replacing the polluting polyphosphates (1974)

In 1962 the zeolites were introduced by Mobil Oil Corporation as new cracking catalysts in refinery technology. They were characterized by higher activity and selectivity in cracking and hydrocracking. At the end of the 1960s, the concept of shape-selective catalysis with zeolites was introduced to petrochemistry (Selecto-forming process), and the zeolites became of increasing importance in catalysis research and applied catalysis [7].

During the last 20 years, great progress was made in the synthesis of molecular sieves and in the understanding of the catalytic transformation of organic molecules on zeolites. This fundamental knowledge was successfully applied to introduce large-scale processes in the fields of oil refining, petrochemicals and, with increasing success, in the clean synthesis of fine chemicals.

1.1.1 Zeolite naming

Zeolite structures are designated by a 3 capital letter code according to rules set by the Commission of the International Zeolite Association (IZA). For instance, FAU stands for the faujasite structure to which the well-known X and Y zeolites belong. The 5th edition of the Atlas of Zeolite Framework Types, recently published by IZA, describes 133 zeolite structures. Regular updates are found on the website of the IZA.

1.1.2 Pore structure

As adsorption and catalytic processes involve diffusion of molecules in the zeolite pores, only those with a minimum of 8 tetrahedral (8T) atoms apertures allowing this diffusion are generally considered. Most of the zeolites can be classified into three categories:

· Small pore zeolites with eight membered-ring pore apertures (8 T atoms and 80) having free diameters of 0.30-0.45 nm.

(Fig. 1-1 shows zeolite A with 8 membered-ring)

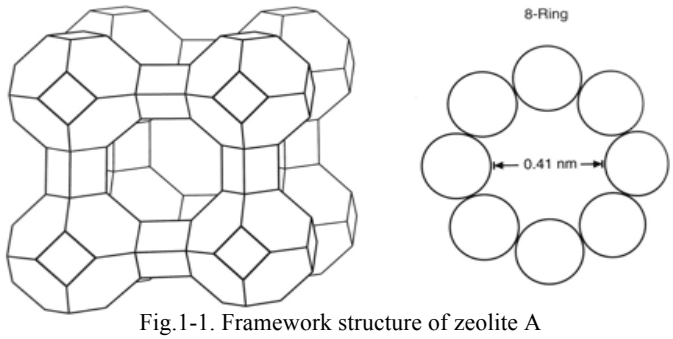

Fig.1-1. Framework structure of zeolite A

· Medium pore zeolites with ten membered-ring apertures, 0.45 – 0.60 nm in free diameter. (Fig. 1-2 shows MFI-type zeolite with 10 membered-ring)

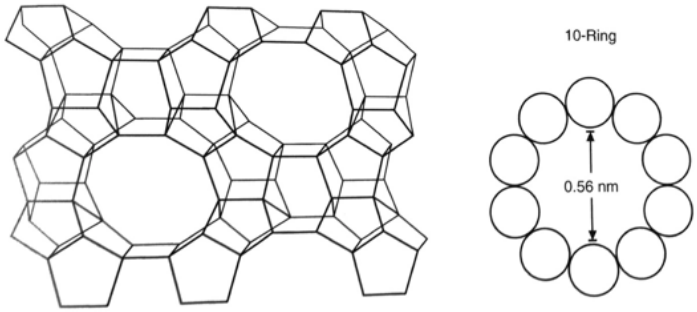

Fig. 1-2. MFI-type zeolite

· Large pore zeolites with 12 membered-ring apertures, 0.6-0.8 nm.
(Fig. 1-3 shows FAU-type zeolite with 12 membered-ring)

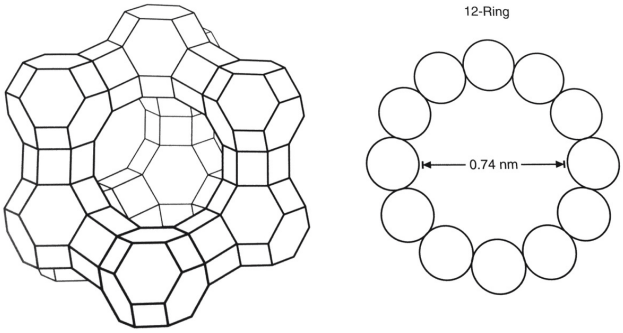

Fig. 1-3. FAU-type zeolite

· Extra large pore zeolites with above 14 membered-ring apertures, 0.8 nm-2nm

1.2 Active sites of zeolite

Zeolites are utilized as acid, base, acid-base, redox and bifunctional catalysts because they can be easily obtained over a wide range of compositions directly by synthesis and/or after various post synthesis treatment. Moreover, various compounds can be introduced or even synthesized within the zeolite pores. However, Most of the applications are being in acid and in bifunctional catalysis.

Zeolites are widely utilized as solid acid catalysts. Zeolite structure containing only SiO_2 tetrahedra would be electrically neutral and no acidity would be developed on its surface. Brønsted acid sites are developed when Si^{4+} is isomorphically substituted by a trivalent metal cation, for instance, Al^{3+}, and a negative charge is created in the lattice, which is compensated by a proton. The proton is attached to the oxygen atom connected

to neighbor silicon and aluminum atoms, resulting in the so-called bridged hydroxyl group which is the site responsible for the Brønsted acidity of zeolites [8].

The most important process involving a zeolite, Fluid Catalytic Cracking (FCC) uses a catalyst containing an acid FAU zeolite. Other examples of processes using acid zeolite catalysts are Methanol to Olefins, Acetylation etc.

1.2.1 Acid properties of zeolites

Acid sites generate in zeolites when Si^{4+} is isomorphically replaced by a trivalent metal cation such as Al^{3+}. This substitution makes a negative charge in the lattice that can be compensated by a proton. Zeolites in the H form are solid acids whose acid strength can be varied over a wide range by modification of the zeolites (ion-exchange, partial dealumination, and isomorphic substitution of the framework Al and Si atoms).

Fig.1-4 showed how does Brønsted acid sites generate on the zeolite. The best method is exchange of the alkali metal ions by NH_4^+ ions, followed by heating the resulting ammonium salts to 500-600℃ [9].

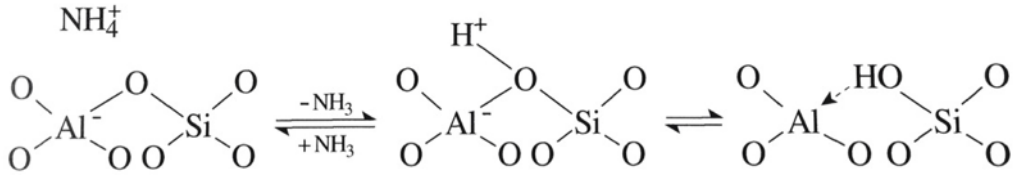

Fig. 1-4. Formation of Brønsted acid sites

Infrared investigations have shown that the protons are mainly bound as silanol groups but have a strongly acidic character due to the strongly polarizing influence of the coordinative unsaturated aluminum center. Brønsted acid centers are generally the catalytically active sites of H-zeolites.

The maximum number of protonic sites is equal to the number of framework aluminum atoms, the actual number being smaller due to cation exchange, dehydroxylation and dealumination during activation at high temperatures. The number (and density) of protonic sites can therefore be adjusted either during the synthesis or during post synthesis treatments of the zeolite: dealumination, ion-exchange, etc. However, as aluminum atoms cannot be adjacent (Lowenstein's rule), the maximum number of protonic sites is obtained for a framework Si/Al ratio of 1 (8.3 mmol H^+ g^{-1}

zeolite). Moreover, no purely protonic zeolite is stable with this low framework Si/Al ratio, hence this maximum number can never be achieved [4].

When an H-zeolite is heated to high temperature, water is driven off and coordinatively unsaturated Al^{3+} ions are formed. These are Lewis acids (Fig. 1-5).

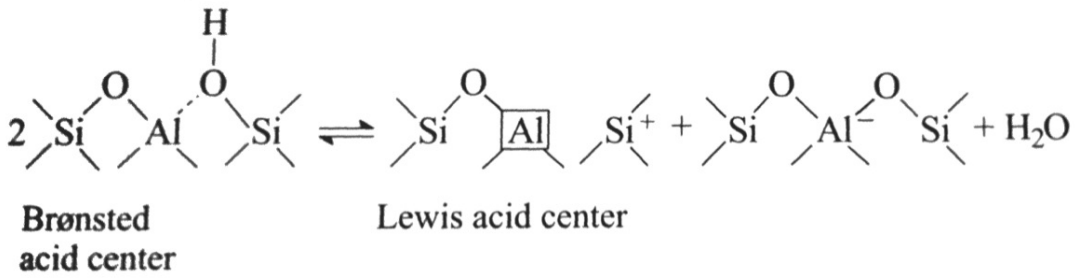

Fig. 1-5. Formation of Lewis acid center

Bases like pyridine are more strongly bound to such lewis acid centers than to Brønsted acid centers, as can be shown by IR spectroscopy and temperature-controlled desorption. Figure 1-6 shows the transformation of Brønsted into Lewis acid centers on calcination of an HY zeolite, monitored by IR spectroscopic measurements on the adsorption of pyridine.

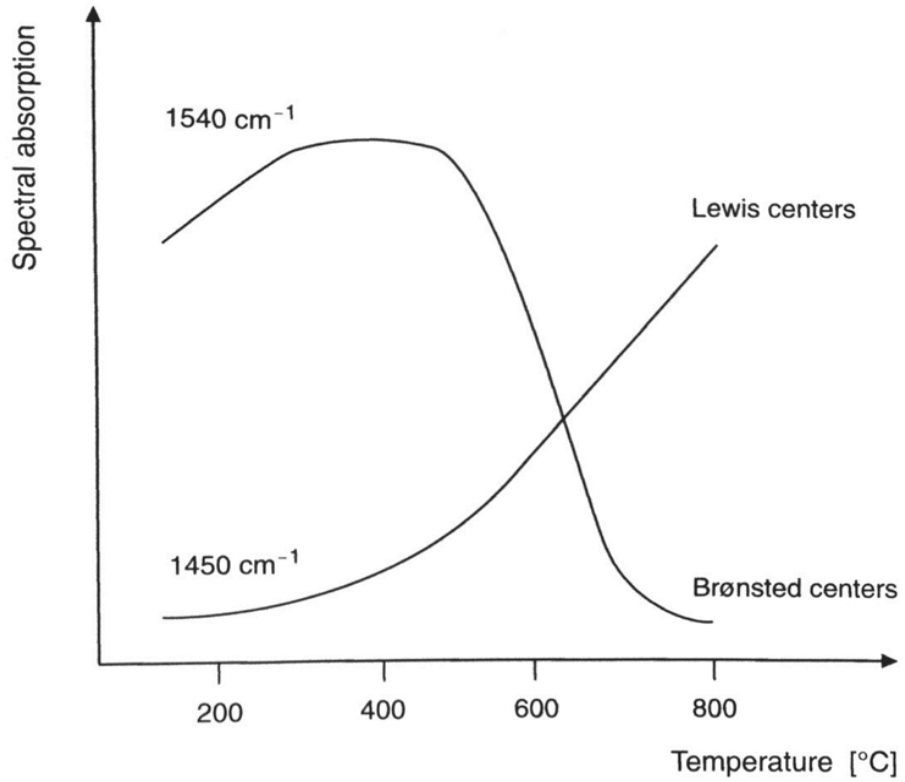

Fig. 1-6. Calcination of an HY zeolite: equilibrium between Brønsted and Lewis acid

1.2.2 Acid strength

Acid strength is one of important parameters of zeolites as catalysts. Most of the hydrocarbon reactions as well as many transformations of functionalized compounds are catalyzed by protionic sites only [10].

The acid strength depends on several factors as follow:

- the kind of metals introduced in the framework
- T-O-T bond angles
- degree of exchange of Na cations
- framework Si/Al ratio

The synthesis of metallosilicates containing trivalent elements in the framework other than Al (B, Ga, In, Fe) is of interest in designing the acid strength. The ranking in acid strength drawn from theoretical calculations is in relatively good agreement with acidity measurement [11]. Thus, according to IR spectroscopy (wavenumber of the OH groups) and ammonia TPD over MFI samples, the acid strength is in the following order: [12]

$$B(OH)Si < In(OH)Si \leq Fe(OH)Si < Ga(OH)Si < Al(OH)Si$$

The protonic site strength depends on the degree of exchange of Na cations in the zeolite. As could be expected, the greater the exchange level, the stronger the pronic sites. However at high exchange degree, there is not only creation of very strong protonic site but also an increase in the strength of the protonic sites already present in the zeolite [13].

A relation exists between the T-O-T bond angles and the acid strength of the associated proton in the zeolites [14]. The greater the angle, the stronger the sites. Thus, the protonic sites of HMOR (bond angle range between 143-180°) and HMFI (133-177°) are stronger than those of HFAU (138-147°). This explains why HMOR is and HFAU is not active in n-butane and n-hexane isomerization at 200-250℃, two reactions requiring very strong acid sites.

Theoretical and experimental approaches of the framework Si/Al ratio effect on the acidity led to the conclusion that the strength of the protonic site of zeolites is influenced by the presence of neighbors [14, 15]. Each framework Al atom has 4 Si atoms (Lowenstein`s rule) in the first surrounding layer (nearest neighbors) and, depending on the zeolite topology, 9-12 Al or Si atoms in the second layer (Next-Nearest-Neighbors or NNN). According to the NNN concept, the acid strength of a protonic site depends on the number of Al atoms in the NNN position; the strength is

maximum at 0 Al as NNN and minimum at full occupancy of the NNN sites with Al. Using statistical calculations, Wachter [16] determined that the Si/Al value for which all Al atoms were isolated was 7 for all zeolites with 9 Al or Si NNN.

1.2.3 Accessibility of the protonic sites

The accessibility of the protonic sites also plays a significant role in the catalytic activity of zeolites. Obviously this accessibility depends both on the location of the OH in the zeolite and on the size of the reactant molecules. Thus, the portion of protonic sites of HFAU zeolites located in the supercages is accessible to many organic molecules whereas the others, located in the hexagonal prisms, are inaccessible to all the organic molecules. HMOR also has protonic sites accessible (in the large channels) to many organic molecules and less accessible sites (in the side pockets). With H-MFI, all the protonic sites being located at the channel intersections are equally accessible (or inaccessible) to reactant molecules. The same can be said for HERI, the protonic sites of which are located in large cages with small apertures, hence only accessible to linear organic molecules.

1.3 Shape selectivity

The term Shape Selectivie Catalysis was coined 40 years ago by Weisz and Frilette to describe the unexpected catalytic behavior of an LTA zeolite exchanged with Ca^{2+} (CaA). They found that at 260℃, CaA dehydrated 60% of 1-butanol but did not convert isobutanol. CaA also cracked n-hexane (but not 3-methyhexane) exclusively into linear products. These results demonstrated that reactions occurred inside the pores of CaA (0.5 nm pore openings) making it impossible for branched molecules to enter or exit these pores. The first shape selective catalytic process Selectoforming, was based on this simple and elegant concept of shape selectivity by sieving.

The accessibility of the pores for molecules is subject to definite geometric or steric restrictions. The shape selectivity of zeolites is based on the interaction of reactants with the well-defined pore system. A distinction is made between three variants.

− Reactant selectivity

− Product selectivity

− Restricted transition state selectivity

Figure 1-7 shows these schematically with examples of reactions.

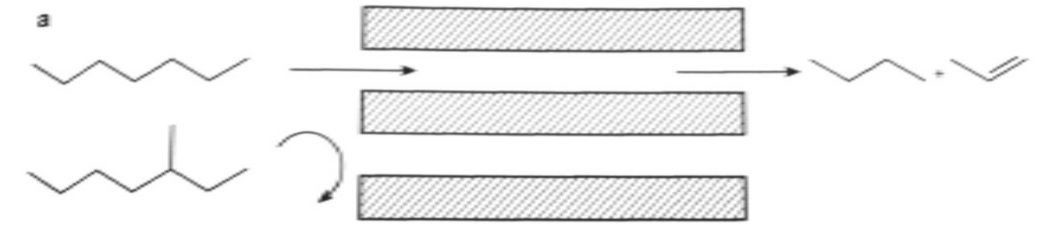

a) Reactant selectivity: cleavage of hydrocarbons

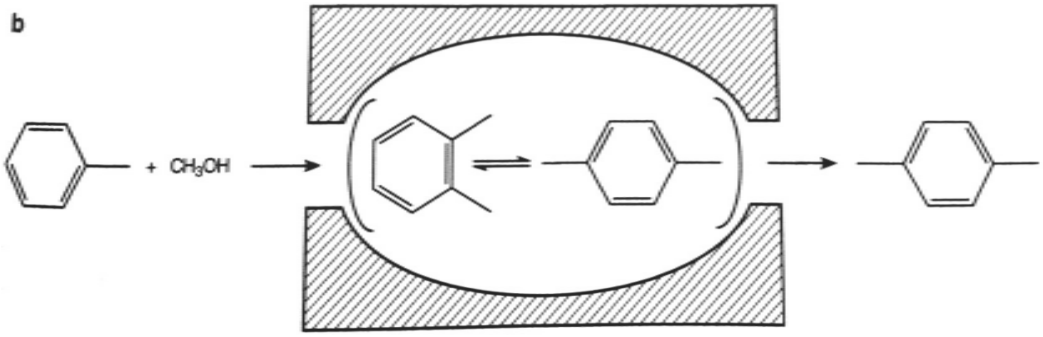

b) Product selectivity: methylation of tuluene

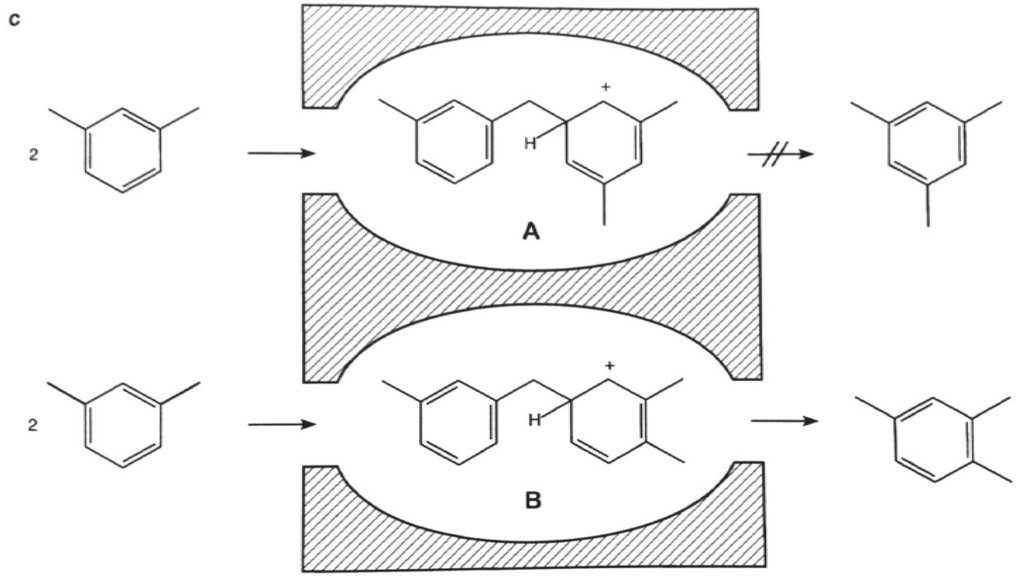

c) Restricted transition state selectivity: disproportionation of *m*-xylene

Fig. 1-7. Shape selectivity of zeolites with examples of reactions

a) Reactant Selectivity

Reactant selectivity means that only starting materials of a certain size and shape can penetrate into the interior of the zeolite pores and undergo reaction at the catalytically active sites. Starting material molecules that are larger than the pore apertures can not react. Hence the term 'molecular sieve' is justified.

b) Product Selectivity

Product selectivity arises when, corresponding to the cavity size of a zeolite, only products of a certain size and shape that can exit from the pore system are formed. Well-known examples of product selectivity are the methylation of toluene and the disproportion of toluene on ZSM-5.

c) Restricted Transition State Selectivity

This third form of shape selectivity depends on the fact that chemical reactions often proceed via intermediates. Owing to the pore system, only those intermediates that have a geometrical fit to the zeolite cavities can be formed during catalysis. This selectivity occurs preferentially when both monomolecular and bimolecular rearrangements are possible. In practice, it is often difficult to distinguish restricted transition state selectivity from product selectivity.

1.4 Characterization for valuating Al distribution and acid properties

1.4.1 ^{27}Al MAS NMR and ^{27}Al MQMAS NMR

Zeolites are made up from corner and edge-sharing SiO_4 and AlO_4 tetrahedra. In commercial zeolites, the ratio of Si/Al is usually in the range of 1-100 and distribution of Al and Si over the tetrahedral sites (T sites) is disordered.

The acidic properties of zeolites are closely related to the nature and distribution of the Al species in the framework. Therefore, detailed characterization of the Al environment is essential for understanding the catalytic properties. It is well recognized that solid-state ^{27}Al magic angle spinning (MAS) NMR spectroscopy is highly effective in the study of zeolites. However, unlike ^{29}Si (I=1/2) MAS NMR, the resolution of ^{27}Al MAS NMR spectra is not high enough to detailed characterize Al species because quadrupolar interaction at Al (I = 5/2) leads to a broadening of the peak; the sizable second-order quadrupolar interaction at Al, which contains higher-rank anisotropic terms, cannot be completely averaged out by MAS [17, 18, 19]. So far, only in zeolite omega and lately also in MCM-22 the crystallographically nonequivalent framework sites of aluminium could be detected [20, 21]. Recently, a very high

magnetic field has become applicable to the NMR measurement, and high-resolution solid-state NMR spectroscopy has established itself as a powerful technique for characterization of zeolites and related materials with respect to structure elucidation, catalytic behavior, and mobility. In addition, a multiple quantum (MQ) method of NMR, which has been developed by Frydman and Harwood [22], has become a promising tool for the study of quadrupolar nuclei in solids, *i.g.*, ^{7}Li, ^{11}B and ^{23}Na with I = 3/2 and ^{17}O, ^{27}Al and ^{25}Mg with I = 5/2 [23-27]. In this study, to investigate the distribution of Al on the Al-containing zeolites, high-resolution solid-state ^{27}Al MAS NMR and ^{27}Al MQMAS NMR techniques have been applied.

1.4.2 FTIR study of CO adsorption

Acid properties of zeolite catalyst have been extensively investigated by various methods including temperature-programmed desorption (TPD)[28, 29], X-ray photoelectron spectroscopy (XPS) [30], infrared (IR) spectroscopy [31, 32] and so on. In the IR method, OH stretching vibrations of the acidic OH groups, the Brønsted acid sites (BAS), of zeolites can be clearly observed. Moreover, the nature of the BAS and the Lewis acid sites (LAS) can be investigated by using basic probe molecules such as pyridine, NH_3 and CD_3CN [33]. These strongly basic probe molecules can distinguish BAS and LAS by different structures of adsorbed species. Pyridine has been often used as probe among various basic molecules for the characterization of 10- and 12-MR zeolites because of the experimental simplicity. However, pyridine cannot be applicable to the 8-mebered ring zeolites because diffusion of pyridine molecule into 8-membered ring micropores is significantly difficult. Meanwhile, CO has become used as probe molecule [34-38]. The advantages of CO as probe are its very weak basicity, small molecular diameter and high sensitivity of the IR band frequency to the strength of the acid sites. Therefore, in this study, *in-situ* FT-IR technique using CO as probe molecule was applied to the characterization of the acid property of the Al-containing **RTH**-zeolites.

1.5 Applications of zeolites

Zeolites have a wide range of applications. They are used as replacements for phosphates in laundry detergents, as adsorbents for purification and separation of materials, and as catalysts. The detergents industry has the largest demand for zeolites (ca. 1.2×10^6 t/a in 1994) and the highest growth rate. Demand for zeolite catalysts is also growing, and in 1994 amounted to ca. 115000 t/a.

Table 1-1 lists important catalytic processes involving zeolites.

Table1-1. Important catalytic processes involving zeolites

Process	Starting material	Zeolite	Products
Catalytic cracking	Crude oil	Faujasite	Gasoline, heating oil
Hydrocracking	Crude oil+H_2	Faujasite	kerosene
Dewaxing	Middle distillate	ZSM-5, mordenite	lubricants
Benzene alkylation	Benzene, ethene	ZSM-5	styrene
Toluene disproportionation	Toluene	ZSM-5	Xylene, benzene
Xylene isomerization	Isomer mixture	ZSM-5	*p*-xylene
MTG	Methanol	ZSM-5	gasoline
MTO	Methanol	ZSM-5	olefins
Intermediate products	Diverse	Acidic and bifunctional zeolites	Chemical raw materials
SCR process	Power station flue gases	mordenite	NO_x-free off-gas

1.6 Extra-large-pore zeolites

Zeolites having more than 12 T-atom for pore windows were delimited as extra-large-pore zeolites.

Zeolites will offer new opportunities for reactions in the field of chemical and fine chemicals. However, for many important applications, the size of the zeolitic pore is too small to react the bulky desired molecules.

Three methods are considered to improve the catalytic properties of zeolites when dealing with bulky molecules. The first is the synthesis of zeolites with nanocrystals. The second is the synthesis of delaminated zeolites. The third is the synthesis of extra-large-pore zeolites. The nanocrystalline zeolites and delaminated zeolites can provide large external surface area to make the reactions process. However, for the first method, the stability of the zeolite upon catalyst regeneration can be an issue. For the second method, the further study is necessary. The third method is the most direct way to expand the possibilities of zeolites for bulky molecule reactions [39].

Prior to 1987, all zeolite and zeolite-like molecular sieves contained large pore (12 oxygen atoms) or smaller [40]. The first extra-large-pore crystalline material was thought to be the mineral cacoxenite, a hydrated basic iron oxyphosphate with a pore diameter of 1.5 nm. However, the application of this microporous crystalline material as an adsorbent or catalyst is limited because the structure collapses after removal of the water molecules by calcinations [41].

VPI-5 (Virginia Polytechnic Institute 5) is the first real zeotype material which contains rings consisting of more than twelve T-atoms. VPI-5 is the aluminophosphate molecular sieve with 18-membered ring (18R) channels with a 1.2 nm pore diameter. However, it was transformed into $AlPO_4$-8 with one-dimensional (1D) 14R channel system when heating in the presence of moisture [42].

Table 1-2 shows the summary of extra-large pore materials. After VPI-5 was reported, several other extra-large-pore phosphate-based molecular sieve were reported to be synthesized successfully such as JDF-20 and Cloverite [43,44].

Table 1-2 Summary of extra-large pore materials.

Material	Year reported	Main framework composition	Ring size (O atoms)	Pore size [a]	Ref.
VPI-5	1988	$AlPO_4$	18	13	[9]
$AlPO_4$-8	1990	$AlPO_4$	14	<10	[14,15]
Cloverite	1991	$GaPO_4$	20	<10	[16]
JDF-20	1992	$AlPO_4$	20	– [c]	[17]
ULM-5	1994	$GaPO_4$	16	NR [d]	[18]
AlMepO-β	1995	$Al_2(CH_3PO_3)_3$	18	6	[19]
TPA-SnS-3	1995	Sn_4S_9	32 [b]	NR	[20]
not named	1996	$V_5O_9(PO_4)_2$	16	NR	[21]
ULM-16	1996	$GaPO_4$	16	NR	[22]
UTD-1	1996	SiO_2	14	10	[23]
ULM-15	1997	$FePO_4$	16	NR	[24]

[a] In Å; proven by adsorption. [b] Contains a total of 32 atoms. [c] Collapse upon activation. [d] NR: not reported.

The extra-large-pore materials were expected to be effect adsorbents or catalysts. However, it was found that the thermal and hydrothermal stability of phosphate-based extra-large-pore material was poor. Davis and his co-workers reported that the origin of the instability of VPI-5 was not due to the presence of extra-large ring, but rather to the nature of the structural units such as the strained, fused four-membered rings [45]. Further more, it is hard to introduce active sites into phosphate-based materials. So the reasons above greatly restrict the application of phosphate-based materials

The poor thermal and hydrothermal stability of phosphate-based extra-large-pore material is harmful for the practical value. Thus, the synthesis of silica-based extra-large-pore zeolites has received much attention. In 1996 a silica-based zeolite containing, UTD-1, was synthesized. UTD-1 is a high-silica zeolite possessing only tetrahedral atoms of silicaon and aluminum and is thermally stable like other known zeolites [46].

The synthesis of UTD-1 just proves that the formation of extra-large-pore material is not limited to phosphate-based materials and provides reason to believe that extra-large-pore material will find practical application in the future.

UTD-1 is synthesized by using bis(pentamethylcyclopentadienyl)cobalt(III)

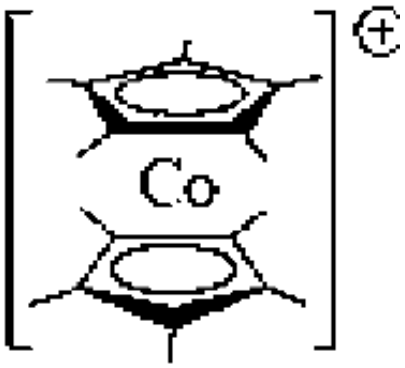

hydroxide as a structure-directing agent. The cost of this structure-directing agent is high. Cobalt will remain in the pore after calcination. Acid treatment is necessary to remove the cobalt in the pore. So it is difficult to utilize UTD-1 as a commercial catalyst.

After discovery of UTD-1, the silica-based zeolites containing extra-large-pore CIT-5 [47], SSZ-53 and SSZ-59 were reported to be synthesized by the quaternary ammonium ion. (Table 1-3) Though all of them have a 1D 14R channel system, the pore shape and effective pore diameters should affect their adsorption and catalytic properties.

Table 1-3: Extra-large-pore zeolites

Structure code	Material	Year	Channel dimension	Framework atoms	Framework density [T atoms nm^{-3}]	Template	Ref.
VFI	VPI-5	1988	1D 18 R	Al, P	14.5	**32, 33**	[10]
AET	AlPO-8	1990	1D 14 R	Al, P	18.2	**33**	[11]
-CLO	Cloverite	1991	3D 20 R	Ga, P	11.1	**8**	[13]
DON	UTD-1	1996	1D 14 R	Si	17.1	**34**	[44]
CFI	CIT-5	1997	1D 14 R	Si	16.8	**35**	[45]
SFH	SSZ-53	2003	1D 14 R	B, Si	16.5	**36**[a]	[47]
SFN	SSZ-59	2003	1D 14 R	B, Si	16.6	**37**[a]	[47]
OSO	OSB-1	2001	3D 14×8×8 R	Be, Si	13.3	K^+	[46]
ETR	ECR-34	2003	3D 18×8×8 R	Ga(Al), Si	15.4	**27** and Na^+, K^+	[48]
UTL	IM-12 or ITQ-15	2004	2D 14×12 R	Ge, Si	15.6	**38**(for IM-12), **39**(for ITQ-15)	[50,51]
-	ITQ-33	2006	3D 18×10×10 R	Ge, Si	12.3[b]	**40**	[52]
	ITQ-37	2009	3D 30 R	Ge, Si	10.3[c]	**41**	[158]

[a] Only one example with this SDA. [b] Taken from Ref. [52]. [c] Taken from Ref. [158].

Table 1-4 showed the adsorption properties of various zeolites reported by Chen and Zones [48]. All the zeolites can easily adsorb small sorbates, such as *n*-hexane, cyclohexane, 2,2-dimethylbutane. But for more bulkier sorbates, such as 1,3,5-triisopropylbenzene with a kinetic diameter of about 0.85 nm, only the 14R zeolites UTD-1, SSZ-53, SSZ-59 with pore diameters over 0.80 nm, the 18R aluminophosphate VPI-5, and the 3D 12R NaY zeolite are able to adsorb significant amounts. So it is thought that silica-based extra-large-pore zeolites are suitable for the bulkier molecule.

After the report of SSZ-53 and SSZ-59 by researchers at Chevron, an 18×8×8R

Table 1-4: Adsorption property of various zeolites

Zeolite	Pore Size [Å]	Pore system	Adsorption capacity [mL g^{-1}]			
			n-hexane (σ=4.4 Å)[a]	cyclohexane (σ=6.0 Å)[a]	2,2-dimethyl-butane (σ=6.2 Å)[a]	1,3,5-triiso-propylbenzene (σ=8.5 Å)[a]
NaY	7.3	12R, 3D	0.28	0.25	0.25	0.18
SSZ-24	7.3	12R, 1D	0.10	0.11	0.13	0.01
CIT-5	7.5×7.2	14R, 1D	0.09	0.09	0.09	0.041
UTD-1	8.2×8.1	14R, 1D	0.12	0.11	0.12	0.11
SSZ-53	8.7×6.4	14R, 1D	0.13	0.10	0.12	0.13
SSZ-59	8.5×6.4	14R, 1D	0.16	0.13	0.12	0.11
VPI-5	12.1	18R, 1D	0.20	0.16	0.15	0.12

[a] σ = Kinetic diameter.

gallosilicate zeolite (ECR-34) with a pore diameter of 1.08 nm for the 18R was reported by Strohmaier and Vaughan [49]. A germanosilicate zeolite with very large pore volume was first reported in the patent literature as ITQ-15 [50], which has a channel system formed by 14×12R pores and has been assigned as zeotype UTL. Recently, Corma et al. reported a silicogermanate zeolite (ITQ-33) with an 18×10×10R pore system. In 2009, extra-large-pore silicogermanate zeolite ITQ-37 with 30R was successfully synthesized by using large and rigid three-dimensional OSDA (organic structure directing agent). Germanium was also thought as a key atom to synthesize extra-large-pore zeolites. However, there are two main drawbacks for the practical use of Ge containing zeolites, the hydrothermal stability and the price of germanium.

Until now, there are few reports about the synthesis and catalytic properties of SSZ-53 and SSZ-59. So we focus on SSZ-53 and SSZ-59 zeolites.

1.6.1 SFH-type zeolite

SSZ-53 (**SFH**-type) zeolite was discovered in Chevron laboratories [51]. Its pore system consists of linear, non-interconnected channels with pore openings formed from elliptical 14-rings with an approximate size of 0.65×0.85 nm(Figure 1-8) [52].

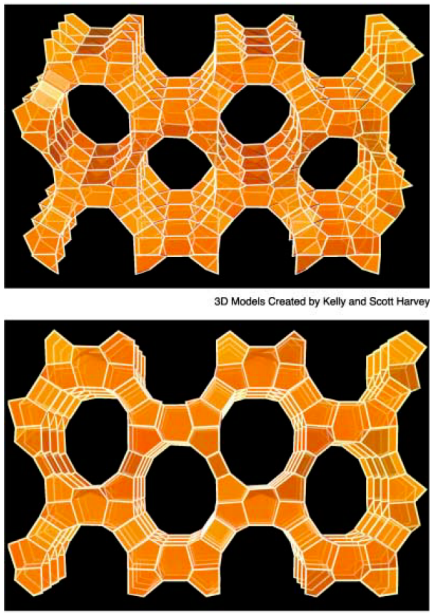

Fig. 1-8. Projection of the SSZ-53 framework topology along a axis.
Oxygen atoms have been omitted for clarity.

Figure 1-9 shows the T sites of SSZ-53. In SSZ-53, there are eight crystallographically distinct tetrahedral T sites where Al cations can be located [53]; seven of them (T1, T2, and T4-T8) are exposed in the channel.

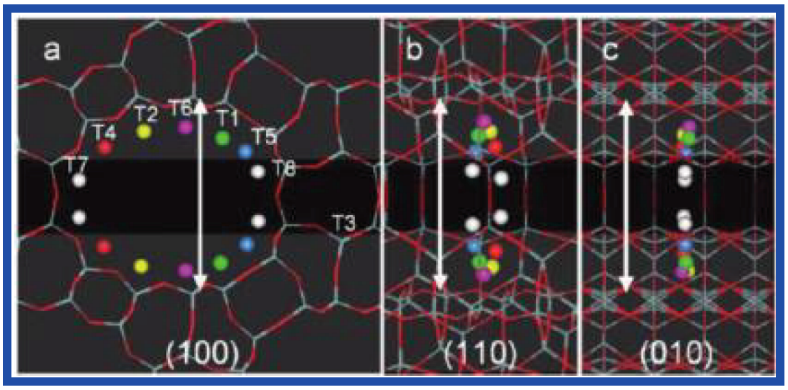

Fig. 1-9. Projection of the SSZ-53 framework topology along *a* axis.
Oxygen atoms have been omitted for clarity.

1.6.2 SFN-type zeolite

SSZ-59 (**SFN**-type zeolite) was also discovered in Chevron laboratories [51]. Its pore system consists of linear, non-interconnected channels with pore openings formed from elliptical 14-rings with an approximate size of 0.63×0.83 nm(Figure 1-10) [52]. In SSZ-53, there are eight crystallographically distinct tetrahedral T sites where Al cations can be located

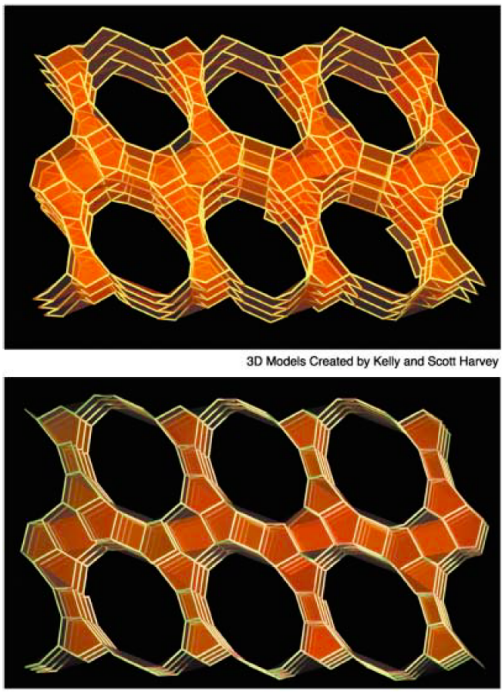

Fig. 1-10. Projection of the SSZ-59 framework topology along a axis.
Oxygen atoms have been omitted for clarity.

1.6.3 Difference between SFH- and SFN-type zeolites

Structure features of SSZ-53 and SSZ-59: The framework structures of SSZ-53 and SSZ-59 are very similar. They both have elliptical 14-ring pores with dimensions (adjusted for the radius of oxygen ≈ 1.35 Å) of approximately 8.5×6.5Å. They also possess the same framework density. Figure 1-11 shows the structural relationship between SSZ-53 and SSZ-59. While the layers in SSZ-53 are related by a twofold rotation about an axis within the plane of the figure, the layers in SSZ-59 are related by a twofold rotation about an axis perpendicular to the figure.

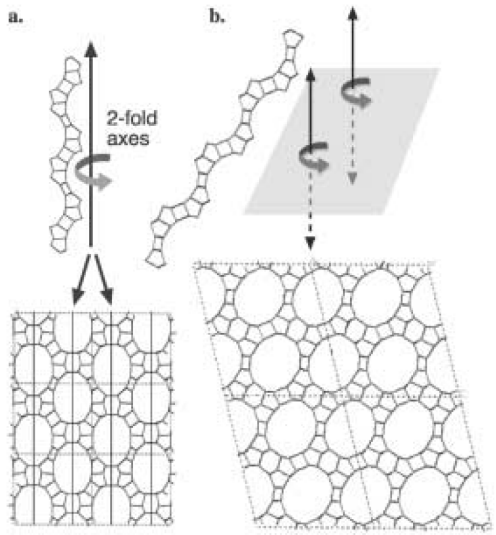

Fig. 1-11. Structural relationship between a) SSZ-53 and b) SSZ-59.

The subtle differences between SSZ-53 and SSZ-59 are exemplified in their different pore structure. Figure 1-12 shows the pore structures of SSZ-53, SSZ-59 and UTD-1. While UTD-1 possesses pore bound by smooth 6-ring ring nets, both SSZ-53 and SSZ-59 have pores with corrugated surfaces. In SSZ-53 these corrugations are centered about the vertices (of the major axis) of the elliptical pore. On the other hand, in SSZ-59 the corrugations are positioned on the sides (i.e., near the vertices of the minor axis) of the elliptical pore [52].

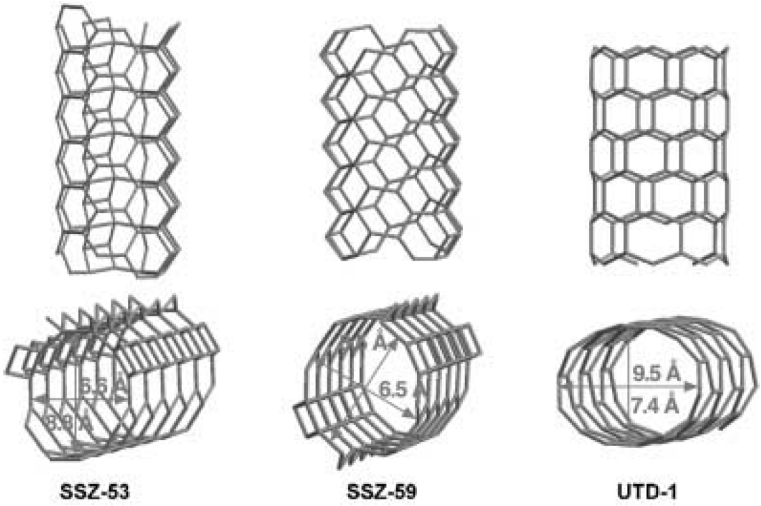

Fig. 1-12. Comparison of the pore structures of SSZ-53, SSZ-59 and UTD-1.

1.7 Small pore zeolites

Recently, 8-membered ring zeolite and zeotype material have attracted much attention in expectation of selective catalysis due to their small pores. For example, CHA-zeotype materials such as SSZ-13 and SAPO-34 showed a catalytic activity for methanol to olefins (MTO) reaction to provide ethylene and propylene, which are important chemicals for the polymer industry [54-57].

1.7.1 RTH-type zeolite

RTH-type zeolites, which consists of the **RTH** cages with the openings of 8-MR and has two-dimensional channels with aperture size of 0.41 x 0.38 nm for non-distorted 8-MR pore and 0.56 x 0.25 nm for distorted 8-MR pore, which run parallel to the a-axis and the c-axis, respectively. As shown in Scheme 1, the **RTH**-zeolite has four different T sites (T1, T2, T3 and T4). T1 site is facing to the non-distorted 8-MR pore (4.1×3.8 Å) [58, 59]. T2 site is facing to both the non-distorted and the distorted 8-MR pores (5.6×2.5 Å). T3 site is not facing either 8-MR pores. T4 site is facing to the distorted 8-MR pore. The **RTH**-type zeolites have been expected to show unique properties in the field of catalysis and adsorption because of its unique structure. However, the synthesis conditions and the diversification of the **RTH**-type zeolite have not been thoroughly investigated. Only two examples on the **RTH**-type zeolites had been reported until 2009. One is the type material, RUB-13 [59], which is the **RTH**-type borosilicate synthesized by using 1,2,2,6,6-pentamethylpiperidine (PMP) in combination with ethylenediamine (EDA) as OSDA (organic structure-directing agent)[60]. The other is SSZ-50, which is the **RTH**-type aluminosilicate and has been synthesized in the presence of *N*-ethyl-*N*-methyl-5,7,7-trimethylazoniumbicyclo octane cation as OSDA [61]. From a practical viewpoint, the use of these OSDA could significantly hinder its industrial applications. Our group found that the amounts of PMP and/or EDA can be decreased by adjusting the gel compositions. Our group have also found that simpler organic amines such as *N*-methylpiperidine and hexamethyleneimine can be used as alternative OSDA in place of PMP for the synthesis of the **RTH**-type zeolites [62,63]. Furthermore, our group have established the synthesis method for preparing the **RTH**-type zeolites without using any OSDAs [62]. The key points are the addition of an appropriate amount of sodium hydroxide as well as calcined [B]-RUB-13 as seeds and the adjustment of the molar composition of water. Thus prepared **RTH**-type zeolites synthesized without any organic-templates are named “TTZ-1” (Tokyo Tech. Zeolite) series.

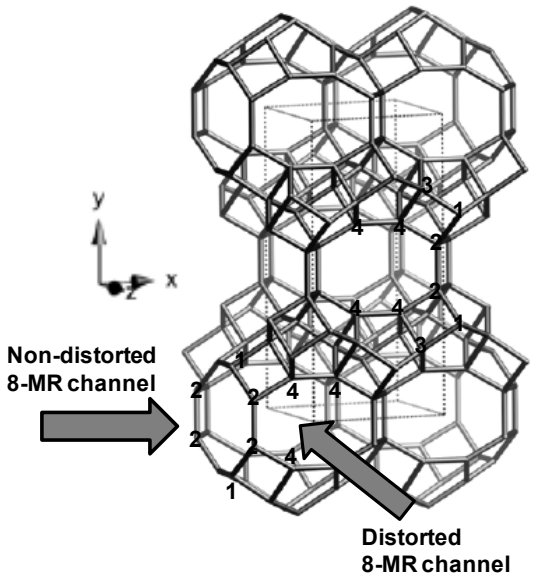

Scheme 1

Framework of the **RTH**-type zeolite viewed along [001].

1.8 Catalytic reaction for evaluating the catalytic properties

1.8.1 Friedel Crafts acylation reaction over zeolite catalysts

There is an urgent need for more environmentally acceptable processes for the synthesis of Fine Chemicals. Indeed, 5 to more than 50 kg waste per kg product are generated, i.e. approximately 10 times more than in the case of Bulk Chemicals [64]. This is because Fine Chemicals synthesis requires various successive steps, but also because many of the steps are carried out in homogeneous phase, stoichiometrically or by using acid catalysts such as H_2SO_4 or $AlCl_3$. These acids which are not reusable have to be neutralized, which generates a large amount of valueless salts. The solution to this problem seems obvious: these polluting technologies have to be substituted with cleaner technologies such as those based on heterogeneous catalysis [65, 66]. Indeed, solid catalysts offer many advantages: easy recovery of reaction products, easy set up of continuous processes, etc. Among them, zeolites with their shape selective properties and the easy tailoring of their acidity, porosity, etc. are particularly well adapted to selective organic synthesis, with, however, the scope limitation to the size of the synthesized molecules [67-71].

Friedel-Crafts acylation of aromatics is one of the most important reactions to produce aromatic ketones, which are useful intermediates for the synthesis of a number of fine chemicals such as pharmaceuticals, fragrances and dyestuffs [72, 73].

"The first mention of acylation related to the later Al_2Cl_6 method of Friedel and Crafts appeared in 1873 in a preliminary communication by Grucarevic and Merz..." [74] With these words G. A. Olah in an historical review about Friedel-Crafts Chemistry [75] reported the earliest reference on the metal-catalyzed acylation of aromatic compounds. The Friedel-Crafts acylation reaction essentially consists of the production of an aromatic ketone by reacting an aromatic substrate with an acyl component in the presence of a catalyst [76]. The conventional processes for the preparation of these aromatic ketones employ metal halides ($AlCl_3$, $FeCl_3$, etc.) or mineral acids (HF or polyphosphoric acid) as homogeneous catalysts [77]. A major drawback of the conventional Lewis-acid metal chloride catalysts for Friedel-Crafts acylation is that they are non-regenerable and must be used in more than stoichiometric amounts.

Zeolites are well-known microcrystalline porous materials largely studied and applied in the petrochemical industry for a long time [78]. Recently they have been utilized in the fine chemicals industry [79]. Owing to the above problems mentioned, many research groups have tried to develop environmentally benign acylation processes using solid acid catalysts such as zeolites.

1.8.1.1 Acylation of 2-methoxynaphthalene (2MN)

The acylation of 2-methoxynaphthalene by aluminum chloride was a step in the first large-scale synthesis of naproxen [80].

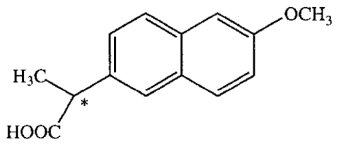

naproxen

Acylation of 2-methoxynaphthalene with acetic anhydride (AA) was investigated over various molecular sieves: FAU [81,82], MFI, MOR [82], MTW [81], MCM-41 [83] and especially BEA [81, 84-92]. With this acetylation, there is an additional problem because of the simultaneous formation of 2-acetyl-6-methoxynaphthalene, which is the desired product (precursor of naproxen), and of its isomers. (Fig.1-13) Generally, acetylation occurs preferentially at the kinetically controlled 1-position with formation of 1-acetyl-2-methoxynaphthalene.

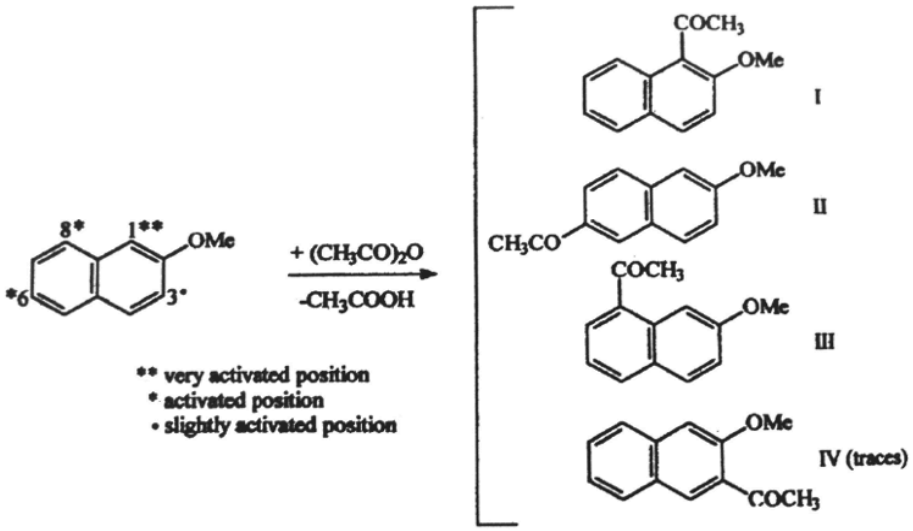

Fig. 1-13 Acetylation of 2-methoxynaphthalene (2MN) reaction products.

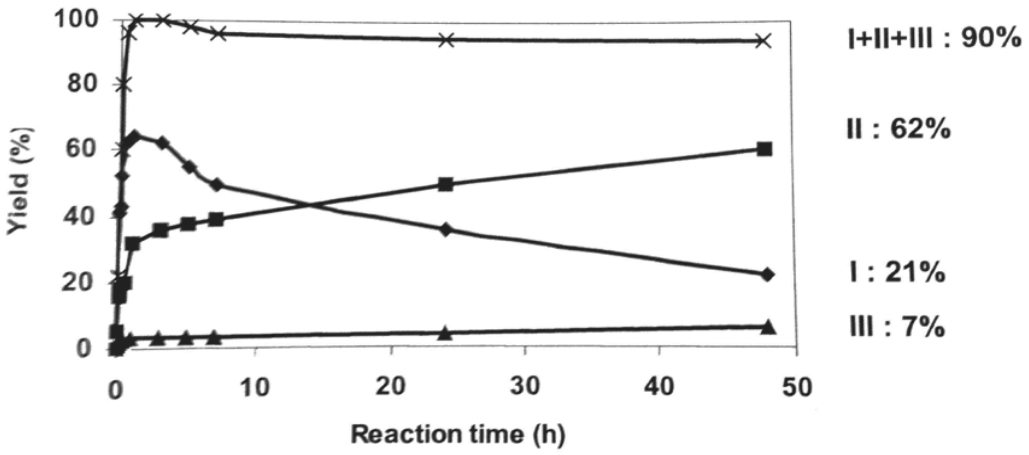

Fig. 1-14 Acetylation of 2-methoxynaphthalene with acetic anhydride in nitrobenzene solvent. Total yield in acetyl-methoxynaphthalene(I + II + III) (X) and yields in isomers I, II, III.

However, as shown in Figure 1-14, over an HBEA zeolite with a Si/Al ratio of 15 (HBEA15), acetylation is followed by secondary reactions of isomer I: isomerization into II and into 1-acetyl-7-methoxynaphthalene(III) and deacylation. Therefore, the transformation the 2MN/AA mixture on HBEA15 can be proposed to occur mainly through the following successive scheme [93]:

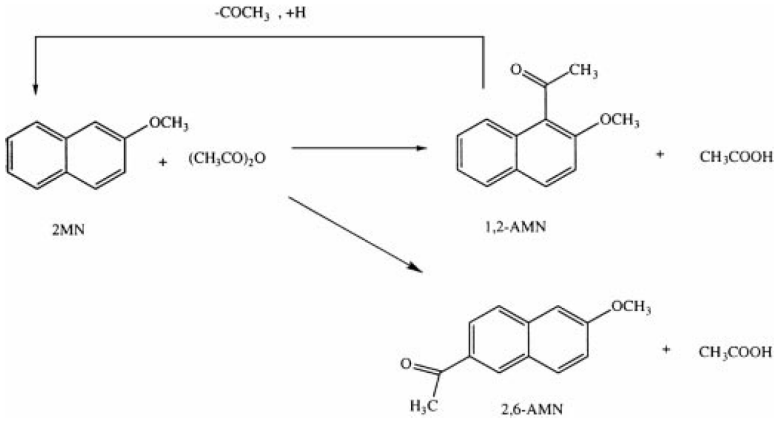

1.8.2 MTO reaction (Methanol-to-Olefins reaction)

Light olefins such as Ethylene, propylene and butenes are important petrochemical products for the polymer industry. These products are mainly produced from the thermal cracking of naphtha. The rapid rise of the crude oil price also causes the prices of light olefins to go up. Furthermore, the large amount formation of carbon dioxide and consumption of energy drives the petrochemical industries out to find new routes to produce light olefins from other carbon sources with lower energy requirement. The methanol-to-olefin (MTO) process has been considered as a strong alternative, because it produces light olefins from natural gas or coal via methanol. Molecular sieves have been known to be effective catalysts for converting methanol and other oxygenates to olefin since the early 1970s [94,95]. Much of the early work was an offshoot of the methanol-to-gasoline (MTG) process development that used catalysts based on the medium-pore sized ZSM-5 zeolite [96,97].

MTO and MTG reactions are generically called MTH (methanol-to-hydrocarbons) reaction. The methanol-to-hydrocarbons technology was considered as a powerful method to convert coal into gasoline or chemicals. By using this technology, one can make almost anything out of coal or natural gas that can be made out of crude oil. Methanol is made from synthesis gas (a mixture of carbon monoxide and hydrogen) which is formed by steam reforming of natural gas or gasification of coal. The methanol is then can be processed catalytically to either gasoline (methanol-to-gasoline, MTG) or olefins (methanol-to-olefin, MTO), depending on the catalyst and/or the process operation conditions. Although methanol itself is a potential motor fuel or can be blended with gasoline, it would be hard to use methanol as a motor fuel directly. The commercial MTG reaction runs at temperatures around 400°C and a methanol partial pressure of several bars and uses a ZSM-5 catalyst. These are the optimal conditions for converting the olefins that form within the catalyst into paraffins and aromatics. However, at one point in the MTG reaction, the product mixture consists of about 40% light olefins. The importance of light olefins as intermediates in the conversion of methanol to gasoline was recognized early. Consequently, a number of attempts were made to selectively form light olefins from methanol, not only on medium-pore zeolites but also on small-pore zeolites, SAPO type molecular sieves and large-pore zeolites (to a much lesser extent). If one interrupted the reaction at the point of about 40% light olefin formation, one could harvest these C_2 –C_4 olefins. By adjusting the reaction conditions (such as, for example, raising the temperature to 500° C) as well as the catalyst applied, one can increase dramatically the olefin yield. This discovery led to the development of the MTO process, which generates mostly propylene and butylene, with

high-octane gasoline as a byproduct.

The MTO process of Mobil has been demonstrated in the experimental 4000 ton $year^{-1}$ plant at Wesseling (Germany) used to prove the fluid-bed MTG process, applying ZSM-5 as catalyst [98]. In cooperation with Norsk Hydro, UOP announced in 1996 that their SAPO-34 based MTO process was to be realized in the construction of a 250 000 ton $year^{-1}$ plant using a natural gas feedstock for production of ethylene. A 0.5 ton $year^{-1}$ demonstration unit operated by Norsk Hydro has verified the olefin yields and catalyst performance. SAPO-34 is extremely selective towards ethylene and propylene formation with the flexibility of altering the ratio between the two olefins by varying the reactor conditions [99].

Besides the process engineering aspects, a huge knowledge concerning the involved microporous materials has been gathered during this research, especially with respect to ZSM-5 (MTG directed) and SAPO-34 (MTO directed) which is of benefit for the 'zeolite' community in general. While the FCC research promoted the insight into the field of large-pore zeolites/ microporous materials, the methanol to hydrocarbons research contributed strongly to the enhancement of the knowledge directed towards the medium- and small-pore molecular sieves.

SAPO molecular sieves, with their mild acidity, are very interesting alternatives to obtain high selectivities for light olefins. The conditions of synthesis, dealumination and cation exchange seem to be very important for obtaining a catalyst with a good performance for methanol conversion into light olefins. Furthermore, the ratio of acid sites on the external surface to acid sites in the porous structure also plays an important role. The smaller the crystallite size, the higher this ratio. Finally, the presence of certain OH groups (ν_{OH}= 3600 cm−1 , which correspond to Al-OH bonds) were found to be the most active ones for the methanol conversion into hydrocarbons. Consequently, it is very important that the access to these acid sites is not blocked [100].

1.9 Outline

Zeolites have been utilized in many industrial technologies, including gas adsorption, ion-exchange, separation and catalysis for their unique porosity and high surface area. In recent decades, extra-large-pore zeolites with more than 14-MR have been paid much attention because of a wide range of applications in catalysts. SSZ-53 and SSZ-59 with the **SFH**- and **SFN**-type topology are specially received much attention due to their high hydrothermal stability. However, SSZ-53 and SSZ-59 to date there are few reports on the preparation and catalytic performance of the two aluminosilicate zeolites. Furthermore, the synthesis conditions have not been fully investigated. Here, Al containing SSZ-53 and SSZ-59 were synthesized under different methods, and the structural and catalytic properties were investigated. **RTH**-type zeolite with 8-MR has attracted much attention due to its high yield of olefins in MTO reaction. Here, **RTH**-type zeolite was synthesized by using different OSDAs or without OSDA. The detailed characterization of Al species in relation to their acidic properties has been conducted.

Chapter 2

The **SFH**-type aluminosilicate zeolites were successfully synthesized by direct- and post-synthesis methods. The ^{27}Al MAS and ^{27}Al MQMAS NMR reveals that most Al species of the samples are located in the framework but there is a marked difference in the distribution of Al atoms in the framework between direct- and post-synthesis methods. [Al,B]-SFH-D (synthesized by direct-synthesis method) exhibited a higher catalytic performance in the acylation compared to [Al,B]-SFH-P (synthesized by post-synthesis method).

Chapter 3

According to the synthesis results of **SFH**-type zeolite in chapter 2, the direct-synthesis method for preparing the **SFN**-type aluminosilicate zeolites, designated as [Al,B]-SFN-D, was successfully improved by increasing the SDA/SiO_2 ratio to 0.3 and adding 10 wt% seeds. However, high Al content containing **SFN**-type zeolite could not be synthesized by direct-synthesis method like **SFN**-type zeolite. Similar ^{27}Al MAS NMR results were obtained to the results of SSZ-53. [Al,B]-SFN-D exhibited a higher catalytic performance in the acylation compared to [Al,B]-SFN-P.

Chapter 4

14 membered ring extra-large-pore zeolite, CIT-5 (California Institute of Technology Number 5), was synthesized by direct-synthesis method according to the literature reported previously. Thus prepared CIT-5 (**CFI**-type) zeolite was characterized in details. Finally, Al containing CIT-5, SSZ-53 and SSZ-59 synthesized by direct-synthesis method were utilized as catalysts for acylation of 2-methoxynaphthalene under same reaction condition in order to compare the catalytic performace. Commercial 12 membered ring zeolites Beta and Mordenite were also used in the same reaction. [Al]-CIT-5 was considered to be the weakest of the five zeolites according to the results of NH_3-TPD. [Al.B]-SSZ-53 showed the highest catalytic performance due to its extra-large-pore and medium degree of acid strength.

Chapter 5

The **RTH**-type aluminosilicates were synthesized with different types of OSDA or without using any OSDAs. Thus obtained zeolite synthesized with different preparation methods were characterized by using various techniques, especially, high-resolution ^{27}Al MAS NMR and CO-adsorbed in-situ FT-IR techniques. All the prepared **RTH**-type zeolites produced propene selectively on the MTO reaction. However, the catalytic properties significantly depended on the type of OSDA used for the zeolite synthesis. The high-resolution ^{27}Al MAS NMR and ^{27}Al MQMAS NMR techniques revealed that the Al distribution over framework T sites was clearly dependent on the type of OSDA.

References

1. A. Corma, *Journal of Catalysis*, **2003**, 216, 298

2. H. van Bekkum, E. M. Flanigen, J. C. Jansen, *Studies in surface science and catalysis*, 58, 13, chapter 2

3. A. F. Cronstedt, Akad. Handl. Stockholm, **1756**, 18, 120

4. Michel Guisnet, Jean-Pierre Gilson, *Zeolites for Cleaner Technologies*, *Catalytic Science Series*, Vol. 3, chapter 1

5. G. W. Morey and E. Ingerson, *Econ. Geol.*, **1937**, 32, 607

6. H. de St. Claire-Deville, *Compt. Rend.*, **1862**, 54, 324

7. J. Hagen, *Industrial Catalysis*, chapter 6, 229

8. A. Corma, *Chem. Rev.* **1995**, 95, 559

9. J. Hagen, *Industrial Catalysis*, chapter 6, 235

10. Guisnet M., and Edimbourg in Supported Catalysts and their Applications, Ed. Sherrington D.C. and Kybett A.P., (The Royal Society of Chemistry, Cambridge, **2001**) 55

11. Martens J.A., Souverijns W., van Rhyn W. and Jacobs P.A., *in Handbook of Heterogeneous Catalysis*, Ed. G. Ertl et al., 1 (Wiley, 1997) 324

12. Graham J. Hutchings, *Catalytic Science Series*, Vol. 3, *Zeolites for Cleaner Technologies*, chapter1

13. Guisnet M., and Edimbourg in Supported Catalysts and their Applications, Ed. Sherrington D.C. and Kybett A.P., (The Royal Society of Chemistry, Cambridge, **2001**) 55

14. Rabo J. and Gajda G. J., in Guidelines for Mastering the Properties of Molecular Sieves, Ed. Barthomeuf D. et al., 221 (NATO ASI Series B: Physics, Plenum Press, New York, **1990**) 273

15. Martens J. A., Souverijns W., van Rhyn W. and Jacobs P.A., *in Handbook of Heterogeneous Catalysis*, Ed. G. Ertl et al., 1(Wiley, 1997) 324.

16. Wachter W. A., Proceedings 6th Int. Zeolite Conference, Ed. Olson D. and Bisio A., (Butterworth, Guildford, 1984) 141

17. E. Lippmaa, A. Samoson, M. Magi, *J. Am. Chem. Soc.* **1986**, 108, 1730-1735.

18. W. Kolodziejski, C. Zicovich-Wilson, C. Corell, J. Perez-Pariente, A. Corma, *J. Phys. Chem.* **1995**, 99*,* 7002-7008.

19. C. A. Fyfe, Y. Feng, H. Grondey, G. T. Kokotailo, H. Gies, *Chem. Rev.* **1991**, 91, 1525-1543.

20. Fyfe, C. A.; Gobbi, G. C.; Kennedy, G. J.; Graham, J. D.; Ozubko, R. S.; Murphy, W. J.; Bothner-By, A.; Radok J.; Chesnick, A. S. *Zeolites,* **1985**, 5, 179.

21. Hunger, M.; Ernst, S.; Weitkamp, J. *Zeolites* **1995**, 15, 188.
22. Medek, J. S. Harwood, L. Frydman, *J. Am. Chem. Soc.*, **1995**, 117, 12779-12787.
23. S.-J. Hwang, C. Fernandez, J. P. Amoureux, J.-W. Han, J. Cho, S. W. Martin, M. Pruski, *J. Am. Chem. Soc.*, **1998**, 120, 7337–7346.
24. S. E. Ashbrook, L. Le Pollès, R. Gautier, C. J. Pickard, R. I. Walton, *Phys. Chem. Chem. Phys.*, **2006**, 8, 3423-3431.
25. K. H. Lim, C. P. Grey *J. Am. Chem. Soc.*, **2000**, 122, 9768-9780.
26. K. Shimoda, Y. Tobu, Y. Shimoikeda, T. Nemoto, K. Saito, *J. Magnetic Resonance* **2007**, *186*, 156-159.
27. K. Shimoda, Y. Tobu, K. Kanehashi, T. Nemoto, K. Saito, *J. Non-Crystalline Solids*, **2008**, 354, 1036-1043.
28. H. G. Karge, V. Dondur and J. Weitkamp, *J. Phys. Chem.* **1991**, 95, 283-288.
29. N. Katada and M. Niwa, *Catal. Surv. Asia* **2004**, 8, 161-170.
30. R. B. Borade, A. Adnot and S. Kaliaguine, *J. Chem. Soc., Faraday Trans*., **1990**, 86, 3949-3956.
31. J. W. Ward, in Zeolite Chemistry and Catalysis, ed. J. A. Rabo, ACS Monograph 171, American Chemical Society, Washington, DC, **1976**, pp. 118-284.
32. Jentys and J. A. Lercher, *Stud. Surf. Sci. Catal.* **2001**, *137*, 345-386, and the references therein.
33. L. M. Kustov, V. B. Kazansky, S. Beran, L. Kuvelkova, P. Jiru, *J. Phys. Chem.* **1987**, 91, 5247-5251.
34. N. Echoufi and P. Gelin, *J. Chem. Soc., Faraday Trans.* **1992**, 88, 1067-1073.
35. Zecchina, S. Bordiga, G. Spoto, D. Scarano, G. Petrini, G. Leofanti, M. Padovan and C. O. Arean, *J. Chem. Soc., Faraday Trans.*, **1992**, 88, 2959-2969.
36. S. Bordiga, E. E. Platero, C. O. M. Arean, C. Lamberti and A. Zecchina, *J. Catal.* **1992**, 137, 179-185.
37. L. Mirojew, S. Ernst, J. Weitkamp and H. Knozinger, Catal. Lett., **1994**, 24, 235-248.
38. J. N. Kondo, R. Nishitani, E. Yoda, T. Yokoi, T. Tatsumia, K. Domenc, *Phys. Chem. Chem. Phys.* **2010**, 12, 11576-11586.
39. A. Corma, *Journal of Catalysis,* **2003,** 216, 298-312
40. M. E. Davis, *Chem. Eur. J.*, **1997**, 3, No.11
41. P.B. Venuto, *Microporous Mater.* **1994**, 2, 297.
42. M. E. Davis, P.E., C. Saldarriaga, C. Montes, J. Garces, C. Crowder, *Nature*, **1988**, 331, 698.

43. Q.S. Huo, R. R. Xu, S. G. Li, Z. G Ma, J. M. Thomas, R. H. Jones, A.M. Chippindale, J. Chem. Soc. Chem. Commun. 1992, 875-876
44. M. Estermann, L. B. McCusker, C. Baerlocher, A. Merrouche, H. Kessler, Nature 1991, 352, 320-323
45. H. Y. Li, M. E. Davis, *Catal. Today* **1994**, 19, 61.
46. (a)M. E. Davis, *Nature*, **1996**, 381, 295, (b)M. E. Davis, *J. Am. Chem. Soc.* **1997**, 119, 8474
47. M. E. Davis, *Nature*, **1996**, 381, 295-298
48. C. Y. Chen, S. I. Zones, A. W. Burton, S. A. Elomari, S. Svelle, *Stud. Surf. Sci. Catal.*, **2007**, 172, 329
49. K.G. Strohmaier, D.E.W. Vaughan, *J. Am. Chem. Soc.*, **2003**, 125, 16035-16039.
50. a. A. Corma, M. J. Diaz-Cabanas, F. Rey, Sp. Pat. ES2186487, **2000**; b. A. Corma, M. J. Diaz-Cabanas, F. Rey, PCT Int. Appl. WO0203820, 2002.
51. S. Elomari (Chevron Research and Tochnology Company), WO-A1 01/9992155, 2001.
52. A. Burton, S. Elomari, C.-Y. chen, R.C. Medrud, I. Y. Chan, L. M. Bull, C. Kibby, T. V. Harris, S. I. Zones, E.S. Vittoratos, *Chem. Eur. J.* 2003, 9, 5737-5748.
53. Ceren Aydin, Jing Lu, Ann J. Liang, Cong-Yan Chen, Nigel D. Browning, and Bruce C. Gates, *Nano Lett.* **2011**, 11, 5537-5541.
54. Q. Zhu, J. N. Kondo, R. Ohnuma, Y. Kubota, M. Yamaguchi, T. Tatsumi, *Microporous Mesoporous Mater.*, **2008**, 112, 153-161.
55. Q. Zhu, M. Hinode, T. Yokoi, J. N. Kondo, Y. Kubota, T. Tatsumi, *Microporous Mesoporous Mater.*, **2008**, 116, 253-257.
56. J. Liang, H. Li, S. Zhao, W. Guo, R. Wang, M. Ying, *Applied Catalysis*, **1990**, 64, 31-40.
57. Q. Zhu, J. N. Kondo, T. Tatsumi, S. Inagaki, R. Ohnuma, Y. Kubota, Y. Shimodaira, K. Domen, *J. Phys. Chem. C*, **2007**, 111, 5409-5415.
58. http://www.iza-structure.org/
59. S. Vortmann, B. Marler, H.Gies, P. Daniels, *Microporous Mater.*, **1995**, 4, 111-121.
60. G. S. Lee, S. I. Zones, *J. Solid State Chem.*, **2002**, 167, 289-298.
61. M. Niwa, K. Katada, *Catal. Surv. Jpn.*, **1997**, 1, 215-226.
62. T. Yokoi, M. Yoshioka, H. Imai, T. Tatsumi, *Angew. Chem. Int. Ed.*, **2009**, 48, 9884-9887.
63. M. Yoshioka, T. Yokoi, H. Imai, S. Inagaki, T. Tatsumi, *Microporous Mesoporous Mater.*, **2012**, 153, 70-78 .
64. R.A. Sheldon, *Chemtech*, March **1994**, 38.

65. Heterogeneous Catalysis and Fine Chemicals 1, 2, 3, 4, Stud. Surf. Sci. Catal. 41(**1988**), 59(**1991**), 78(**1993**), 108(**1997**).
66. Sheldon R.A. and van Bekkum H., Fine Chemicals through Heterogeneous Catalysis, (Wiley-VCH. Weinheim, **2001**)
67. Holderich W.F. and van Bekkum H., Fine Chemicals through Heterogeneous Ctalysis, (Wiley-VCH. Weinheim, **2001**).
68. Venuto P.B., *Microporous Materials*, **1994**, 2, 297.
69. Perot G. and Guisnet M., Precision Process Technology, Ed. Weijnen M.P.C. and Drinkenburg A.A.H., (Kluwer Academic Publishers, **1993**) 157
70. Holderich W.F., Heitnmannn G., Catalysis Today 38 (1997) 227
71. Corma A., Garcia H., Catalysis Today, 38 (1997) 257
72. J.A. Horseley, CHEMTECH, **1997**, 45.
73. K. Bauer, D. Garbe, H. Surburg, Common Fragrance and Flavor Materials, VCHVerlagsgesellschaft, Weinheim, **1990**, P. 83.
74. Grucarevic, S.; Merz, V., *Chem. Ber.* **1873**, 6, 60.
75. Olah, G. A. *Friedel-Crafts Chemistry*; Wiley: New York, **1973**.
76. Gore, P. H. in Friedel-Crafts and Related Reactions; Olah, G. A., Ed.; John Wiley & Sons Inc.: London, **1964**; Vol. III, Part 1, p 1.
77. P.H. Gore, in: G.A. Olah (Ed.), Friedel Crafts and Related Reactions, Vol. III, Wiley Insterscience, New York, **1964**, P. 64
78. A. Corma, *Chem. Rev.*, **1995**, 95, 559
79. Sen, S. E.; Smith, S. M.; Sullivan, K. A. Tetrahedron, **1999**, 55, 12657.
80. Harrington, P. J., and Lodewijk, E., Org. Process Res. Develop. 1, 72, **1997**.
81. Harvey G. and Mader G., Collect. Czech., *Chem. Commun.*, **1992**, 57, 862.
82. Yadav G.D. and Krishnan M.M.S., Chem. Eng. Sci., **1999,** 54, 4189
83. Gunnewegh, E. A., Gopie, S. S. and van Bekkum, H., *J. Mol. Catal. A*, **1996**, 106,151.
84. Harvey G., Binder G. and Prins R., *Stud. Surf. Sci. Catal.*, **1998**, 94, 397.
85. Heinichem H.K. and Holderich W.F., *J. Catal.*, **1999,** 185, 408.
86. Kim S.D. et al., *J. Mol. Catal. A: Chem.*, **2003**, 152, 33
87. Fromentin E., Coustard J.M. and Guisnet M., *J. Mol. Catal.*, **2000,** 159, 377
88. Fromentin E., Coustard J.M. and Guisnet M., *J. Catal.*, 2000, 190, 433.
89. Andy P. et al., *J. Catal.*, **2000**, 192, 215
90. Casagrande M., Storaro L., Lenarda M. and Ganzerla R., *Appl. Catal. A: Gen.*, **2000**, 201, 263.
91. Botella P., Corma A. and Sastre G., *J. Catal.*, **2001**, 197, 81.

92. Berreghis A., Ayrault P., Fromentin E. and Guisnet M., *Catal. Letters*, **2000**, 68, 121.
93. M. E. Davis, *Journal of catalysis*, **2002**, 192, 215-223
94. Chang C.D., Lang W.H. and Silvestri A.J., U.S. Patent 4,062,905, **1977**.
95. Chang C.D. and Silvestri A.J., *J. Catal*., **1977**, 47, 249.
96. Chang C.D., *Catal. Rev.-Sci. Eng.*, **1984**, 10, 323.
97. Chang C.D., Hydrocarbons from Methanol (M. Dekker, New York, **1983**).
98. C.D. Chang, A.J. Silvestri, Chemtech. 10 (**1987**) 624.
99. B.V. Vora, T.L. Marker, P.T. Barger, H.R. Nilsen, S. Kvisle, T. Fuglerud, in: M. de Pontes, R.L. Espinoza, C.P. Nicolaides, J.H. Scholz, M.S. Scurrell (Eds.), Stud. Surf. Sci. Catal., vol. 107, Elsevier, Amsterdam, **1997**, p. 87.
100. G.F. Froment, W.J.H. Dehertog, A.J. Marchi, *A review of the literature, Catalysis*, **1992**, 9, 1.

Chapter 2

Synthesis, characterization and catalytic properties of SFH-type zeolites

Abstract

The direct-synthesis method for preparing the **SFH**-type aluminosilicate zeolites, designated as [Al,B]-SFH-D, was successfully improved by adding the calcined **SFH**-type borosilicate zeolite as seeds into the mother gel in the presence of *N*, *N*, *N*-trimethylphenylcyclohexylmethylammonium hydoxide as organic-structure-directing agent. As a control, by the conventional post-synthesis method, the **SFH**-type aluminosilicate zeolites, designated as [Al,B]-SFH-P, were prepared. Thus prepared **SFH**-type aluminosilicate zeolites were characterized in details. The high-resolution ^{27}Al MAS NMR results implied that there are marked differences in the distribution of Al atoms in the framework between the zeolites obtained by the direct- and post-synthesis methods. [Al,B]-SFH-D exhibited a higher catalytic performance in the acylation of 2-methoxynaphthalene with acetic anhydride than [Al,B]-SFH-P.

2.1 Introduction

Zeolites have been widely utilized in the petroleum catalysis and refining industry. Among them, 8-, 10-, and 12-membered rings (MR) zeolites that consist of 8, 10, and 12 oxygen atoms to construct the rings of the pores are called small-, medium-, and large-pore zeolites, respectively. When more than 12 oxygen atoms are used to construct the pores, thus zeolites are called "extra-large-pore zeolite". In recent decades, extra-large-pore zeolites with more than 14-MR has been receiving much attention because of a wide range of applications in catalysis, adsorption, separation, chromatography, *etc.*, in particular, for bulky molecules that cannot enter 12 MR pores [1].

The first extra-large-pore zeolite is VPI-5 (an aluminophosphate material) with the **VFI**-type topology and pores larger than 10 Å, which was reported in 1988 [2]. The large pores of the VPI-5 sieves consist of one-dimensional channels circumscribed by 18-MR and possess free diameters of approximately 12-13 Å. However, its poor thermal and hydrothermal stability limits its usefulness. Since this report, extra-large-pore zeolites have been extensively investigated, and the synthesis of silica-based aluminosilicate zeolites, UTD-1 (**DON**, 0.74×0.95 nm) and CIT-5 (**CFI**, 0.72×0.75 nm) that possess one-dimensional channel with 14-MR pores, have been reported [3,4]. These zeolites have both high thermal stability and favorable Brønsted acidity. However, a highly elaborated organic compound, (pentamethyl)cyclopentadienyl cobalticinium complex, is necessary for the synthesis of UTD-1, and thus has limited its synthesis and application. Although CIT-5 has 14 MR channels, its pore dimensions (0.72×0.75 nm) are approximately the same as those of 12-MR windows of **FAU**- and [*]**BEA**-type zeolites [5].

One of the recently discovered extra-large-pore zeolites is "SSZ-53" with the **SFH**-type topology [6]. This zeolite that consists of one-dimensional 14MR pores (0.65 × 0.85 nm) has been synthesized with *N*, *N*, *N*-trimethyl-phenylcyclohexylmethylammonium hydroxide as organic-structure-directing agent (OSDA). The pore structure of this zeolite with high hydrothermal stability would be efficient for a wide range of applications in catalysis for large molecular reaction. Originally, this zeolite was synthesized as borosilicate in 2002 [6]. Burton *et al.* reported on the synthesis of aluminosilicate ones by the direct-and post-synthesis methods in 2003 [7]. The catalytic application of the

SFH-type aluminosilicate was also reported [8]. Recently, its unique structural properties and detailed characterization were reported [9]. However, to date, there are few reports on the preparation and catalytic performance of the **SFH**-type aluminosilicate. Furthermore, the synthesis conditions of the **SFH**-type aluminosilicate have not been fully investigated, although its unique structural and catalytic properties have attracted considerable attention.

Here, we report the synthesis of the **SFH**-type aluminosilicate zeolites by the direct- and post-synthesis methods, and the differences in the structural and acid properties between the products obtained by the two methods. The influences of the synthesis conditions on the crystallization behavior, composition and physicochemical properties of the product were investigated in detail. The high-resolution ^{27}Al MAS NMR results have revealed that there are marked differences in the conditions of tetrahedral Al species between the products obtained by the two methods.

2.2 Experimental

2.2.1 Synthesis of SFH-type zeolites

2.2.1.1 Synthesis of SFH-type zeolites by direct-synthesis method

First, *N*, *N*, *N*-trimethyl-phenylcyclohexylmethylammonium hydroxide was synthesized according to the patent reported [6] and used as OSDA for synthesizing the **SFH**-type zeolite, its successful synthesis was confirmed by liquid state ^{13}C and ^{1}H NMR spectra.

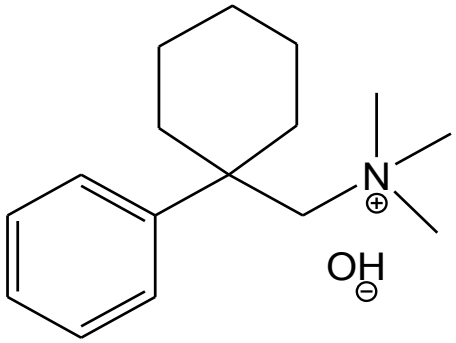

N, *N*, *N*-trimethyl-phenylcyclohexylmethylammonium hydroxide

The **SFH**-type borosilicate, designated as [B]-SFH, was hydrothermally synthesized from the mother gel containing colloidal silica (Ludox HS-40, Sigma-Aldrich)**,** sodium borate decahydrate ($Na_2B_2O_7 \cdot 10H_2O$, Aldrich) and OSDA according to the previous report [7]. The molar composition of the mother gel was SiO_2: OSDA: Na_2O: B_2O_3: H_2O = 1: 0.25: 0.05: 0.033: 44. The mother gel was hydrothermally treated at 160 ºC for 8 days. The atomic ratios of Si/B in the gel and the solid product were 15 and 38, respectively.

The **SFH-**type zeolite containing both Al and B was directly synthesized by hydrothermal synthesis method with the amount of Al content varied. $Al(NO_3)_3 \cdot 9H_2O$ was used as Al source. The molar composition of the mother gel was SiO_2: OSDA: Na_2O: Al_2O_3: B_2O_3: H_2O = 1: 0.25: 0.0125: *x*: 0.033: 44 (*x* = 0.02, 0.01, 0.005, or 0.0025). 5 wt% of the calcined [B]-SFH (Si/B = 38) as seeds was added into the mother gel. Thus prepared gels were hydrothermally treated at 160-180 ºC for 5-11 days. The solid product was recovered by filtration, washing with distilled water and drying overnight at 100ºC. Thus obtained Na-type samples were calcined in air at 550ºC, and then were converted to the H-type ones by treating with 1 M NH_4NO_3 aq. followed by calcination at 550 ºC to exchange Na^+ ions for H^+. The products were

designated as [Al,B]-SFH-D-*x* (*y*) where *x* and *y* are the Si/Al atomic ratio in the gel and the product, respectively.

2.2.1.2 Synthesis of SFH-type zeolites by post-synthesis method

The **SFH**-type aluminosilicate was prepared by the post-synthesis method as follows [7]. The calcined [B]-SFH and [B]-SFN was treated in the aqueous solution containing aluminium nitrate for 12 h at 95 ºC. After the treatment, the resulting solid was washed with 0.1 N hydrochloric acid. The concentration of $Al(NO_3)_3$ was varied from 0.25 to 1.0 M in order to change the Al content incorporated. After drying at 100 ºC for 12 h and a final calcination at 550ºC, a H-type form of the aluminosilicate zeolites were obtained. Thus obtained product was designated as [Al,B]-SFH-P-*m* (*n*) and [Al,B]-SFN-P-*m* (*n*), where *m* and *n* are the concentration of $Al(NO_3)_3$ solution and the Si/Al atomic ratio in product, respectively.

2.2.2 Characterizations

2.2.2.1 Structural characterization

The prepared zeolites were characterized by XRD, ICP, SEM, N_2 adsorption, high resolution ^{27}Al MAS NMR and NH_3-TPD. XRD patterns were collected on a Rint-Ultima III (Rigaku) using a Cu Kα X-ray source (40 kV, 20 mA). Nitrogen adsorption measurements to determine the BET surface area (S_{BET}), S_{EXT}, and micropore volume (V_{micro}) were conducted at 77 K on a Belsorp-mini II (Bel Japan). Field-emission scanning electron microscopic (FE-SEM) images of the powder samples were obtained on an S-5200 microscope (Hitachi) operating at 1-30 kV. The sample was mounted on a carbon-coated microgrid (Okenshoji Co.) without any metal coating. The Si/Al ratios of the samples were determined by using an inductively coupled plasma-atomic emission spectrometer (ICP-AES, Shimadzu ICPE-9000).

2.2.2.2 Detailed characterizations of Al species by high-resolution ^{27}Al MAS NMR and ^{27}Al 3Q MQMAS NMR spectroscopies

To investigate the Al environment, solid-state ^{27}Al magic-angle spinning (MAS) NMR spectra were obtained on a JEOL ECA-600 spectrometer (14.1 T). The relaxation delay time was 10 ms. The ^{27}Al chemical shift was referenced to $AlNH_4(SO_4)_2 \cdot 12H_2O$ at -0.54 ppm and samples were spun at 17 kHz by using a 4 mm ZrO_2 rotor.

2.2.2.3 Estimation of acid amount by NH_3-TPD

Temperature-programmed NH_3 desorption (NH_3-TPD) profiles were recorded on a BELCAT (Japan BEL). Typically, 30 mg catalyst was pretreated at 773 K in He (50 mL min^{-1}) for 1 h and then cooled to 423 K. Prior to the adsorption of NH_3, the sample was evacuated at 423 K for 1 h. Approximately 2500 Pa of NH_3 was allowed to make contact with the sample at 423 K for 10 min. Subsequently, the sample was evacuated to remove weakly adsorbed NH_3 at the same temperature for 30 min. Finally, the sample was cooled to 423 K and heated from 423 to 873 K at a ramping rate of 10 K min^{-1} in a He flow (50 mL min^{-1}). A quadrupole mass spectrometer was used to monitor desorbed NH_3 (m/e = 16). The amount of acid sites was determined by using the area of the so-called "*h*-peak" in the profiles [10].

2.2.3 Catalytic reaction

To evaluate the catalytic performance of the **SFH**-type aluminosilicate prepared, Friedel-Crafts acylation of 2-methoxynaphthalene (2-MN) with acetic anhydride was conducted in the liquid-phase under batch conditions. Before the reaction, 50 mg of the catalyst was pretreated at 400ºC for 1 h under vacuum conditions in a glass reactor. Under argon atmosphere, 2 mmol of 2-MN, 1 mmol of acetic anhydride and 2 ml of *o*-dichlorobenzene as solvent were put into the glass reactor. The reaction temperature and time were set at 100 ºC and 5-30 min, respectively. The reactant and products were analyzed by a gas chromatograph (Shimadzu, GC-2014) equipped with an FID detector with a DB-5 column.

2.3 Results and discussion

2.3.1 Direct-synthesis method

First, [B]-SFH was directly synthesized in the presence of the OSDA by the conventional method under the hydrothermal conditions at 160 ºC for 8 days. It showed the typical XRD pattern attributed to the **SFH** structure (Fig. 1 a) [7]. By the ICP analyses, the Si/B ratio of [B]-SFH was found to be 38. The ^{11}B MAS NMR spectrum exhibited one sharp peak at -2.6 ppm, indicating that boron atoms are in the framework [11, 12]. In this study, thus prepared calcined [B]-SFH was used as seeds in preparing Al-containing **SFH**-type zeolite via a direct-synthesis route.

2.3.2 Modification of synthesis conditions of SFH-type zeolite

The introduction of the Al source into the mother gel of [B]-SFH was tested under the same conditions as those for [B]-SFH. Attempts to directly synthesize [Al,B]-SFH by adding the Al source into the mother gel of [B]-SFH with the Si/Al ratio of 200 were unsuccessful; the product was amorphous (Fig. 1 b). By adding 5 wt% of the calcined [B]-SFH as seed crystals, two diffraction peaks attributed to the **SFH**-type zeolite were slightly observed at 2θ = 6.7 and 8.3˚ after the hydrothermal treatment at 160 ºC for 11 days, although the main product was cristobalite that typically gave a strong diffraction peak at 2θ = 22.0˚ (Fig. 1 c) [13]. When the $NaOH/SiO_2$ ratio was decreased from 0.1 to 0.025, the formation of cristobalite was completely suppressed with the peaks attributed to the **SFH**-type zeolite retained (Fig. 1 d). The formation of the **SFH**-type zeolite was not significantly enhanced any more when the period of the hydrothermal treatment was prolonged. Meanwhile, by increasing the hydrothermal temperature from 160 to 180 ºC, the SFH-type zeolite was successfully formed after the hydrothermal treatment for 5 days (Fig. 1 e). The yield of the product was almost 100 %, and the Si/Al and Si/B ratios in the product were found to be 190 and 38, respectively. The product was designated as [Al,B]-SFH-D-200 (190).

The **SFH**-type aluminosilicate was not formed under the same conditions as those for [Al,B]-SFH-D-200 except the absence of the seed crystals, even when the hydrothermal treatment at 180 ºC was prolonged to 14 days, suggesting that the presence of the seeds crystal is indispensable for directly crystallizing the **SFH**-type aluminosilicate zeolite. Hereafter, the crystallization of the **SFH**-type aluminosilicate zeolite was conducted at the $NaOH/SiO_2$ ratio of 0.025 at 180 ºC in the presence of the

seeds (5 wt%).

The effect of the Al content in the gel on the **SFH**-type structure was investigated with the Si/B ratio in the gel kept as 15. Fig. 2 shows the XRD patterns of the as-synthesized products after the hydrothermal treatment at 180 ºC with the Al content in the gel varied. At the Si/Al ratios of 100 and 80, a pure phase of the **SFH**-type zeolite was obtained after the hydrothermal treatment for 8 and 11 days, respectively. The Si/Al ratios in the products were found to be 107 and 91, respectively. The solid state ^{27}Al MAS NMR indicated that all of the Al species are in the framework for [Al,B]-SFH-D-91. However, when the Si/Al in the gel was decreased to 50, several diffraction peaks due to unknown phases were observed at 2θ = 15.3, 16.0, 24.0, 26.1, and 27.4˚ in addition to those due to the **SFH** phase after the hydrothermal treatment for 11 days. At the Si/Al in the gel below 50, the product was amorphous. These results suggest that the high amount of the Al source in the gel retarded the crystallization.

Fig. 3 shows the SEM images of the representative products synthesized. [B]-SFH was composed of needle-like crystallites around 0.5-1 μm in length. A high-silica type sample, [Al,B]-SFH-200 was almost similar to [B]-SFH in morphology. However, the low-silica sample [Al,B]-SFH-80 and [Al,B]-SFH-100 consisted of slightly larger crystals 1-2 μm in length. For [Al,B]-SFH-50, which exhibited the XRD pattern of a mixture of unknown and the **SFH**-phases, irregular-shaped small particles were dominantly observed with needle-like crystallites around 1-2 μm in length. N_2 adsorption-desorption analyses revealed that all the samples had a specific surface area of about 400-450 $m^2 \cdot g^{-1}$ and a micropore volume of about 0.13-0.15 $cm^3 \cdot g^{-1}$. The values are similar to those for SSZ-53 previously reported [4].

In conclusion, an efficient method for directly incorporating Al atoms into the **SFH**-type framework with B atoms has been developed by optimizing the gel compositions and hydrothermal conditions.

2.3.3 Post-synthesis method

As a control, the **SFH**-type aluminosilicate was prepared by a one-pot post-synthesis method [22]; both deboronation and Al insertion were simultaneously achieved by means of treating the calcined [B]-SFH (Si/B = 38) with an aqueous solution containing $Al(NO_3)_3$. The influence of the concentration of $Al(NO_3)_3$ as Al

source in the gel on the Al content was investigated.

Fig. 4 shows the XRD patterns, indicating that the **SFH** structure was retained irrespective of the concentration of $Al(NO_3)_3$. When the concentration was 0.25, 0.5 and 1.0 M, the pH of the treatment solution was 2.7, 2.3 and 1.8, respectively, and the resultant Si/B ratio was found to be 174, 185 and 184, respectively. Thus acidic conditions caused the deboronation from the framework but the deboronation was not significantly enhanced by increasing the concentration of $Al(NO_3)_3$. However, the Al content introduced was varied by changing the concentration of the Al source; when the concentration was 0.25, 0.5 and 1.0 M, the Si/Al ratio was found to be 144, 125 and 50, respectively. ^{27}Al MAS NMR spectra revealed that the Al atoms are mainly incorporated into the framework and that extra-framework Al species are also slightly formed. The morphology and porosity were not changed even after the deboronation followed by the Al insertion using 0.25 M $Al(NO_3)_3$. Thus, the post-treatment of [B]-SFH with $Al(NO_3)_3$ simultaneously led to the deboronation and the Al insertion into the framework with the structure and the morphology intact.

2.3.4 Al distribution

High-resolution ^{27}Al MAS NMR spectra (600 MHz, 14.1 T) of the representative calcined samples are shown in Fig. 5. A main broad peak at 50-65 ppm, which is assigned to tetrahedrally coordinated Al species in the framework, and a small peak at 0 ppm, which is assigned to octahedrally-coordinated Al species, were observed irrespective of the preparation route and the Al content. The intensity of the small peak at 0 ppm increased along with an increase in the Al content. Note that the main broad peak attributed to the framework Al species consists of at least three peaks; the peaks at 61, 57 and 55 ppm are designated as Al^F_A, Al^F_B and Al^F_C, respectively (Fig. 5). The intensity ratio of the three peaks is dependent on the preparation route and/or Al content. The proportions of the peak areas of Al^F_A :Al^F_B :Al^F_C for [Al,B]-SFH-D-200 (190), [Al,B]-SFH-D-100 (107) and [Al,B]-SFH-D-80 (91) was estimated at 40 :28 :32, 32 :50 :18 and 28 :60 :12, respectively. For the products by the direct-synthesis method, the proportions of Al^F_A and Al^F_C as well as the peak at 0 ppm were increased with an increase in the Al content. Note that, for the products by the post-synthesis method, the peak of Al^F_A was clearly dominant irrespective of the Al content; the proportions for [Al,B]-SFH-P-1M, -0.5M and -0.25M were estimated at 73 :22 :5,

71 :25 :4 and , 70 : 24 : 6, respectively.

To further clarify the difference in the Al distribution between the zeolites prepared by the direct- and post-synthesis methods, the ^{27}Al 3Q MQMAS NMR spectra were measured (Fig. 6). The axis F1 in the MQMAS NMR spectra after an appropriate shearing consists of isotropic lines accompanied by second-order quadrupolar shifts for the central transition with their respective anisotropic quadrupolar features on the axis F2 [14].

The spectrum of the directly prepared [Al,B]-SFH-D-100 sample showed five cross-sections indicated by arrows (Fig. 6(a)); it has at least five crystallographically distinct Al sites (a, b, c, d and e) in the **SFH** framework. On the other hand, only three cross-sections (a, b and c) were observed in the spectrum of [Al,B]-SFH-P-1M (Fig. 6(b)). These results suggest that the direct incorporation of Al species into the framework would lead to a more uniform distribution, and that the proportion of Al atom occupying each of the 8 different T-sites (T1~T8) in the **SFH**-type zeolite is dependent on the preparation route.

When Al and B species are directly incorporated, they are distributed with being accompanied by *N*, *N*, *N*-trimethyl-phenylcyclohexylmethylammonium cation (OSDA cation) as well as Na^+ ions because the isomorphic substitution of Si by Al or B in tetrahedral T sites in the framework generates a negative charge. In general, large OSDA cation would occupy well-defined positions within the void of the 14-MR pores, while Na^+ ions are uniformly distributed in the pores. Because the **SFH**-type zeolite consists of the one-dimensional 14-MR pore, the OSDA cation and Na^+ ions are considered to be uniformly distributed in the pore. Hence, the direct-synthesis method led to the formation of at least five crystallographically distinct Al sites.

On the other hand, in the post-synthesis method, Al atoms are incorporated into the T sites originally occupied by B atoms in [B]-SFH. The incorporation of Al atoms into the specific T sites might be caused by the incorporation of B atom into specific T sites and/or the deboronation of B atoms at specific T sites in the framework. The high-resolution ^{11}B MAS NMR spectra (600 MHz, 14.1 T) of the [B]-SFH, [Al,B]-SFH-D-100 and [Al,B]-SFH-P-0.25M samples are representatively shown in Fig. 7 (a). For [B]-SFH, a main peak centered at around -3 ppm, which is assigned to tetrahedrally coordinated B atoms in the framework, was observed in all the spectra and the peaks attributed to extra-framework trigonal B species (10-20 ppm) were not

observed. Note that this main peak consists of at least three peaks; there is a main peak at -2.6 ppm and two shoulder peaks at -3.0 and -3.8 ppm. They are designated as B^F_A, B^F_B and B^F_C, respectively (Fig. 7 (b)), It is suggested that there are at least three crystallographically distinct B sites, and that B atoms are incorporated into specific T sites derived from B^F_A. On the whole, the intensities of the peaks were decreased by the post-treatment, in agreement with the fact that the Si/B ratio was dramatically increased from 38 to 170. The incorporation of Al atoms into the specific T sites would result from the incorporation of B atoms into the specific T sites. The mechanisms of the incorporation of Al and B atoms into the **SFH**-type framework and the attributions of the peaks to the T sites are under investigation.

To date, high-resolution ^{27}Al MAS NMR and ^{27}Al MQMAS NMR techniques have been extensively applied to ZSM-5, MCM-22, USY and Beta to obtain information about the acid property as well as Al distribution in T sites [15-20]. Based on these reports, the chemical shift of ^{27}Al MAS NMR spectrum is shifted to the higher magnetic field as T-O-T angle is increased. Therefore, it is considered that Brønsted acid sites with larger T-O-T angles are formed to a larger extent in the zeolite prepared by the direct-synthesis method than in the zeolite prepared by the post-synthesis method.

2.3.5 Acid properties

The acid amounts of samples were determined by NH_3-TPD, and are listed in Table 1. Fig. 8 shows the NH_3-TPD profiles of the representative samples of the **SFH**-type zeolites prepared and a Beta zeolite as a control. The profiles show two NH_3 desorption peaks. The low temperature peak (100–230 ˚C) corresponds to NH_3 adsorbed on non-acidic -OH groups and NH_4^+, which is formed by the reaction of NH_3 and Bronsted acid sites (BASs), and does not correspond to NH_3 adsorbed on catalytically active BASs or Lewis acid sites (LASs). On the other hand, the high temperature peak, so-called "*h*-peak", (300 - 500 ˚C) corresponds to NH_3 desorption from catalytically active BASs or LASs [10].

The temperature of the *h*-peak for the samples prepared by the direct-synthesis method was slightly lower than that by the post-synthesis method; e.g., the temperatures were estimated as 325 and 340 ºC for [Al,B]-SFH-D-200 (190) and [Al,B]-SFH-P-0.5M (125), respectively. These results imply that the acid strength of

the samples prepared by the direct-synthesis method was slightly lower than that by the post-synthesis method. The temperature of the *h*-peak increase to 350 ºC for [Al,B]-SFH-P-1M (50). However, considering a low Al content and re-adsorption of NH_3 molecules onto acid sites during the measurements, it is considered that the difference in the temperature would not be caused by that of the acid strength.

The amounts of acid sites for the samples estimated by the *h*-peak areas are listed in Table 1. Assuming that all Al species in the solid work as acid sites, the acid amount based on the Al content should be 0.088, 0.166 and 0.208 mmol/g for [Al,B]-SFH-D-200 (190), [Al,B]-SFH-D-100 (107) and [Al,B]-SFH-D-80 (91), respectively (Table 1). The proportion of the Al species that can work as acid sites to the total Al species in the solid is calculated at 77, 72 and 66 %, respectively. As revealed by the ^{27}Al MAS NMR spectra, the proportion of extra-framework Al species was increased along with the Al content. For the samples prepared by the post-synthesis method, the proportion is calculated at 46, 57 and 58% for [Al,B]-SFH-P-0.25M (134), [Al,B]-SFH-P-0.5M (125) and [Al,B]-SFH-P-1M (50), respectively (Table 1). The lower values compared to those for the products prepared by the direct-synthesis method are probably due to the presence of the extra-framework Al species; a part of Al species would not be incorporated into the framework and such Al species might be deposited on the particle surface and would not work as acid sites.

2.3.6 Catalytic performances of the SFH-type aluminosilicate zeolites

Table 2 summarizes the results of the acylation of 2-methoxynaphalene (2-MN) over the **SFH**-type aluminosilicate zeolites. The reaction did not proceed in the absence of catalysts, and [B]-SFH did not exhibit a catalytic activity for this reaction. For this reaction, 1,2-AMN is proved to be a kinetically favored product. When the **SFH**-type aluminosilicate zeolites were used as a catalyst, 1,2-AMN was mainly obtained and other products were hardly detected. Considering that the size of 14-MR pore (0.65×0.85 nm) is larger than the cross section of 1,2-AMN (ca. 0.41×0.81 nm), the reaction would occur inside the 14-MR pores and the kinetically favored product, 1,2-AMN was preferentially formed. When Beta was used as a control catalyst, 2,6-AMN (ca. 0.41×0.62×1.23 nm) was also formed in addition to 1,2-AMN. The formation of 2,6-AMN over the Beta zeolite would be due to the shape-selectivity of the 12-MR pores and 1,2-AMN would be formed on the acid sites located near pore mouth and at the external surface because the pore size of the *BEA-type zeolite (0.56×0.56 nm) is smaller than 1,2-AMN but larger than 2,6-AMN [21].

In order to quantitatively compare of the catalytic performance of the different **SFH**-type aluminosilicates prepared by the direct- and post-synthesis methods, the specific catalytic activity per acid site (i.e., turnover number, TON) on the basis of the acid amount estimated by the *h*-peak areas in the NH_3-TPD profiles has been considered. At similar conversions of 2-MN (ca. 40 %), the TON values for [Al,B]-SFH-D-100 (107), [Al,B]-SFH-D-200 (190) and [Al,B]-SFH-P-1M (50) are calculated at 61, 118 and 40, respectively, clearly indicating that acid sites on the zeolite prepared by the direct-synthesis method effectively worked as the active sites for this reaction compared to those by the post-synthesis method.

The ^{27}Al MAS and ^{27}Al 3Q MQMAS NMR suggest that the zeolite prepared by the direct-synthesis method has the Al species attributed from the peaks of Al^F_B and Al^F_C at a higher magnetic field or the cross-sections “d” and “e” to a larger extent compared to that by the post-synthesis method. These Al species contribute to the generation of the Brønsted acid sites with larger T-O-T angles, which will be more effective active sites for the catalysis regarding large molecules compared to those with small T-O-T angles. Hence, the **SFH**-type zeolite prepared by the direct-synthesis method exhibited a higher catalytic performance in the acylation of 2-MN than that by the post-synthesis method.

2.4 Conclusions

The **SFH**-type aluminosilicate zeolites were successfully synthesized by direct- and post-synthesis methods. The ^{27}Al MAS and ^{27}Al MQMAS NMR reveals that most Al species of the samples are located in the framework but there is a marked difference in the distribution of Al atoms in the framework between direct- and post-synthesis methods; at least five kinds of framework Al species are formed in the zeolites prepared by the direct-synthesis method. [Al,B]-SFH-D exhibited a higher catalytic performance in the acylation compared to [Al,B]-SFH-P. We conclude that the differences in the catalytic performance as well as acid property are due to the difference in the distribution of Al atoms in the framework, and the distribution of Al atoms is strongly dependent on the preparation route. Our findings will contribute to the development of zeolite catalysts with acid sites in the pores controlled, and also accelerate a study on synthesis and catalytic application of extra-large pore zeolite catalysts.

References:

1. M.E. Davis, Chem. Eur. J. 3 (1997) 1745-1750.
2. M.E. Davis, C. Saldarriaga, C. Montes, J. Garces, C. Crowder, Nature, 331 (1988) 698-699.
3. K.J. Balkus, A.G. Gabrielov, US 5489424 (1996).
4. P. Wagner, M. Yoshikawa, M. Lovallo, K. Tsuji, M. Tsapatsis, M.E. Davis, Chem. Commun. (1997) 2179-2180.
5. Y. Kubota, S. Tawada, K. Nakagawa, C. Naitoh, N. Sugimoto, Y. Fukushima, T. Hanaoka, Y. Imada, Y. Sugi, Micropor. Mesopor. Mat. 37 (2000) 291-301.
6. S. Elomari, US 2002/0104780 A1.
7. A. Burton, S. Elomari, C.-Y. Chen, R.C. Medrud, I.Y. Chan, L.M. Bull, C. Kibby, T.V. Harris, S.I. Zones, E.S. Vittoratos, Chem. Eur. J. 9 (2003) 5737-5748.
8. S. Tontisirin, S. Ernst, Angew. Chem. Ind. Ed. 46 (2007) 7304-7306.
9. C. Aydin, J. Lu, A.J. Liang, C. Chen, N.D. Browning, B.C. Gates, Nano Lett. 11 (2011) 5537-5541.
10. M. Niwa, K. Katada, Catal. Surv. Jpn. 1 (1997) 215-226.
11. Z. Gabelica, J.B. Nagy, P. Bodart, G. Debras, Chemistry Letters (1984) 1059-1062.
12. K.F.M.G.J. Scholle, W.S. Veeman, Zeolites 5 (1985) 118-122.
13. J.M. Elzea, I.E. Odom, W.J. Miles, Anal. Chim. Acta 286 (1994) 107-116.
14. O. H. Han, C.-S. Kim, S. B. Hong, Angew. Chem. Int. Ed. 41 (2002) 469-472.
15. A. P. M. Kentgens, D. Iuga, M. Kalwei, H. Koller, J. Am. Chem. Soc. 123 (2001) 2925-2926.
16. P. Sarv, C. Fernandez, J.-P. Amoureux, K. Keskinen, J. Phys. Chem. 100 (1996) 19223-19226.
17. D. Ma, X. Han., S. Xie, X. Bao, H. Hu, S. C. F. Au-Yeung, Chem. Eur. J. 8 (2002) 162-170.
18. A. Zheng, L. Chen, J. Yang, M. Zhang, Y. Su, Y. Yue, C. Ye, F. Deng, J. Phys. Chem. B 109 (2005) 24273-24279.
19. N. Katada, S. Nakata, S. Kato, K. Kanehashi, K. Saito, M. Niwa, J. Mol. Catal. A 236 (2005) 239-245.
20. J. A. van Bokhoven, D. C. Koningsberger, P. Kunkeler, H. van Bekkum, A. P. M. Kentgens, J. Am. Chem. Soc. 122 (2000) 12842-12847.

21 A. Corma, J. Catal. 216 (2003) 298-312.

Table 1

Physicochemical properties of Al containing **SFH**-type zeolites via direct- and post-synthesis routes

a) Si/Al and Si/B: atomic ratio of Si/Al and Si/B in the sample

Sample No	Cat.	Si/Al[a)]	Si/B[a)]	S_{BET}[b)]	V_{micro}[c)]	S_{EXT}[d)]	Acid amount[e)]	Al amount[f)]	Acid amount / Al amount	B amount[g)]
				[m^2/g]	[ml/g]	[m^2/g]	[mmol/g]	[mmol/g]	(%)	[mmol/g]
1	[B]-SFH	--	38	431	0.139	68	--	--	--	0.439
7	[Al,B]-SFH-D-80	91	51	400	0.114	110	0.137	0.208	66	0.327
6	[Al,B]-SFH-D-100	107	61	423	0.125	98	0.119	0.166	72	0.273
5	[Al,B]-SFH-D-200	190	38	451	0.151	58	0.068	0.088	77	0.439
10	[Al,B]-SFH-P-1M	50	174	393	0.124	73	0.192	0.333	58	0.096
11	[Al,B]-SFH-P-0.5M	125	185	431	0.132	85	0.076	0.134	57	0.090
12	[Al,B]-SFH-P-0.25M	134	184	433	0.135	80	0.057	0.124	46	0.90

b) S_{BET}: BET surface area

c) V_{micro}: Micropore volume

d) S_{EXT}: External surface area

e) Acid amount: Estimated by the NH_3-TPD

f) Al amount: Estimated by the ICP

g) B amount: Estimated by the ICP

Table 2

The results of the acylation of 2-methoxynaphalene (2-MN) over the **SFH**-type aluminosilicate zeolites

Sample No	Cat.	Si/Al	Acid amount (mmol/g)	Conversion (%)		Yield (%)			TON
				Acetic anhydride	2-MN	1,2-AMN	2,6-AMN	CH_3COOH	
6	[Al,B]-SFH-D-100	107	0.119	56	42	38	<1	27	65
5	[Al,B]-SFH-D-200	190	0.068	61	49	45	<1	30	135
10	[Al,B]-SFH-P-1M	50	0.192	57	40	38	<1	25	40
-	Beta	150	0.074	41	20	20	3	23	62

Reaction condition: 2-MN, 2 mmol; Acetic anhydride, 1 mmol; *o*-Dichlorobenzene, 2 ml; Catalyst, 50 mg; Temperature, 120ºC. Reaction time, 10 min.

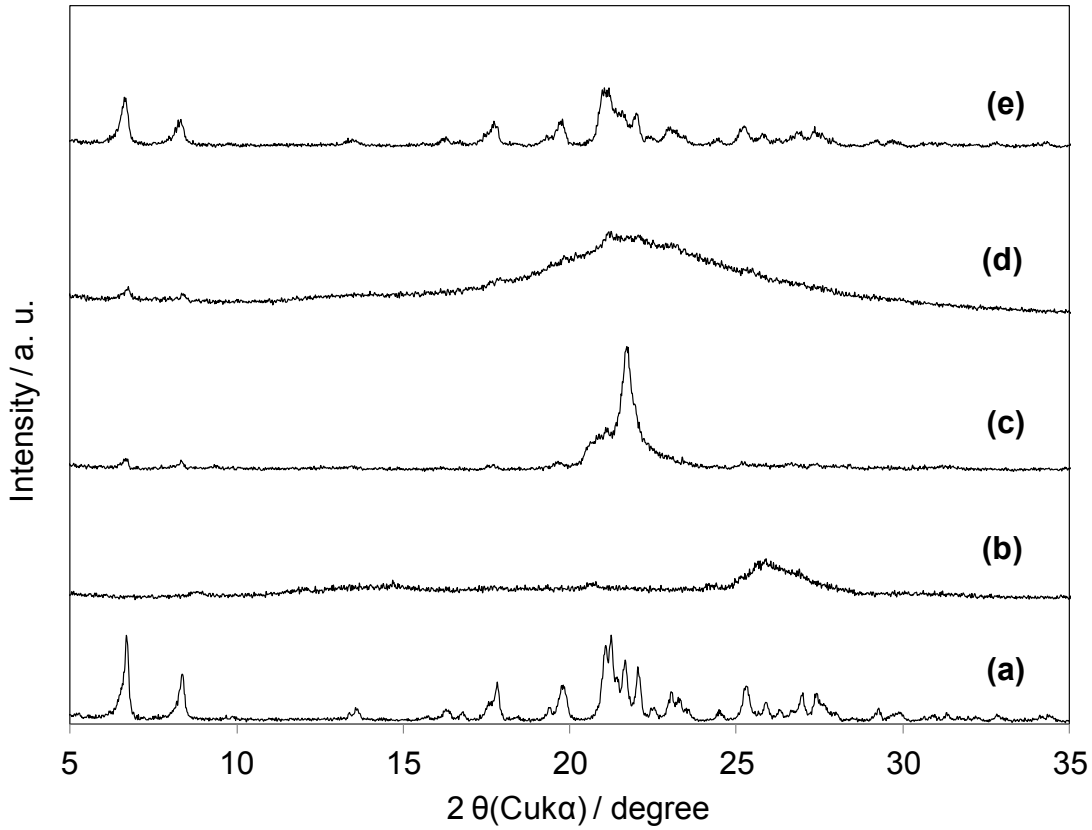

Figure 1

XRD patterns of the synthesized samples under different conditions:

(a) [B]-SFH (Sample 1), (b) Sample 2 (c) Sample 3 (d) Sample 4

(e) [Al,B]-SFH-D-200 (Sample 5).

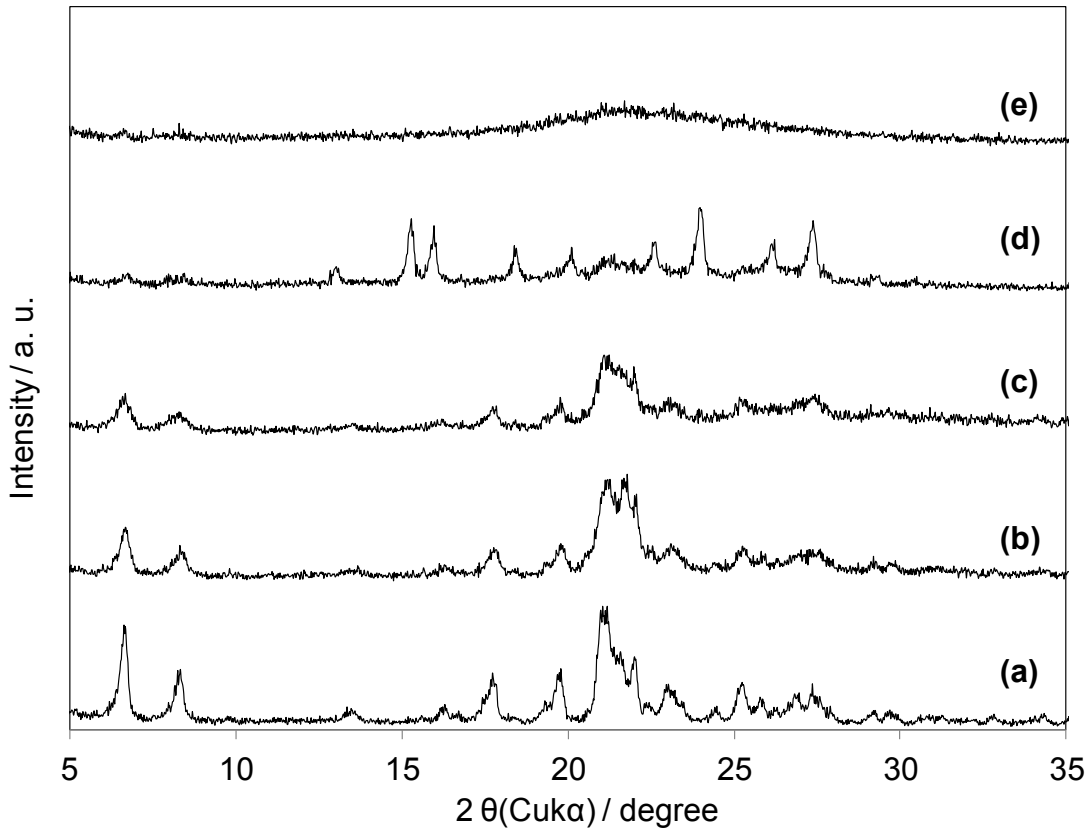

Figure 2

The XRD patterns of the samples synthesized with different Al content: (a) [Al,B]-SFH-D-200 (Sample 5), (b) [Al,B]-SFH-D-100 (Sample 6), (c) [Al,B]-SFH-D-80 (Sample 7), (d) [Al,B]-SFH-D-50 (Sample 8), (e) [Al,B]-SFH-D-25 (Sample 9).

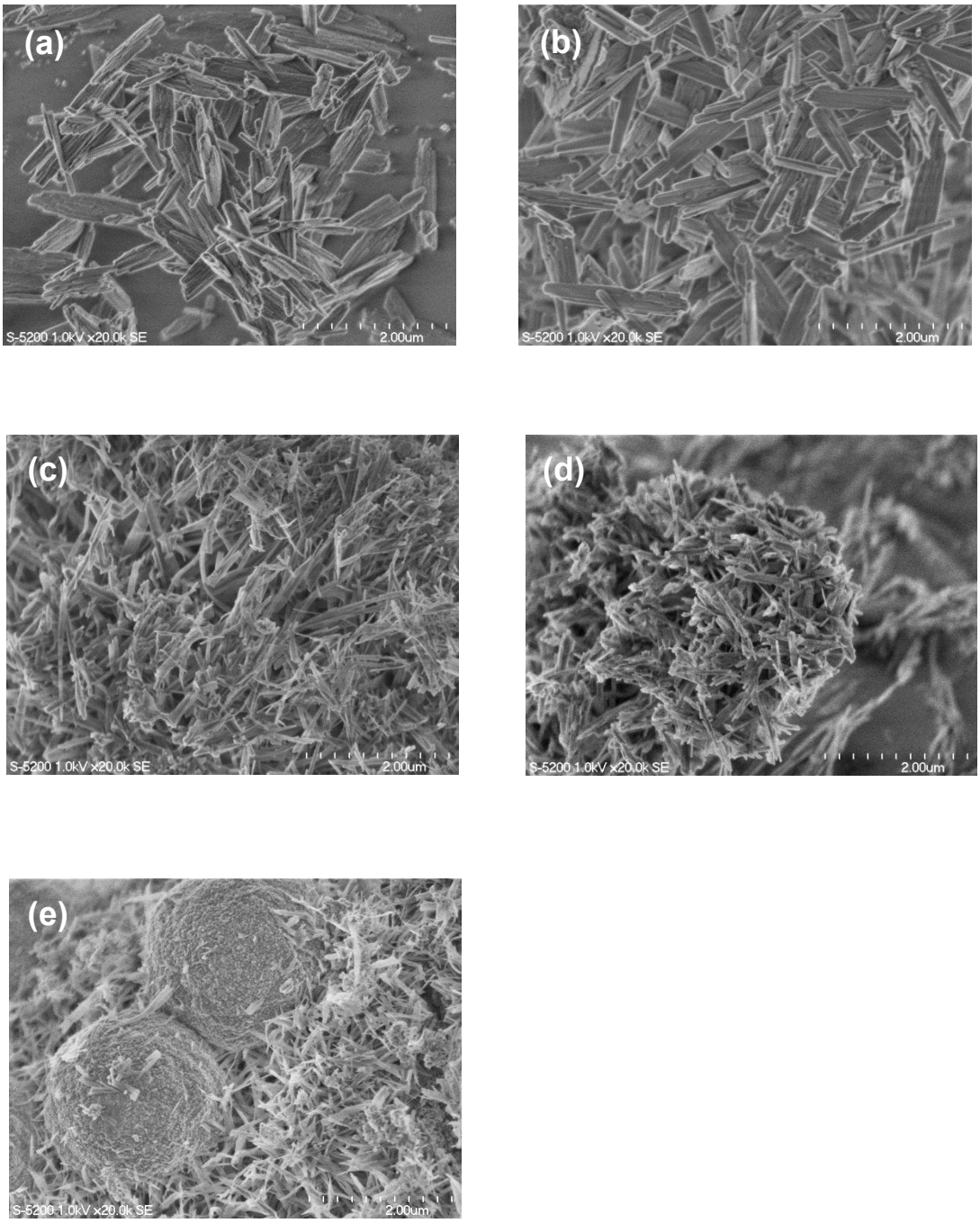

Figure 3

SEM images of the samples after calcinations: (a) [B]-SFH (Sample 1), (b) [Al,B]-SFH-D-200 (Sample 5), (c) [Al,B]-SFH-D-100 (Sample 6), (d) [Al,B]-SFH-D-80 (Sample 7), (e) [Al,B]-SFH-D-50 (Sample8).

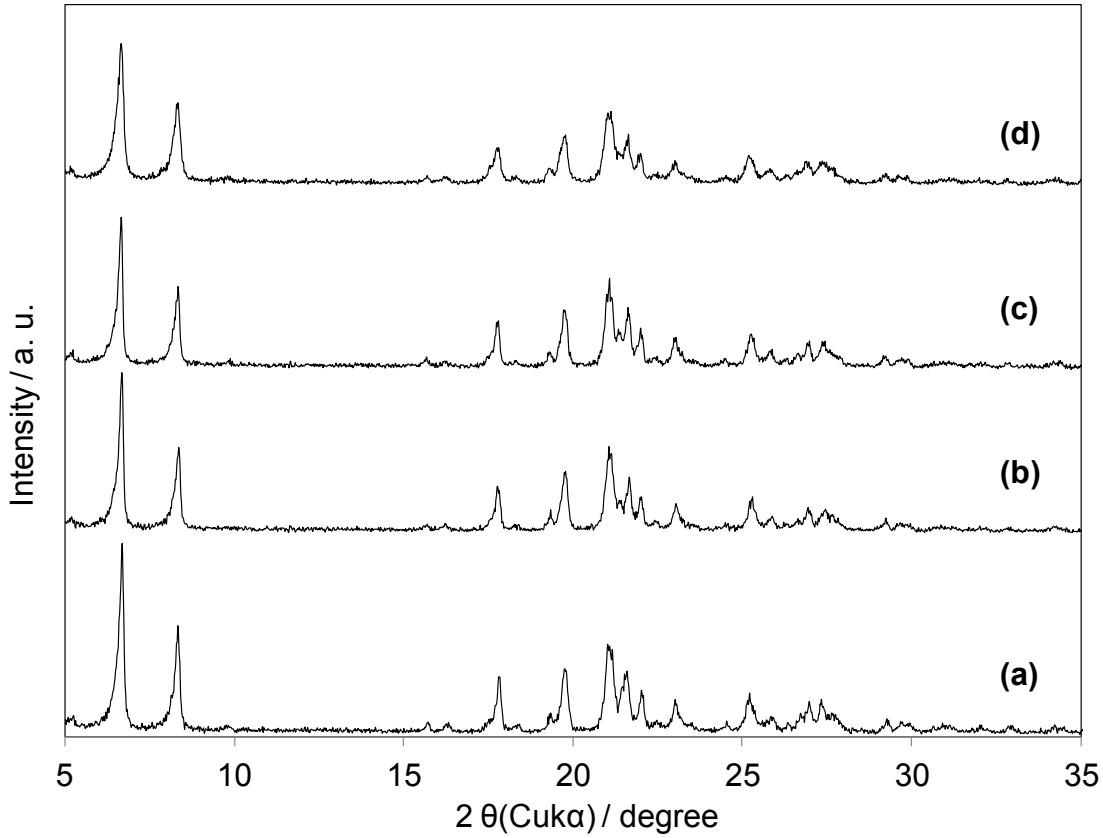

Figure 4

XRD patterns of the samples synthesized under different conditions:

(a) [B]-SFH (Sample 1), (b) [Al,B]-SFH-P-1 M (Sample 10), (c) [Al,B]-SFH-P-0.5 M (Sample 11), (d) [Al,B]-SFH-P-0.25 M (Sample 12).

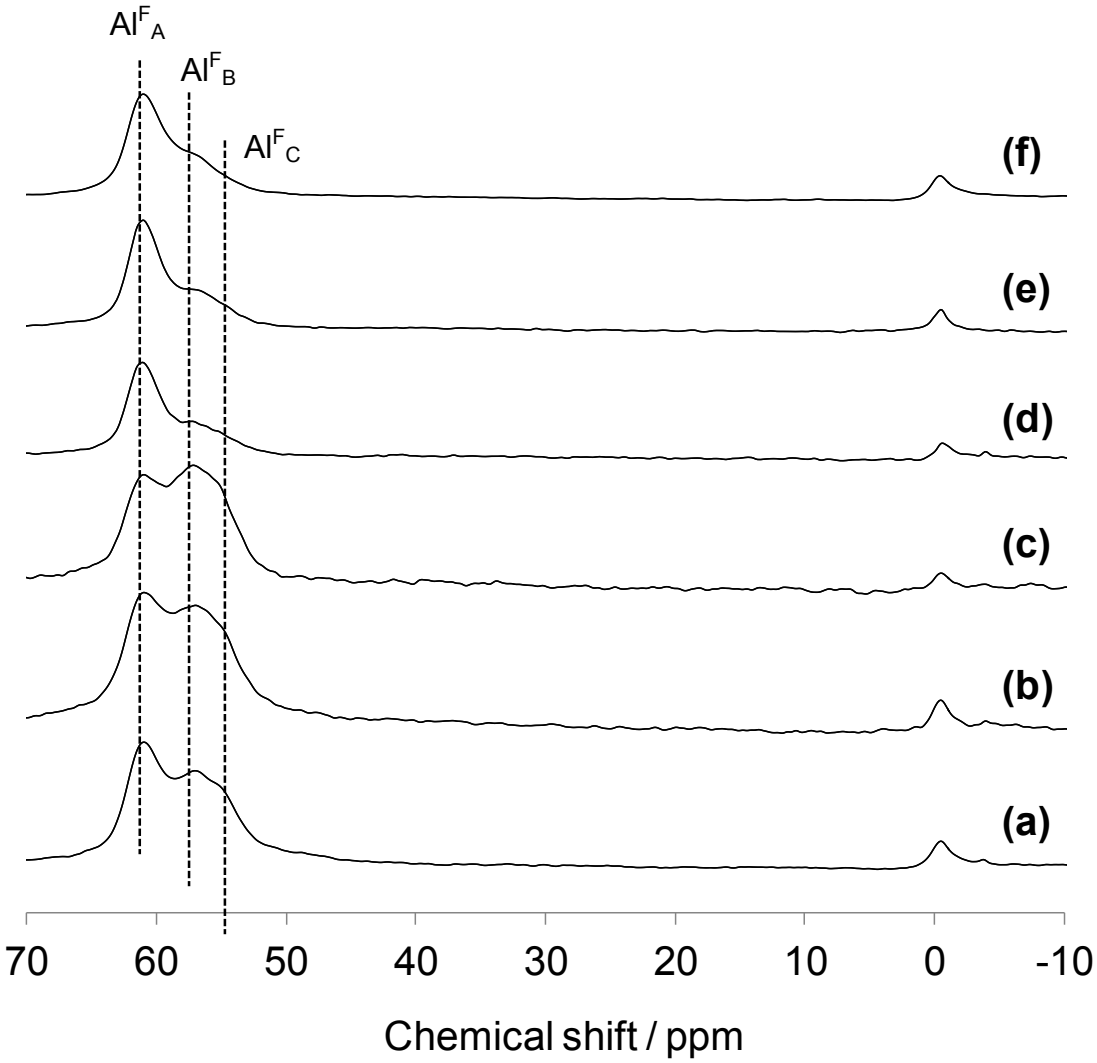

Figure 5

High-resolution ^{27}Al MAS NMR spectra of the representative calcined samples:

(a) [Al,B]-SFH-D-200 (Sample 5), (b) [Al,B]-SFH-D-100 (Sample 6),

(c) [Al,B]-SFH-D-80 (Sample 7), (d) [Al,B]-SFH-P-0.25 M (Sample 12),

(e) [Al,B]-SFH-P-0.5 M (Sample 11), (f) [Al,B]-SFH-P-1 M (Sample 10).

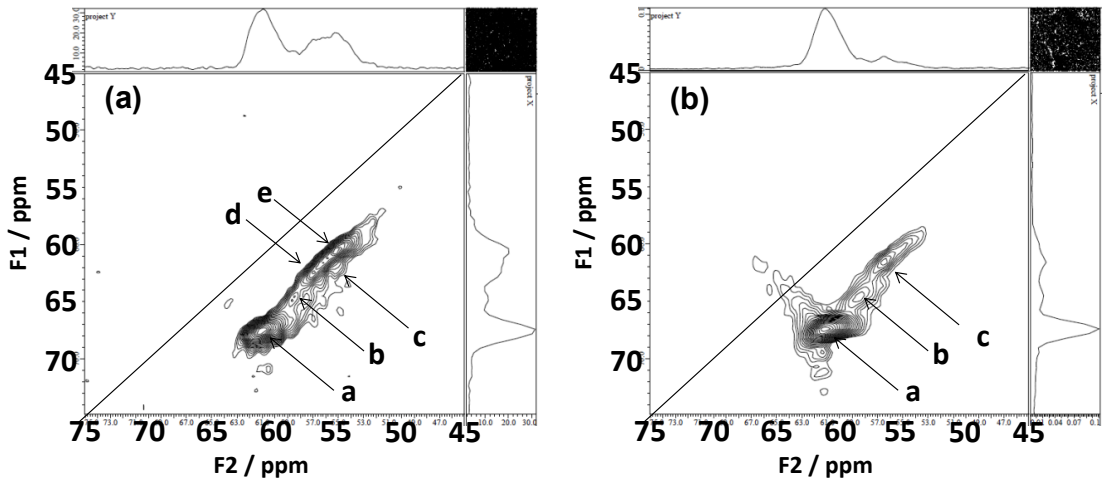

Figure 6

^{27}Al MQ MAS NMR spectra of samples prepared with direct- and post-synthesis method:

(a) [Al,B]-SFH-D-100 (Sample 6), (b) [Al,B]-SFH-P-1M (Sample 10)

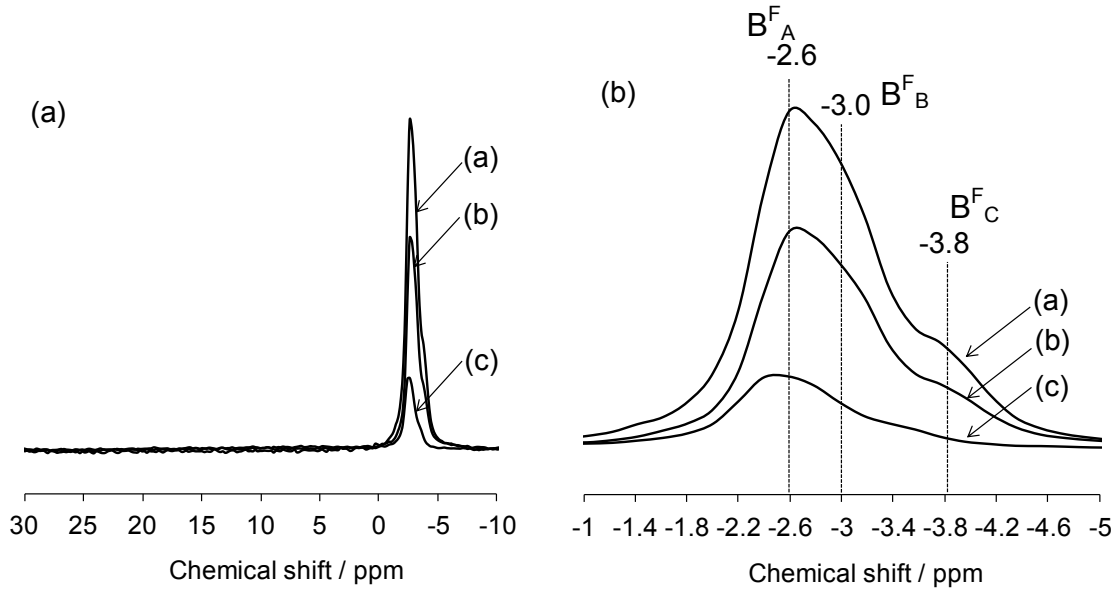

Figure 7

High-resolution ^{11}B MAS NMR spectra of samples prepared with direct- and post-synthesis method: (a) [B]-SFH (Sample 1), (b) [Al,B]-SFH-D-200 (Sample 5), (c) [Al,B]-SFH-P-0.25M (Sample 10).

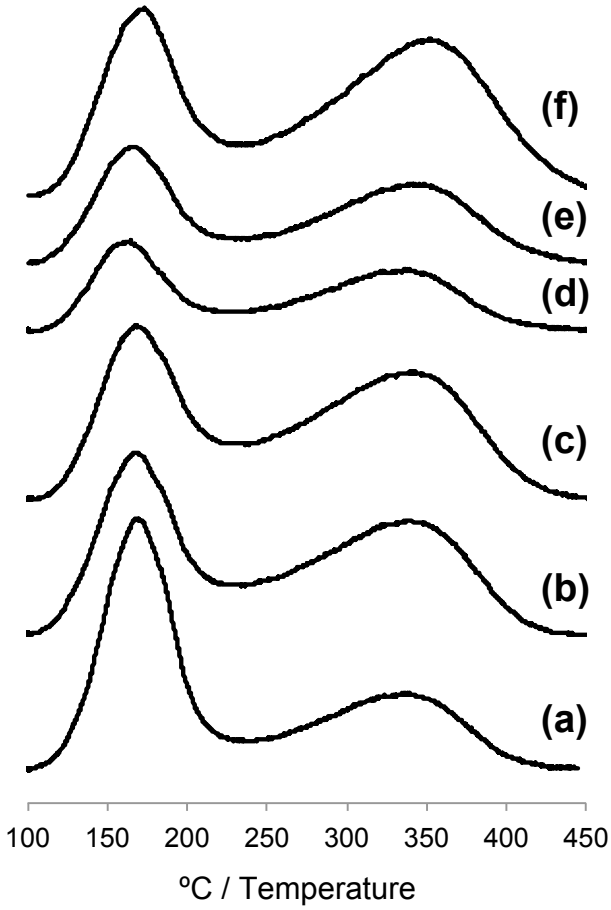

Figure 8

NH_3-TPD profiles of the samples prepared with direct- and post-synthesis method:

(a) [Al,B]-SFH-D-200 (Sample 5), (b) [Al,B]-SFH-D-100 (Sample 6),

(c) [Al,B]-SFH-D-80 (Sample 7), (d) [Al,B]-SFH-P-0.25 M (sample 12),

(e) [Al,B]-SFH-P-0.5 M (sample 11), (f) [Al,B]-SFH-P-1 M (sample 10).

Chapter 3

Synthesis, characterization and catalytic properties of SFN-type zeolites

Abstract

According to the synthesis results of **SFH**-type zeolite in chapter 2, the direct-synthesis method for preparing the **SFN**-type aluminosilicate zeolites, designated as [Al,B]-SFN-D, was successfully improved by increasing the SDA/SiO_2 ratio to 0.3 and adding 10 wt% seeds. However, high Al content containing **SFN**-type zeolite could not be synthesized by direct-synthesis method like **SFN**-type zeolite. As a control, by the same post-synthesis method with **SFH**-type zeolite, the **SFN**-type aluminosilicate zeolites, designated as [Al,B]-SFN-P, were prepared. Thus prepared **SFN**-type aluminosilicate zeolites were characterized in details. The high-resolution ^{27}Al MAS NMR results implied that there are marked differences in the distribution of Al atoms in the framework between the zeolites obtained by the direct- and post-synthesis methods similar to the results of **SFH**-type zeolites. [Al,B]-SFN-D exhibited a higher catalytic performance in the acylation of 2-methoxynaphthalene with acetic anhydride than [Al,B]-SFN-P.

3.1 Introduction

As mentioned in chapter 1, **SFN**-type zeolite is also one of extre-large-pore zeolites and was discovered in Chevron laboratories. This zeolite consists of one-dimensional 14MR pores (0.62×0.85 nm) has been synthesized with *N*-methyl-*N*-[(1-phenylcyclopentyl)methyl]piperidinium hydroxide as organic-structure-directing agent (OSDA).

SFN-type zeolite is expected to be efficient for a wide range of applications in catalysis for its high hydrothermal stability. **SFN**-type zeolite was originally synthesized as borosilicate in 2002 [1]. Burton *et al.* reported on the synthesis of aluminosilicate ones by the direct-and post-synthesis methods in 2003 [2]. However, **SFN**-type aluminosilicate also have the same problems with **SFH**-type zeolite. Few reports about the preparation and catalytic performance were made even though its unique structural and catalytic properties have received considerable attention.

In this study, we report the synthesis of the **SFN**-type aluminosilicate zeolites by the direct- and post-synthesis methods, and the differences in the structural and acid properties between the products obtained by the two methods like **SFH**-type zeolite in chapter 2. The influences of the synthesis conditions on the crystallization behavior, composition and physicochemical properties of the product were also investigated in detail. We obtained similar high-resolution ^{27}Al MAS NMR results of **SFN**-type zeolites to that of **SFH**-type zeolites. The conditions of tetrahedral Al species are marked different between the products synthesized by the two methods. In the acylation of 2-methoxynaphthalene with acetic anhydride, the catalysis synthesized by direct-synthesis method showed higher TON than that synthesized by post-synthesis method.

3.2 Experimental

3.2.1 Synthesis of SFN-type zeolites

3.2.1.1 Synthesis of SFN-type zeolites by direct-synthesis method

The synthesis condition of **SFN**-type zeolite was similar to that of **SFH**-type zeolite. *N*-methyl-*N*-[(1-phenylcyclopentyl)methyl]piperidinium hydroxide was utilized as OSDA for the synthesis of **SFN**-type zeolite. CAB-O-SIL M5 was used as silica source. Other chemicals used in this synthesis were the same with **SFH**-type zeolite.

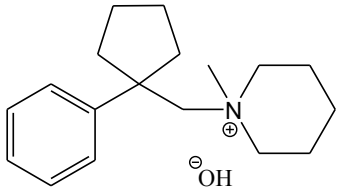

N-methyl-*N*-[(1-phenylcyclopentyl)methyl]piperidinium hydroxide

The **SFN**-type borosilicate, designated as [B]-SFN, was hydrothermally synthesized at 160 ºC for 8 days . The molar composition of the mother gel was SiO_2: OSDA: Na_2O: B_2O_3: H_2O = 1: 0.25: 0.05: 0.022: 41. The atomic ratios of Si/B in the gel and the solid product were 23 and 46, respectively.

In the case of direct-synthesis method for Al and B containing **SFN**-type zeolite, $Al(NO_3)_3 \cdot 9H_2O$ was used as Al source. The molar composition of the mother gel was SiO_2: OSDA: Na_2O: Al_2O_3: B_2O_3: H_2O = 1: 0.3: 0.0125: *x*: 0.022: 41 (*x* = 0.01, 0.005, or 0.0025). 10 wt% of the calcined [B]-SFN (Si/B = 46) as seeds was added into the mother gel. Thus prepared gels were hydrothermally treated at 180 ºC for 8 days.

3.2.1.2 Synthesis of SFN-type zeolites by post-synthesis method

The **SFN**-type aluminosilicate was prepared by the post-synthesis method as follows [3]. The calcined [B]-SFN was treated in the aqueous solution containing aluminium nitrate for 12 h at 95 ºC. After the treatment, the resulting solid was washed with 0.1 N hydrochloric acid. The concentration of $Al(NO_3)_3$ was varied from 0.25 to 1.0 M in order to change the Al content incorporated. After drying at 100 ºC for 12 h and a final calcination at 550ºC, an H-type form of the aluminosilicate zeolites were obtained. Thus obtained product was designated as [Al,B]-SFN-P-*m* (*n*), where *m* and *n* are the concentration of $Al(NO_3)_3$ solution and the Si/Al atomic ratio in product, respectively.

3.2.2 Characterizations

The prepared zeolites were characterized by XRD, ICP, SEM, N_2 adsorption, high resolution ^{27}Al MAS NMR and NH_3-TPD. XRD patterns were collected on a Rint-Ultima III (Rigaku) using a Cu Kα X-ray source (40 kV, 20 mA). Nitrogen adsorption measurements to determine the BET surface area (S_{BET}), S_{EXT}, and micropore volume (V_{micro}) were conducted at 77 K on a Belsorp-mini II (Bel Japan). Field-emission scanning electron microscopic (FE-SEM) images of the powder samples were obtained on an S-5200 microscope (Hitachi) operating at 1-30 kV. The sample was mounted on a carbon-coated microgrid (Okenshoji Co.) without any metal coating. The Si/Al ratios of the samples were determined by using an inductively coupled plasma-atomic emission spectrometer (ICP-AES, Shimadzu ICPE-9000).

To investigate the Al environment, solid-state ^{27}Al magic-angle spinning (MAS) NMR spectra were obtained on a JEOL ECA-600 spectrometer (14.1 T). The relaxation delay time was 10 ms. The ^{27}Al chemical shift was referenced to $AlNH_4(SO_4)_2 \cdot 12H_2O$ at -0.54 ppm and samples were spun at 17 kHz by using a 4 mm ZrO_2 rotor.

Temperature-programmed NH_3 desorption (NH_3-TPD) profiles were recorded on a BELCAT (Japan BEL). Typically, 30 mg catalyst was pretreated at 773 K in He (50 mL min^{-1}) for 1 h and then cooled to 423 K. Prior to the adsorption of NH_3, the sample was evacuated at 423 K for 1 h. Approximately 2500 Pa of NH_3 was allowed to make contact with the sample at 423 K for 10 min. Subsequently, the sample was evacuated to remove weakly adsorbed NH_3 at the same temperature for 30 min. Finally, the sample was cooled to 423 K and heated from 423 to 873 K at a ramping rate of 10 K min^{-1} in a He flow (50 mL min^{-1}). A quadrupole mass spectrometer was used to monitor desorbed NH_3 (m/e = 16). The amount of acid sites was determined by using the area of the so-called "*h*-peak" in the profiles [4].

3.2.3 Catalytic reaction

To evaluate the catalytic performance of the **SFN**-type aluminosilicate prepared, Friedel-Crafts acylation of 2-methoxynaphthalene (2-MN) with acetic anhydride was conducted in the liquid-phase under batch conditions. Before the reaction, the catalyst was pretreated at 400ºC for 1 h under vacuum conditions in a glass reactor. Under argon atmosphere, 2 mmol of 2-MN, 1 mmol of acetic anhydride and 2 ml of *o*-dichlorobenzene as solvent were put into the glass reactor. The reaction temperature and time were set at 100 ºC and 30 min, respectively. The reactant and products were analyzed by a gas chromatograph (Shimadzu, GC-2014) equipped with an FID detector with a DB-5 column.

3.3 Results and discussion

3.3.1 Direct-synthesis method

First, [B]-SFN was directly synthesized in the presence of the OSDA by the conventional method under the hydrothermal conditions at 160ºC for 8 days. It showed the typical XRD pattern attributed to the **SFN** structure (Fig. 1 a) [2]. By the ICP analyses, the Si/B ratio of [B]-SFN was found to be 46. In this study, thus prepared calcined [B]-SFN was used as seeds in preparing Al-containing **SFN**-type zeolite via a direct-synthesis route.

3.3.2 Modification of synthesis conditions of SFN-type zeolite

Attempts to directly synthesize [Al,B]-SFN by adding the Al source into the mother gel of [B]-SFN with the Si/Al ratio of 200 were unsuccessful after hydrothermal treatment 180 ºC for 5 days (Fig. 2 a); the peaks attributed to the **SFN**-type zeolite were slightly observed at 2θ = 6.1, 7.2 and 8.3˚. Pure phase of **SFN**-type zeolite was not obtained even prolonging the crystallization time to 11 days (Fig. 2 c).

By increasing the seed amount from 5 wt% to 10 wt%, the **SFN**-type zeolite was successfully formed after the hydrothermal treatment for 8 days (Fig. 3 a). However, a slight peak at 2θ = 22.0˚ attributed to the cristobalite was observed. Finally, by increasing the OSDA/SiO_2 ratio to 0.3, the **SFN**-type zeolite was successfully synthesized after the hydrothermal treatment for 8 days (Fig. 3 b).

The yield of the product was about 80 %, and the Si/Al and Si/B ratios in the product were found to be 162 and 107, respectively. The product was designated as [Al,B]-SFN-D-200 (162).

The effect of the Al content in the gel on the **SFH**-type structure was investigated with the Si/B ratio in the gel kept as 23. Fig. 4 shows the XRD patterns of the as-synthesized products after the hydrothermal treatment at 180 ºC with the Al content in the gel varied. The Si/Al ratios were 50 and 100. Pure phase of the **SFN**-type zeolite was not obtained after the hydrothermal treatment for 8 days. Amorphous phase remained in the product. **SFN**-type zeolite could not crystallize at high amount of the Al source in the gel.

In conclusion, an efficient method for directly incorporating Al atoms into the **SFN**-type framework with B atoms has been developed by optimizing the gel compositions and seeds amount.

3.3.3 Post-synthesis method

As a control, the **SFN**-type aluminosilicate was prepared by a one-pot post-synthesis method [3]; both deboronation and Al insertion were simultaneously achieved by means of treating the calcined [B]-SFN (Si/B = 46) with an aqueous solution containing $Al(NO_3)_3$. The influence of the concentration of $Al(NO_3)_3$ as Al source in the gel on the Al content was investigated.

Fig. 5 shows the XRD patterns, indicating that the SFN structure was retained irrespective of the concentration of $Al(NO_3)_3$. When the concentration was 0.25 and 1.0 M, the pH of the treatment solution was 2.7 and 1.8, respectively, and the resultant Si/B ratio was found to be 172, 240, respectively. The Al content introduced was varied by changing the concentration of the Al source; when the concentration was 0.25 and 1.0 M, the Si/Al ratio was found to be 73 and 175, respectively. ^{27}Al MAS NMR spectra revealed that the Al atoms are mainly incorporated into the framework and that extra-framework Al species are also slightly formed.

Fig. 6 shows the SEM images of the representative products synthesized. [B]-SFN was composed of needle-like crystallites around 0.5-1 μm in length (Fig. 6 a). There was no significant change after the introduction of Al by post treatment (Fig. 6 b). A high-silica type sample synthesized by directing method, [Al,B]-SFN-D-200, was smaller than those of [B]-SFN in morphology (Fig. 6 c). N_2 adsorption-desorption analyses revealed that the BET surface and micropore volume increased when the sample was synthesized by direct synthesis method. No significant change in N_2 adsorption-desorption was observed when the sample was treated by post synthesis method.

The morphology and porosity were not changed even after the deboronation followed by the Al insertion. Thus, the post-treatment of [B]-SFN with $Al(NO_3)_3$ simultaneously led to the deboronation and the Al insertion into the framework with the structure and the morphology intact.

3.3.4 Al distribution

High-resolution ^{27}Al MAS NMR spectra (600 MHz, 14.1 T) of the representative calcined samples are shown in Fig. 7. A main broad peak at 50-65 ppm, which is assigned to tetrahedrally coordinated Al species in the framework, and a small peak at 0 ppm, which is assigned to octahedrally-coordinated Al species. Note that the main broad peak attributed to the framework Al species consists of at least three peaks; the peaks at 61, 57 and 55 ppm are designated as Al^F_A, Al^F_B and Al^F_C, respectively (Fig. 7). The proportions of the peak areas of Al^F_A :Al^F_B :Al^F_C for [Al,B]-SFN-D-200 (162), was estimated at 43 :31 :26. Note that, for the products by the post-synthesis method, the peak of Al^F_A was clearly dominant irrespective of the Al content; the proportions for [Al,B]-SFN-P-1M, and -0.25M were estimated at 70 :27 :3 and , 73 : 25 : 2, respectively.

To date, high-resolution ^{27}Al MAS NMR techniques have been extensively applied to ZSM-5, MCM-22, USY and Beta to obtain information about the acid property as well as Al distribution in T sites [5-10]. According to the results and discussion of Al distribution in chapter 2, it is considered that Brønsted acid sites with larger T-O-T angles are formed to a larger extent in the zeolite prepared by the direct-synthesis method than in the zeolite prepared by the post-synthesis method.

3.3.5 Acid properties

The acid amounts of samples were determined by NH_3-TPD, and are listed in Table 1. Fig. 8 shows the NH_3-TPD profiles of the representative samples of the **SFN**-type zeolites prepared. The profiles show two NH_3 desorption peaks. The low temperature peak (100–230 ˚C) corresponds to NH_3 adsorbed on non-acidic -OH groups and NH_4^+, which is formed by the reaction of NH_3 and Bronsted acid sites (BASs), and does not correspond to NH_3 adsorbed on catalytically active BASs or Lewis acid sites (LASs). On the other hand, the high temperature peak, so-called "*h*-peak", (300 - 500 ˚C) corresponds to NH_3 desorption from catalytically active BASs or LASs [10].

The temperature of the *h*-peak for the samples prepared by the direct-synthesis method was slightly lower than that by the post-synthesis method; e.g., the temperatures were estimated as 328 and 344 ºC for [Al,B]-SFN-D-200 (162) and [Al,B]-SFN-P-0.25M (175), respectively. These results imply that the acid strength of the samples prepared by the direct-synthesis method was slightly lower than that by the

post-synthesis method. The temperature of the *h*-peak increase to 350 ºC for [Al,B]-SFN-P-1M (73). However, considering a high Al content and re-adsorption of NH_3 molecules onto acid sites during the measurements, it is considered that the difference in the temperature would not be caused by that of the acid strength.

The amounts of acid sites for the samples estimated by the *h*-peak areas are listed in Table 1. Assuming that all Al species in the solid work as acid sites, the acid amount based on the Al content should be 0.103, 0.228 and 0.095 mmol/g for [Al,B]-SFH-D-200 (162), [Al,B]-SFN-P-0.25M (175) and [Al,B]-SFN-P-1M (73), respectively (Table 1). The proportion of the Al species that can work as acid sites to the total Al species in the solid is calculated at 61 % for [Al,B]-SFN-D-200. For the samples prepared by the post-synthesis method, the proportion is calculated at 76 and 68% for [Al,B]-SFH-P-0.25M (175), [Al,B]-SFN-P-1M (73), respectively (Table 1). In the case of **SFH**-type zeolite, the values of the products prepared by the post-synthesis method are lower compared to those for the products prepared by the direct-synthesis method. The **SFN**-type zeolites showed different results from **SFH**-type zeolites.

3.3.6 Catalytic performances of the SFN-type aluminosilicate zeolites

Table 2 summarizes the results of the acylation of 2-methoxynaphalene (2-MN) over the **SFN**-type aluminosilicate zeolites. For this reaction, 1,2-AMN is proved to be a kinetically favored product. When the **SFN**-type aluminosilicate zeolites were used as a catalyst, 1,2-AMN was mainly obtained and other products were hardly detected. Considering that the size of 14-MR pore (0.62×0.85 nm) is larger than the cross section of 1,2-AMN (ca. 0.41×0.81 nm), the reaction would occur inside the 14-MR pores and the kinetically favored product, 1,2-AMN was preferentially formed. When Beta was used as a control catalyst, 2,6-AMN (ca. 0.41×0.62×1.23 nm) was also formed in addition to 1,2-AMN.

In order to quantitatively compare of the catalytic performance of the different **SFN**-type aluminosilicates prepared by the direct- and post-synthesis methods, the specific catalytic activity per acid site (i.e., turnover number, TON) on the basis of the acid amount estimated by the *h*-peak areas in the NH_3-TPD profiles has been considered. With the same weight amount of catalysts, [Al,B]-SFN-P-1M (75) showed higher conversion of 2-MN than [Al,B]-SFN-D-200 (162). However, the TON values for [Al,B]-SFN-D-200 (162) and [Al,B]-SFN-P-1M (75) are calculated at 89 and 49, respectively, clearly indicating that acid sites on the zeolite prepared by the direct-synthesis method effectively worked as the active sites for this reaction compared to those by the post-synthesis method.

The ^{27}Al MAS NMR suggest that the zeolite prepared by the direct-synthesis method has the Al species attributed from the peaks of Al^F_B and Al^F_C at a higher magnetic field to a larger extent compared to that by the post-synthesis method similar to the results of **SFH**-type zeolites. These Al species contribute to the generation of the Brønsted acid sites with larger T-O-T angles, which will be more effective active sites for the catalysis regarding large molecules compared to those with small T-O-T angles. Hence, the **SFN**-type zeolite prepared by the direct-synthesis method exhibited a higher catalytic performance in the acylation of 2-MN than that by the post-synthesis method.

3.4 Conclusions

The **SFN**-type aluminosilicate zeolites were successfully synthesized by direct- and post-synthesis methods. The ^{27}Al MAS NMR reveals that most Al species of the samples are located in the framework but there is a marked difference in the distribution of Al atoms in the framework between direct- and post-synthesis methods. [Al,B]-SFN-D exhibited a higher catalytic performance in the acylation compared to [Al,B]-SFN-P. I conclude that the differences in the catalytic performance as well as acid property are due to the difference in the distribution of Al atoms in the framework, and the distribution of Al atoms is strongly dependent on the preparation route.

References:

1. S. Elomari, US 2002/0104780 A1.
2. A. Burton, S. Elomari, C.-Y. Chen, R.C. Medrud, I.Y. Chan, L.M. Bull, C. Kibby, T.V. Harris, S.I. Zones, E.S. Vittoratos, *Chem. Eur. J.* 9 (2003) 5737-5748.
3. S. Tontisirin, S. Ernst, *Angew. Chem. Ind. Ed.* 46 (2007) 7304-7306.
4. M. Niwa, K. Katada, *Catal. Surv. Jpn.* 1 (1997) 215-226.
5. A. P. M. Kentgens, D. Iuga, M. Kalwei, H. Koller, *J. Am. Chem. Soc.* 123 (2001) 2925-2926.
6. P. Sarv, C. Fernandez, J.-P. Amoureux, K. Keskinen, *J. Phys. Chem.* 100 (1996) 19223-19226.
7. D. Ma, X. Han., S. Xie, X. Bao, H. Hu, S. C. F. Au-Yeung, *Chem. Eur. J.* 8 (2002) 162-170.
8. A. Zheng, L. Chen, J. Yang, M. Zhang, Y. Su, Y. Yue, C. Ye, F. Deng, *J. Phys. Chem. B* 109 (2005) 24273-24279.
9. N. Katada, S. Nakata, S. Kato, K. Kanehashi, K. Saito, M. Niwa, *J. Mol. Catal. A* 236 (2005) 239-245.
10. J. A. van Bokhoven, D. C. Koningsberger, P. Kunkeler, H. van Bekkum, A. P. M. Kentgens, *J. Am. Chem. Soc.* 122 (2000) 12842-12847.

Table 1

Physicochemical properties of Al containing **SFN**-type zeolites via direct- and post-synthesis routes

Cat.	Si/Al[a)]	Si/B[a)]	S_{BET}[b)]	V_{micro}[c)]	S_{EXT}[d)]	Acid amount[e)]	Al amount[f)]	Acid amount / Al amount	B amount[g)]
			[m²/g]	[ml/g]	[m²/g]	[mmol/g]	[mmol/g]	(%)	[mmol/g]
[B]-SFN	--	46	436	0.140	73	--	--	--	0.362
[Al,B]-SFN-D-200	162	107	543	0.159	139	0.063	0.103	61	0.156
[Al,B]-SFN-P-1M	73	240	460	0.144	86	0.154	0.228	68	0.069
[Al,B]-SFN-P-0.25M	175	172	427	0.130	73	0.072	0.095	76	0.097

a) Si/Al and Si/B: atomic ratio of Si/Al and Si/B in the sample

b) S_{BET}: BET surface area

c) V_{micro}: Micropore volume

d) S_{EXT}: External surface area

e) Acid amount: Estimated by the NH_3-TPD

f) Al amount: Estimated by the ICP

g) B amount: Estimated by the ICP

Table 2

The results of the acylation of 2-methoxynaphalene (2-MN) over the **SFN**-type aluminosilicate zeolites

Cat.	Si/Al	Acid amount (mmol/g)	Catalyst weight (mg)	Conversion (%)		Yield (%)			TON
				Acetic anhydride	2-MN	1,2-AMN	2,6-AMN	CH_3COOH	
[Al,B]-SFN-D-200	162	0.063	50	50	33	28	0	20	89
[Al,B]-SFN-P-1M	73	0.154	50	51	43	38	<1	21	49
[Al,B]-SFN-P-1M	73	0.154	22	37	34	25	0	18	73

Reaction condition: 2-MN, 2 mmol; Acetic anhydride, 1 mmol; *o*-Dichlorobenzene, 2 ml; Temperature, 100ºC. Reaction time, 30 min.

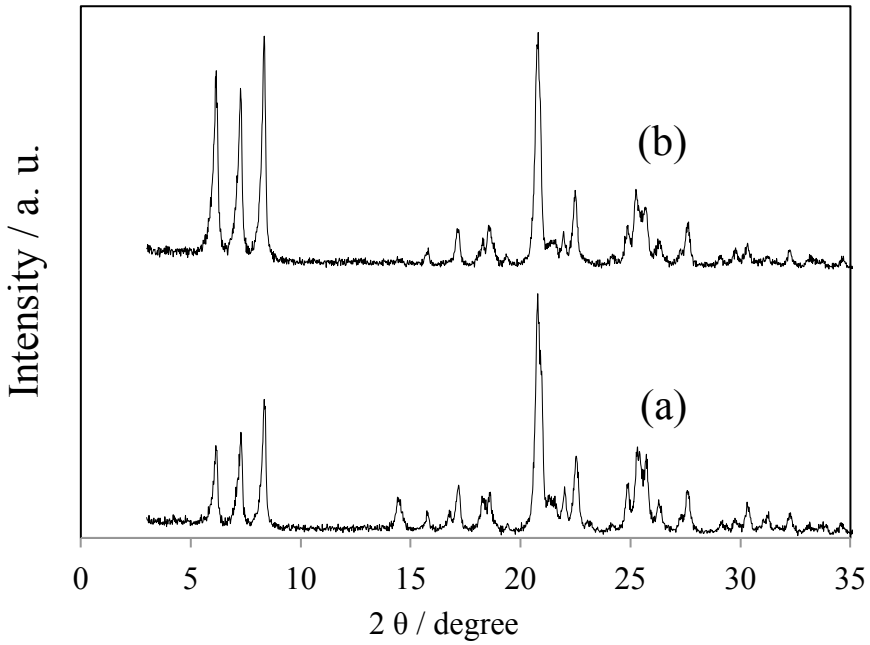

Figure 1

XRD patterns of [B]-SFN

(a) As-made, (b) After calcination

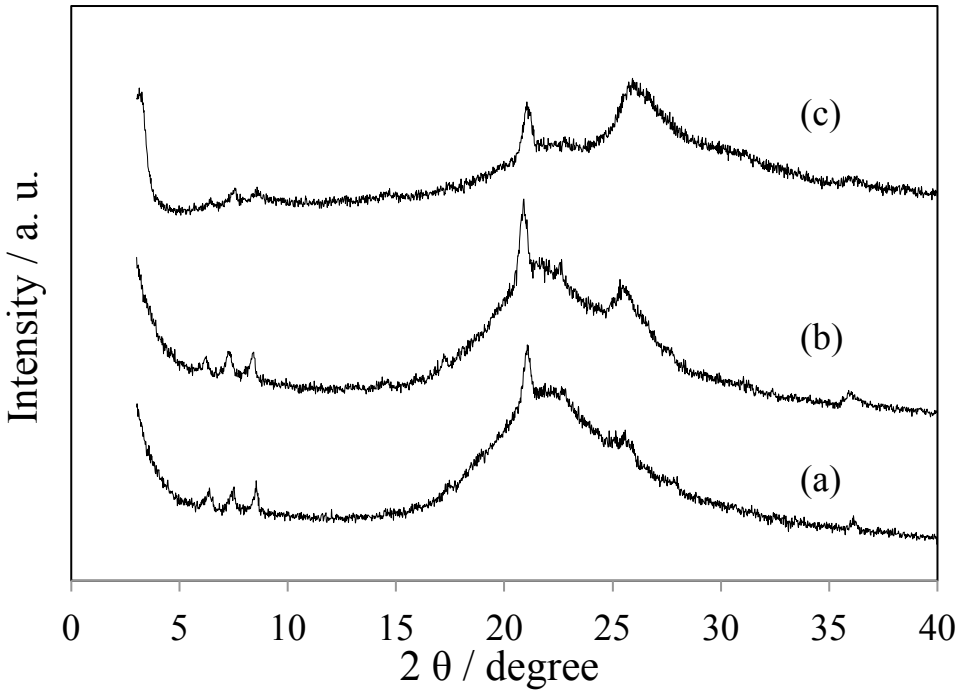

Figure 2

The XRD patterns of the [Al,B]-SFN-D synthesized under different crystallization time: (a) 5 days, (b) 8 days, (c) 11 days.

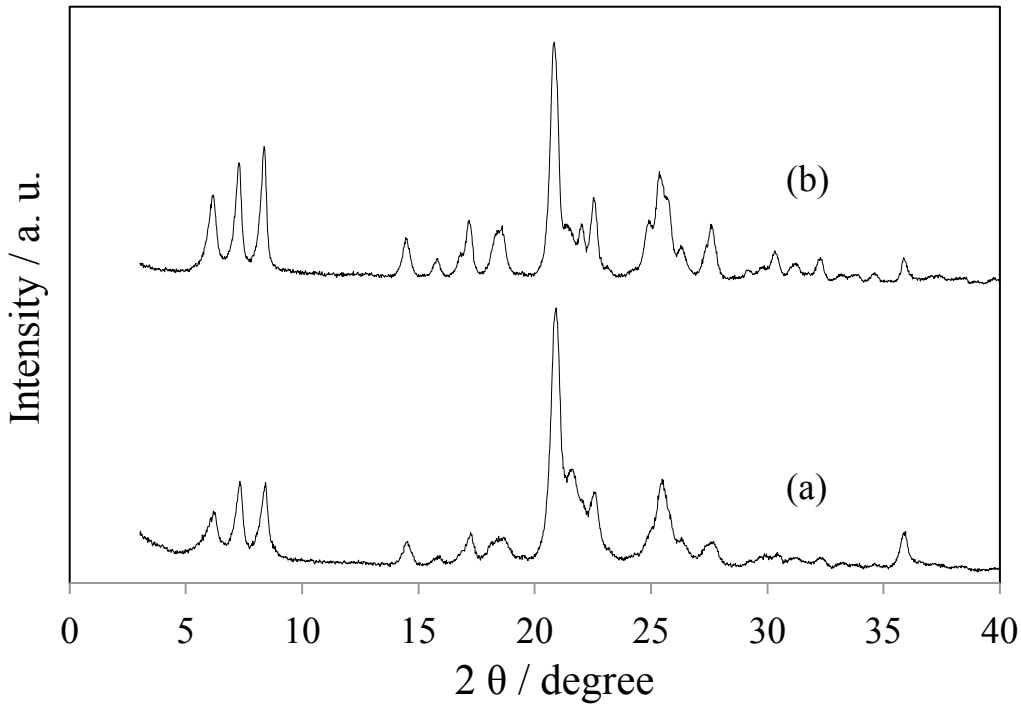

Figure 3

The XRD patterns of the [Al,B]-SFN-D synthesized under different crystallization conditions: (a) $SDA/SiO_2 = 0.25$, seed 10 wt%, (b) $SDA/SiO_2 = 0.3$, seed 10 wt%.

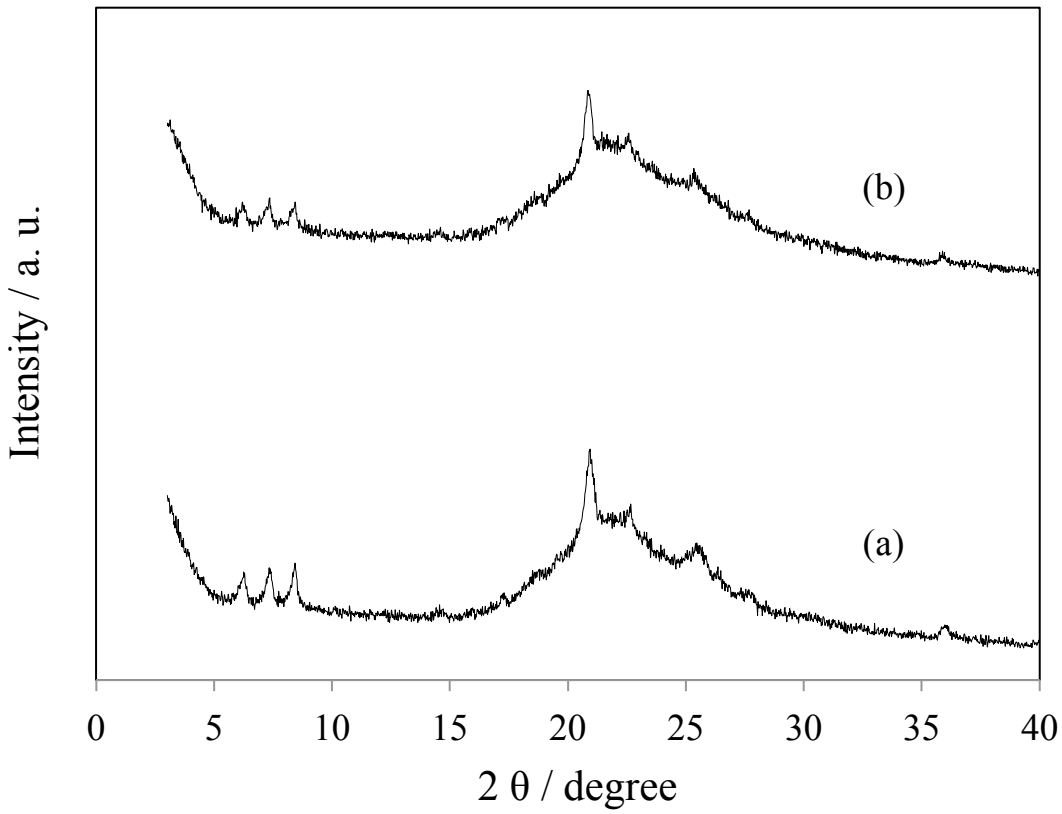

Figure 4

The XRD patterns of the [Al,B]-SFN-D synthesized under different crystallization time:

(a) Si/Al = 50, (b) Si/Al = 100.

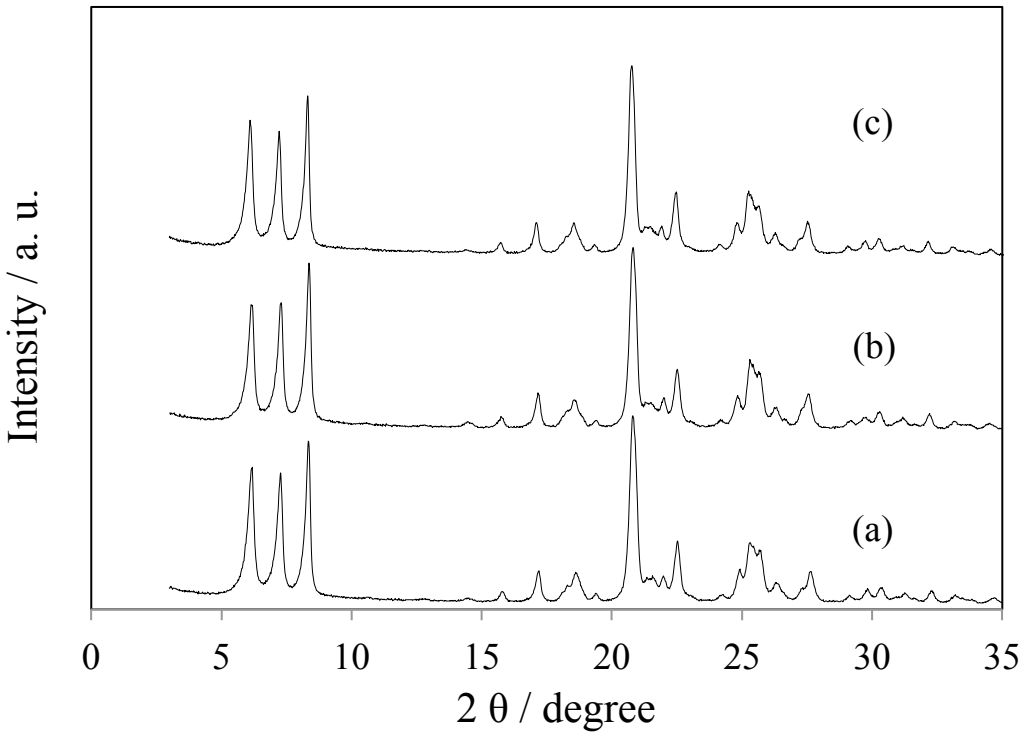

Figure 5

XRD patterns of the samples synthesized under different conditions:

(a) [B]-SFN, (b) [Al,B]-SFN-P-1 M, (c) [Al,B]-SFN-P-0.5 M.

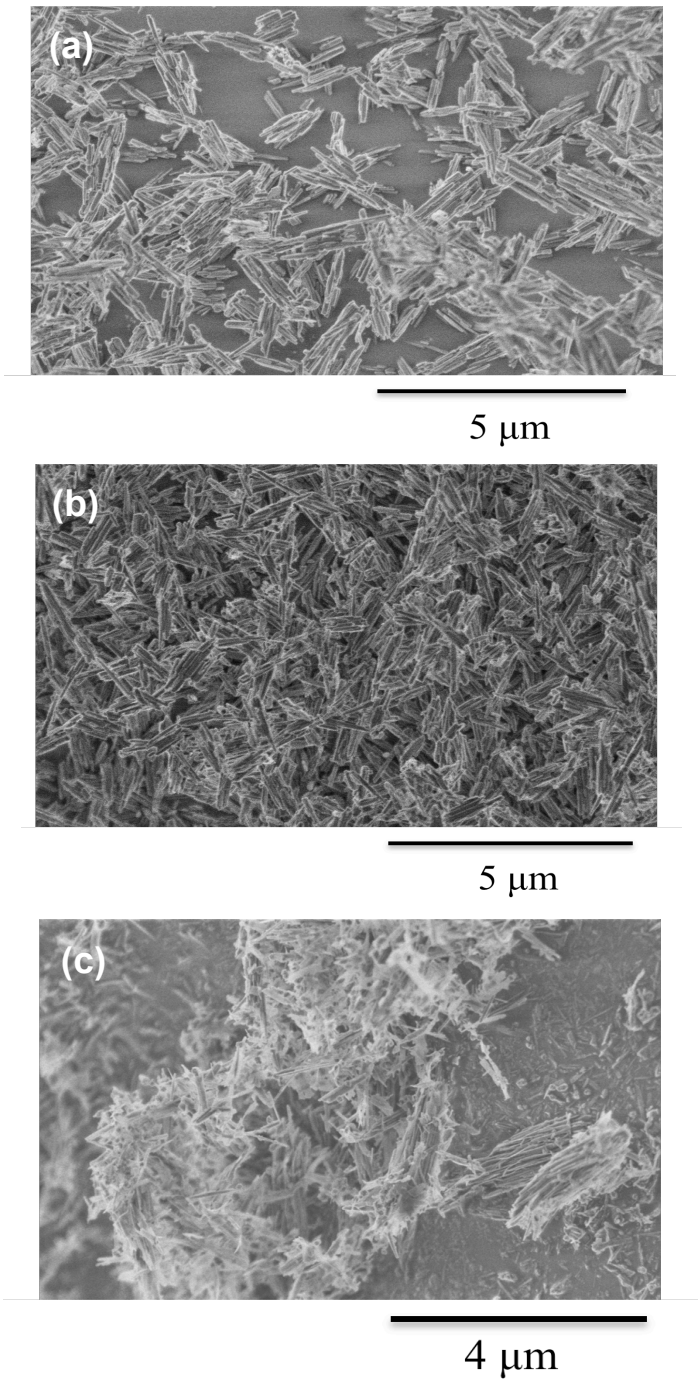

Figure 6

SEM images of the samples after calcinations:

(a) [B]-SFN, (b) [Al,B]-SFN-P-1M, (c) [Al,B]-SFN-D-200.

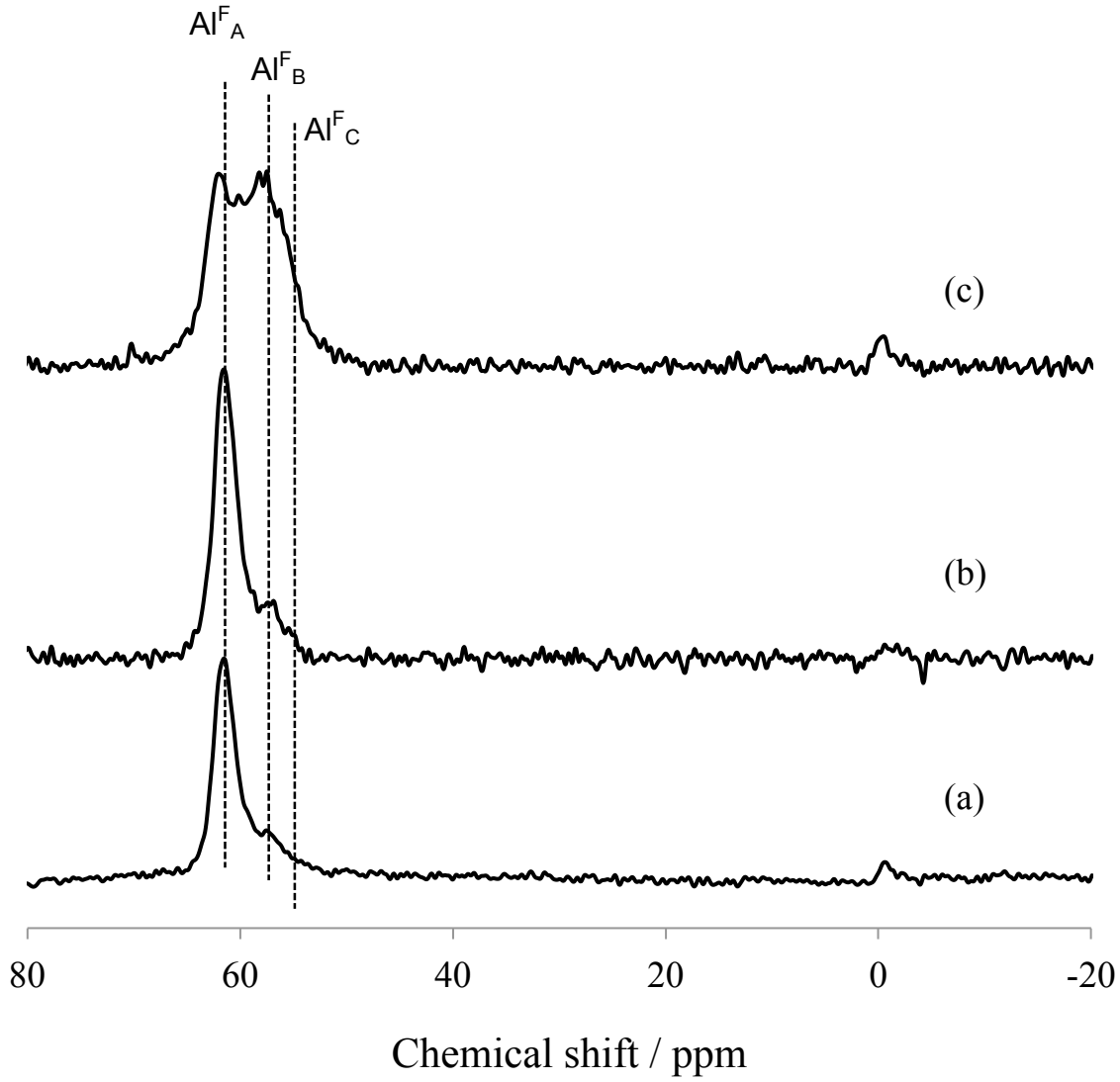

Figure 7

High-resolution ^{27}Al MAS NMR spectra of the representative calcined samples:

(a) [Al,B]-SFH-P-1 M, (b) [Al,B]-SFN-P-0.25 M , (c) [Al,B]-SFH-D-200.

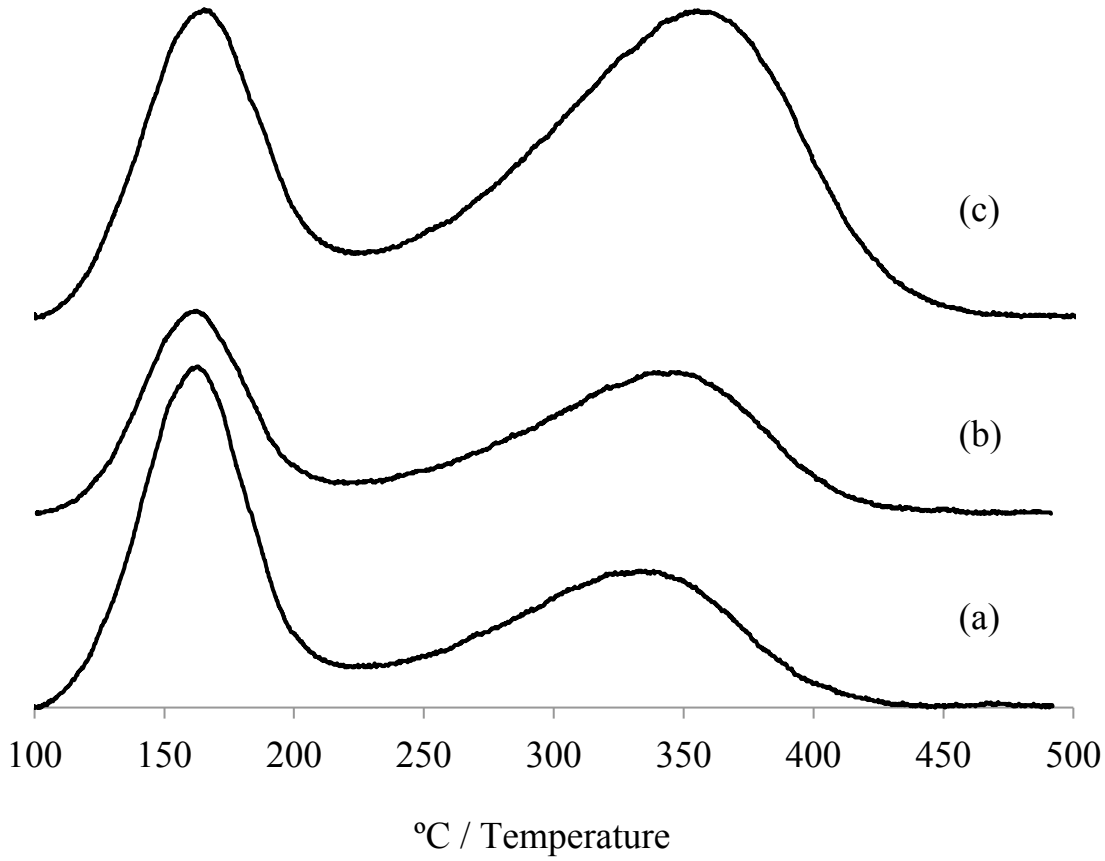

Figure 8

NH_3-TPD profiles of the samples prepared with direct- and post-synthesis method:

(a) [Al,B]-SFH-D-200 , (b) [Al,B]-SFN-P-0.25 M, (c) [Al,B]-SFH-P-1 M.

Chapter 4

Comparison of the Catalytic performance of extra-large-pore zeolites and large-pore zeolites

Abstract

14 membered ring extra-large-pore zeolite, CIT-5 (California Institute of Technology Number 5), was synthesized by direct-synthesis method according to the literature reported previously. Thus prepared CIT-5 (**CFI**-type) zeolite was characterized in details. Finally, Al containing CIT-5, SSZ-53 and SSZ-59 synthesized by direct-synthesis method were utilized as catalysts for acylation of 2-methoxynaphthalene under same reaction condition in order to compare the catalytic performance. Commercial 12 membered ring zeolites Beta and Mordenite were also used in the same reaction in order to compare the catalytic performance with 14 membered ring extra-large-pore zeolites.

4.1 Introduction

14 membered ring extra-large-pore zeolites, SSZ-53 and SSZ-59, are expected to be effective catalysts for their large pore size and high hydrothermal stability. Another extra-large-pore zeolite CIT-5 [1], which is also aluminosilicate zeolite, is also expected to be an effective catalyst. **CFI**-type zeolite was high-silica molecular sieve, and it contains one-dimensional pores circumscribed by 14 tetrahedral atoms [2]. The pore diameter is 7.3Å. CIT-5 was the first extra-large-pore zeolite which is synthesized using an organic cation as SDA. CIT-5 was synthesized by using *N*(16)-methylsparteinium hydroxide (MeSPAOH) as organic structure-directing agent (OSDA) as shown below.

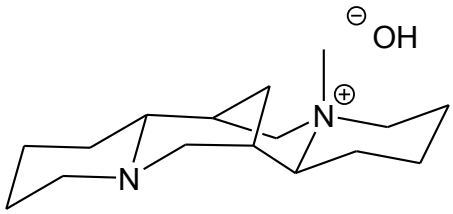

In this chapter, **CFI**-type aluminosilicate zeolite was synthesized according to the literature previously reported [3]. Thus prepared **CFI**-type zeolite, designated as [Al,B]-CIT-5-D, were characterized in details. Finally, [Al]-CIT-5-D was used as a catalyst for 2-methoxynaphthalene acylation reaction. The catalytic performance was compared to the three 14 membered ring zeolites.

4.2 Experimental

4.2.1 Synthesis of CFI-type zeolite

N(16)-methylsparteinium hydroxide (MeSPAOH) was prepared according to the previous report [4]. Al containing CIT-5 was synthesized by direct-synthesis method under hydrothermal conditions. The gel composition was 1 SiO_2 : 0.1 LiOH : 0.02 Al $(OH)_3$: 0.25 SDAOH : 50 H_2O. Gel was heated to 180 ºC for 7 days in order to produce CIT-5. Al containing SSZ-53 and SSZ-59 synthesized by direct-synthesis method were prepared by the method reported in chapter 2 and 3. Beta and Mordenite zeolites were purchased from ZEOLYST and TOSOH, respectively.

4.2.2 Characterization

The prepared zeolites were characterized by XRD, ICP, SEM, N_2 adsorption, high resolution ^{27}Al MAS NMR and NH_3-TPD. XRD patterns were collected on a Rint-Ultima III (Rigaku) using a Cu Kα X-ray source (40 kV, 20 mA). Nitrogen adsorption measurements to determine the BET surface area (S_{BET}), S_{EXT} , and micropore volume (V_{micro}) were conducted at 77 K on a Belsorp-mini II (Bel Japan). Field-emission scanning electron microscopic (FE-SEM) images of the powder samples were obtained on an S-5200 microscope (Hitachi) operating at 1-30 kV. The sample was mounted on a carbon-coated microgrid (Okenshoji Co.) without any metal coating. The Si/Al ratios of the samples were determined by using an inductively coupled plasma-atomic emission spectrometer (ICP-AES, Shimadzu ICPE-9000).

To investigate the Al environment, solid-state ^{27}Al magic-angle spinning (MAS) NMR spectra were obtained on a JEOL ECA-600 spectrometer (14.1 T). The relaxation delay time was 10 ms. The ^{27}Al chemical shift was referenced to $AlNH_4(SO_4)_2 \cdot 12H_2O$ at -0.54 ppm and samples were spun at 17 kHz by using a 4 mm ZrO_2 rotor.

Temperature-programmed NH_3 desorption (NH_3-TPD) profiles were recorded on a BELCAT (Japan BEL). Typically, 30 mg catalyst was pretreated at 773 K in He (50 mL min^{-1}) for 1 h and then cooled to 423 K. Prior to the adsorption of NH_3, the sample was evacuated at 423 K for 1 h. Approximately 2500 Pa of NH_3 was allowed to make contact with the sample at 423 K for 10 min. Subsequently, the sample was evacuated to remove weakly adsorbed NH_3 at the same temperature for 30 min. Finally, the sample was cooled to 423 K and heated from 423 to 873 K at a ramping rate

of 10 K min^{-1} in a He flow (50 mL min^{-1}). A quadrupole mass spectrometer was used to monitor desorbed NH_3 (*m*/*e* = 16). The amount of acid sites was determined by using the area of the so-called "*h*-peak" in the profiles [5].

4.2.3 Catalytic reaction

To evaluate the catalytic performance of the extra-large-pore and large pore zeolites, Friedel-Crafts acylation of 2-methoxynaphthalene (2-MN) with acetic anhydride was conducted in the liquid-phase under batch conditions. Before the reaction, the catalyst was pretreated at 400ºC for 1 h under vacuum conditions in a glass reactor. Under argon atmosphere, 2 mmol of 2-MN, 1 mmol of acetic anhydride and 2 ml of *o*-dichlorobenzene as solvent were put into the glass reactor. The reaction temperature and time were set at 100 ºC and 30 min, respectively. The reactant and products were analyzed by a gas chromatograph (Shimadzu, GC-2014) equipped with an FID detector with a DB-5 column.

4.3 Results and Discussion

The X-ray diffraction (XRD) patterns of zeolites synthesized by direct-synthesis method were showed in Figure 1. Zeolites were confirmed to be successfully synthesized. The Si/Al ratios of the calcined samples were showed in Table 1. The Si/Al ratios of the **SFH**-, **SFN**- and **CFI**-type zeolites were 190, 162 and 45, respectively. The Si/Al ratios of commercial zeolites Beta and Mordenite were 150 and 110. All zeolties had similar acid amount except **CFI**-type zeolite. The BET surface area and micropore volume estimated from N_2 adsorption-desorption analysis were showed in table 1. The specific surface area and micropore volume of **CFI**-type zeolite was lower than that of other zeolites. Figure 2 shows the SEM images of **SFH**-, **SFN**- and **CFI**-type zeolites. All samples were composed of needle-like crystallites around 0.5-2 μm. The crystal of **SFN**-type zeolite was smaller than other samples.

High-resolution ^{27}Al MAS NMR spectra (600 MHz, 14.1 T) of the representative calcined samples are shown in Fig. 3. A main broad peak at 50-65 ppm, which is assigned to tetrahedrally coordinated Al species in the framework, and a small peak at 0 ppm, which is assigned to octahedrally-coordinated Al species, were observed. Fig. 8 shows the NH_3-TPD profiles of the representative samples. The amount of samples was adjusted and the samples measured were expected to have the same acid amount totally. So from the temperature of h-peak, the acid strength of each sample can be compared. The h-peak temperatures of five zeolites were estimated to be 408ºC (Mordenite), 340ºC ([Al,B]-SSZ-59-D), 324ºC ([Al,B]-SSZ-53), 304ºC (Beta) and 285ºC ([Al]-CIT-5-D). So according to the h-peak temperature, the acid strength of these five zeolites was considered to be the order as below:

[Al]-CIT-5-D ≤ Beta < [Al,B]-SSZ-53-D < [Al,B]-SSZ-59-D < Mordenite

The acid strength of Mordenite was considered to be the strongest among these five zeolites. The pore size of these five zeolites was 7.0×6.5Å (Mordenite), 7.5×7.2Å ([Al]-CIT-5-D), 7.7 × 6.6Å (Beta), 8.5 × 6.2Å ([Al,B]-SSZ-59-D) and 8.7 × 6.4Å ([Al,B]-SSZ-53-D). So the order of the pore size was considered as below (according to the larger diameter):

Mordenite < [Al]-CIT-5-D < Beta < [Al,B]-SSZ-59-D < [Al,B]-SSZ-53-D

Table 2 shows the reaction results of 2-MN acylation, the amount of catalysts were adjusted to let each of them have the same acid amount totally. In order to quantitatively compare of the catalytic performance of these five zeolites, the specific

catalytic activity per acid site (i.e., turnover number, TON) on the basis of the acid amount estimated by the h-peak areas in the NH_3-TPD profiles has been considered. The order of TON is showed as below:

[Al]-CIT-5-D < Mordenite < Beta < [Al,B]-SSZ-59-D < [Al,B]-SSZ-53-D

The reaction did not proceed in the absence of catalysts. When the [Al,B]-SSZ-53-D zeolites were used as a catalyst, 1,2-AMN was mainly obtained and other products were hardly detected. Considering that the size of 14-MR pore (0.65×0.85 nm) is larger than the cross section of 1,2-AMN (ca. 0.41×0.81 nm), the reaction would occur inside the 14-MR pores and the kinetically favored product, 1,2-AMN was preferentially formed. [Al,B]-SSZ-59-D showed lower TON due to the smaller pore than that of [Al,B]-SSZ-53-D. When Beta was used as a control catalyst, 2,6-AMN (ca. 0.41×0.62×1.23 nm) was also formed in addition to 1,2-AMN. The formation of 2,6-AMN over the Beta zeolite would be due to the shape-selectivity of the 12-MR pores and 1,2-AMN would be formed on the acid sites located near pore mouth and at the external surface because the pore size of the *BEA-type zeolite (0.77×0.66 nm) is smaller than 1,2-AMN but larger than 2,6-AMN [4]. Although Mordenite had the strongest acid strength, reaction did not process because the pore size is small to inhibit the diffusion of the reactant. No product was obtained over [Al]-CIT-5-D. It is thought that the weak acid strength and smaller pore size were the reasons [Al]-CIT-5-D did not show any activity.

Conclusion

Al containing CIT-5 was successfully synthesized by direct-synthesis method under hydrothermal conditions. According to the results of NH_3-TPD, the acid strength of [Al]-CIT-5 was considered to be the weakest of the five zeolites. [Al.B]-SSZ-53 showed the highest catalytic performance due to its extra-large-pore and medium degree of acid strength.

References

1. Davis, M. E., *Nature*, **1991**, 352, 281.

2. Davis, M. E., *Chem. Commun.*, **1997**, 2179

3. Kubota, Y. et al, *Microporous and Mesoporous Materials*, **2000**, 37, 291-301.

4. Lobo, R. F.; Davis, M. E., *Microporous Mater.*, **1994**, 3, 61.

5. M. Niwa, K. Katada, *Catal. Surv. Jpn.*, **1997**, 1, 215-226.

Table 1

Physicochemical properties of Al containing zeolites containing extra-large-pore and large pore.

Cat.	Si/Al[a)]	Si/B[a)]	S_{BET}[b)]	V_{micro}[c)]	S_{EXT}[d)]	Acid amount[e)]	Al amount[f)]	Acid amount / Al amount
			[m^2/g]	[ml/g]	[m^2/g]	[mmol/g]	[mmol/g]	(%)
[Al,B]-SFH-D-200	190	38	477	0.151	87	0.068	0.088	77
[Al,B]-SFN-D-200	162	107	543	0.159	139	0.063	0.103	61
[Al]-CIT-5	45	--	365	0.106	91	0.134	0.370	36
Beta	150	--	609	0.161	199	0.074	0.111	67
Mordenite	110	--	557	0.185	90	0.072	0.152	47

a) Si/Al and Si/B: atomic ratio of Si/Al and Si/B in the sample

b) S_{BET}: BET surface area

c) V_{micro}: Micropore volume

d) S_{EXT}: External surface area

e) Acid amount: Estimated by the NH_3-TPD

f) Al amount: Estimated by the ICP

g) B amount: Estimated by the ICP

Table 2

The results of the acylation of 2-methoxynaphalene (2-MN) over the aluminosilicate zeolites containing extra-large-pore and large pore.

	Si/Al	Acid amount (mmol/g)	Catalyst weight (mg)	Conversion (%)		Yield (%)		TON
				Ac_2O	2-MN	1,2-AMN	2,6-AMN	
[Al,B]-SSZ-53-D	190	0.068	50	58	47	42	<1	124
[Al,B]-SSZ-59-D	162	0.063	50	50	33	28	0	89
[Al]-CIT-5-D	45	0.134	25	14	10	1	0	3
Beta	150	0.074	47	44	27	25	3	80
Mordenite	110	0.072	46	22	11	5	0	15

Reaction condition: 2-MN, 2 mmol; Acetic anhydride, 1 mmol; *o*-Dichlorobenzene, 2 ml; Temperature, 100ºC. Reaction time, 30 min.

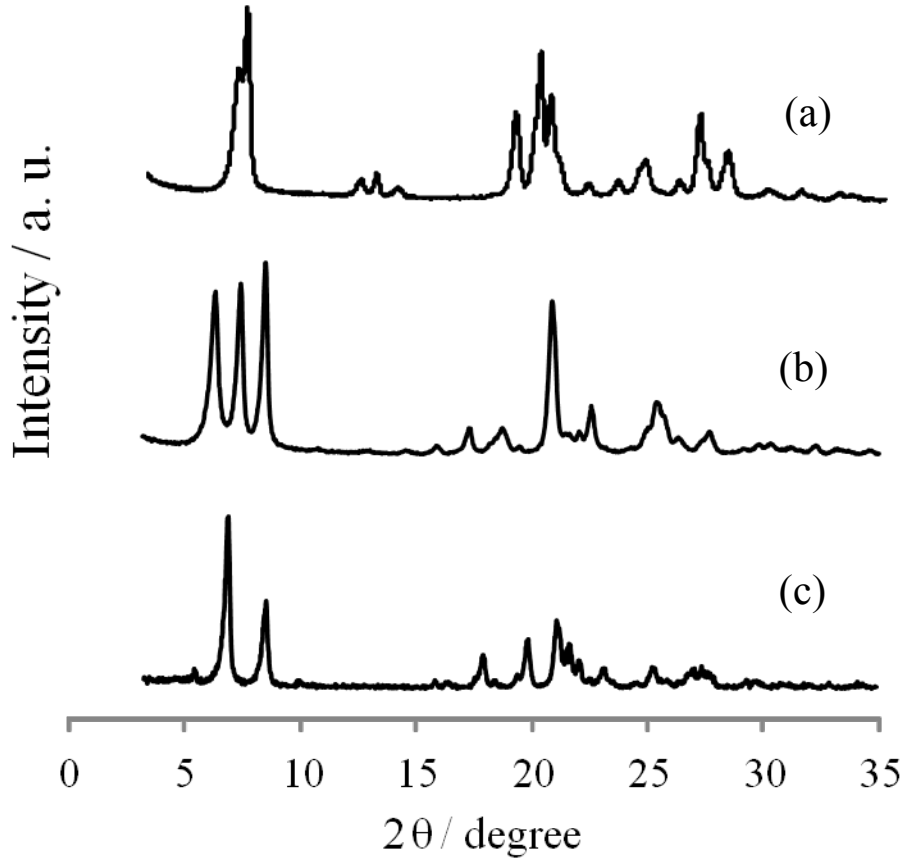

Figur 1

XRD patterns of the synthesized samples:

(a) [Al,B]-CIT-5-D, (b) [Al,B]-SFH-D-200 and (c) [Al,B]-SFN-D-200.

(a)

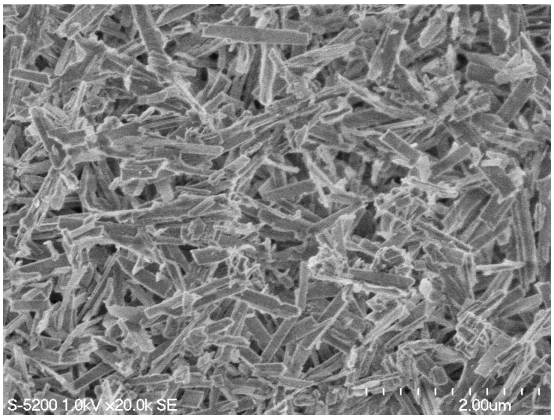

(b)

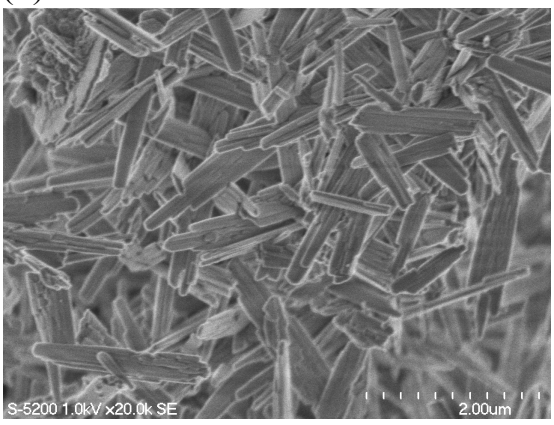

(c)

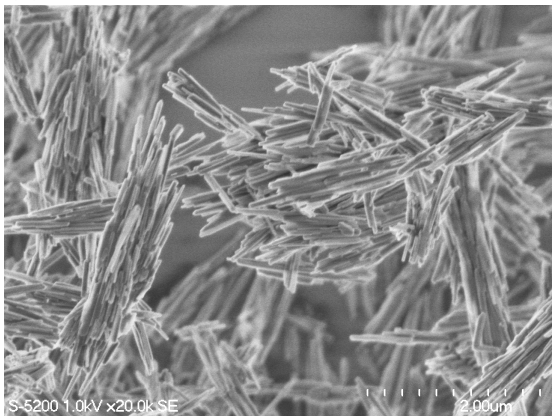

Figure 2

SEM images of the samples after calcinations:

(a) [Al,B]-CIT-5-D, (b) [Al,B]-SFH-D-200 and (c) [Al,B]-SFN-D-200.

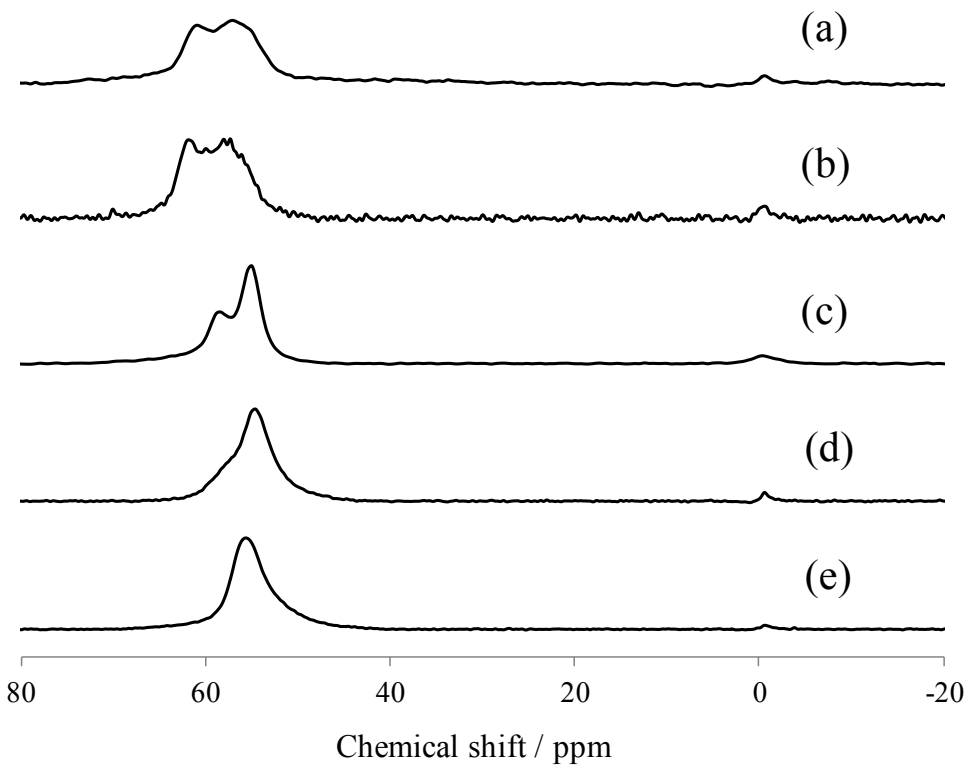

Figure 3

High-resolution ^{27}Al MAS NMR spectra of samples:

(a) [Al,B]-SFH-D-200, (b) [Al,B]-SFN-D-200 and (c) [Al,B]-CIT-5-D, (d) Beta

(e) Mordenite

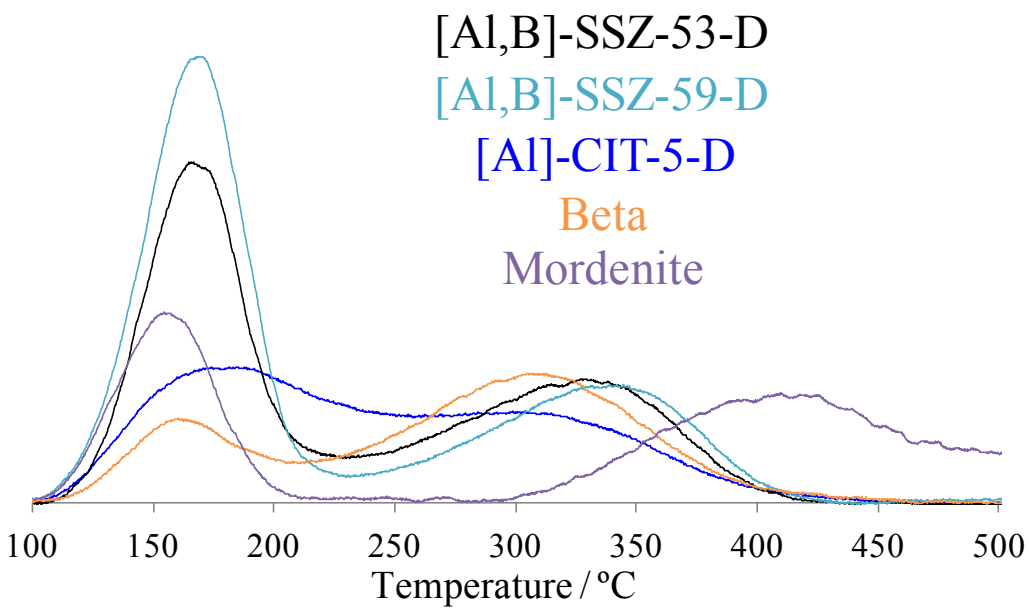

Figure 4. NH_3-TPD profile of the samples.

Chapter 5

Synthesis, characterization and catalytic properties of RTH-type zeolites

Abstract

In addition to original preparation route to the **RTH**-type zeolites using 1,2,2,6,6-pentamethylpiperidine (PMP) as organic structure directing agent (OSDA), we have found that simpler organic amines such as *N*-methylpiperidine and pyridine can be used as alternative OSDA in place of PMP for the **RTH**-type zeolites. Furthermore, we have established the synthesis method for preparing the **RTH**-type zeolites without using any OSDAs. In this study, the **RTH**-type aluminosilicates were synthesized with different types of OSDA or without using any OSDAs. Thus obtained zeolite synthesized with different preparation methods were characterized by using various techniques, especially, high-resolution ^{27}Al MAS NMR and CO-adsorbed in-situ FT-IR techniques. The relationship between the preparation method and the catalytic performance in the methanol to olefins (MTO) reaction was discussed. Finally, the distribution of Al species in the **RTH**-framework was clarified.

5.1 Introduction

Zeolites have been utilized in many industrial technologies, including gas adsorption, ion exchange, separation and catalysis for their unique porosity and high surface area [1, 2]. Recently, 8-membered ring (8-MR) zeolites and zeotype materials have attracted much attention in expectation of selective catalysis due to their small pores. For example, **CHA**-zeotype materials such as SSZ-13 and SAPO-34 showed a catalytic activity for methanol to olefins (MTO) reaction to provide ethylene and propylene, which are important chemicals for the polymer industry [3-6]. The high yield of olefins obtained from these catalysts is usually explained by its 8-MR pores and relatively weak acidity. In this reaction, however, the catalytic activity is decreased along with the deposition of coke derived from polymethylbenzene and aromatic polycyclic compounds, which are formed in the large cavity in the **CHA**-type zeolite [7]. Therefore, the development of an alternative high-silica zeolite with 8MR pores has been strongly desired.

We have focused on the **RTH**-type zeolites, which consists of the **RTH** cages with the openings of 8-MR and has two-dimensional channels with aperture size of 0.41 x 0.38 nm for non-distorted 8-MR pore and 0.56 x 0.25 nm for distorted 8-MR pore, which run parallel to the a-axis and the c-axis, respectively. As shown in Scheme 1, the **RTH**-zeolite has four different T sites (T1, T2, T3 and T4). T1 site is facing to the non-distorted 8-MR pore (4.1×3.8 Å) [8,9]. T2 site is facing to both the non-distorted and the distorted 8-MR pores (5.6×2.5 Å). T3 site is not facing either 8-MR pores. T4 site is facing to the distorted 8-MR pore.

The **RTH**-type zeolites have been expected to show unique properties in the field of catalysis and adsorption because of its unique structure. However, the synthesis conditions and the diversification of the **RTH**-type zeolite have not been thoroughly investigated. Only two examples on the **RTH**-type zeolites had been reported until 2009. One is the type material, RUB-13 [9], which is the **RTH**-type borosilicate synthesized by using 1,2,2,6,6-pentamethylpiperidine (PMP) in combination with ethylenediamine (EDA) as OSDA (organic structure-directing agent) [10]. The other is SSZ-50, which is the **RTH**-type aluminosilicate and has been synthesized in the presence of *N*-ethyl-*N*-methyl-5,7,7-trimethylazoniumbicyclo[4.1.1]octane cation as OSDA [34].

From a practical viewpoint, the use of these OSDA could significantly hinder its industrial applications.

We found that the amounts of PMP and/or EDA can be decreased by adjusting the gel compositions. We have also found that simpler organic amines such as *N*-methylpiperidine and hexamethyleneimine can be used as alternative OSDA in place of PMP for the synthesis of the **RTH**-type zeolites [11, 12]. Furthermore, we have established the synthesis method for preparing the **RTH**-type zeolites without using any OSDAs [11]. The key points are the addition of an appropriate amount of sodium hydroxide as well as calcined [B]-RUB-13 as seeds and the adjustment of the molar composition of water. Thus prepared **RTH**-type zeolites synthesized without any organic-templates are named "TTZ-1" (Tokyo Tech. Zeolite) series. Furthermore, we have demonstrated that the **RTH**-type aluminosilicate has a high potential for the selective production of propylene through the MTO reaction [11].

Interestingly, we have also found that there are significant differences in the catalytic performance in the MTO reaction between the **RTH**-type aluminosilicates that are synthesized with and without using PMP and EDA, and similar in the Al content [11]. We have considered that these differences would be due to the different distributions of Al species in the framework. However, to date, the detailed characterization of Al species in the **RTH**-type aluminosilicates in relation to their acidic properties has not been conducted.

The acidic properties of zeolites are closely related to the nature and distribution of the Al species in the framework. Therefore, detailed characterization of the Al environment is essential for understanding the catalytic properties. It is well recognized that solid-state ^{27}Al magic angle spinning (MAS) NMR spectroscopy is highly effective in the study of zeolites; the peaks at 50-60 and 0 ppm in ^{27}Al MAS NMR spectrum are ascribed to tetrahedral framework Al species and extra- framework octahedral Al atoms, respectively [13]. However, unlike ^{29}Si (I=1/2) MAS NMR, the resolution of ^{27}Al MAS NMR spectra is not high enough to detailedly characterize Al species because quadrupolar interaction at Al (I = 5/2) leads to a broadening of the peak; the sizable second-order quadrupolar interaction at Al, which contains higher-rank anisotropic terms, cannot be completely averaged out by MAS [14-16]. Recently, a very high magnetic field has become applicable to the NMR measurement, and high-resolution solid-state NMR spectroscopy has established itself as a powerful

technique for characterization of zeolites and related materials with respect to structure elucidation, catalytic behavior, and mobility. In addition, a multiple quantum (MQ) method of NMR, which has been developed by Frydman and Harwood [17], has become a promising tool for the study of quadrupolar nuclei in solids, *i.g.*, ^{7}Li, ^{11}B and ^{23}Na with I = 3/2 and ^{17}O, ^{27}Al and ^{25}Mg with I = 5/2 [18-22]. In this study, to investigate the distribution of Al on the Al-containing **RTH**-zeolites, high-resolution solid-state ^{27}Al MAS NMR and ^{27}Al MQMAS NMR techniques have been applied.

Acid properties of zeolite catalyst have been extensively investigated by various methods including temperature-programmed desorption (TPD) [23, 24], X-ray photoelectron spectroscopy (XPS) [25], infrared (IR) spectroscopy [26, 27], and so on. In the IR method, OH stretching vibrations of the acidic OH groups, the Brønsted acid sites (BAS), of zeolites can be clearly observed. Moreover, the nature of the BAS and the Lewis acid sites (LAS) can be investigated by using basic probe molecules such as pyridine, NH_3 and CD_3CN [27]. These strongly basic probe molecules can distinguish BAS and LAS by different structures of adsorbed species. Pyridine has been often used as probe among various basic molecules for the characterization of 10- and 12-MR zeolites because of the experimental simplicity. However, pyridine cannot be applicable to the 8-mebered ring zeolites because diffusion of pyridine molecule into 8-membered ring micropores is significantly difficult. Meanwhile, CO has become used as probe molecule [28-33]. The advantages of CO as probe are its very weak basicity, small molecular diameter and high sensitivity of the IR band frequency to the strength of the acid sites. Therefore, in this study, *in-situ* FT-IR technique using CO as probe molecule was applied to the characterization of the acid property of the Al-containing **RTH**-zeolites.

Here, to examine our hypothesis that the distribution of Al might be dependent on the synthesis method, the detailed characterizations of the **RTH**-type aluminosilicates synthesized with different types of OSDA or without using any OSDAs were conducted by using various techniques, especially, high-resolution ^{27}Al MAS NMR and CO-adsorbed *in-situ* FT-IR techniques. The relationship between the preparation method and the catalytic performance in the MTO reaction was discussed. Finally, the distribution of Al species in the RTH-framework was also considered.

5.2 Experimental

5.2.1 Chemicals

Fumed silica, Cab-O-Sil M5, produced by Cabot was used as silica source. The original OSDAs for RUB-13, 1,2,2,6,6-pentamethylpiperidine (PMP), and ethylenediamine (EDA) were purchased from Wako and TCI, respectively. Pyridine (PY) and *N*-methylpiperidine (MP) were purchased from TCI and Aldrich, respectively. Inorganic chemicals including H_3BO_3, NaOH and $Al_2(SO_3)_3$ were purchased from Wako. All chemicals were used as received without further purification.

5.2.2 Synthesis of RTH-type zeolite

5.2.2.1 OSDAs-directed RTH-type zeolites

Al- and B- containing RTH-type zeolites were synthesized by using 1,2,2,6,6-pentamethylpiperidine (PMP), 1-methylpiperidine (MP) and pyridine (PY) as OSDA in the presence of ethylenediamine (EDA) [11]. In a typical synthesis, H_3BO_3 (0.108 g) and $Al_2(SO_4)_3$ (0.006 g) were dissolved in an aqueous solution of NaOH (0.056 g), OSDA (3.5 mmol) and EDA (7.0 mmol) with stirring at ambient temperature. The fumed silica (0.42 g) was added to the mixture. The molar composition of the resulting mixture was 1 SiO_2 : 0.0025 $Al_2(SO_4)_3$: 0.25 H_3BO_3 : 0.2 NaOH : 0.5 OSDA : 2.0 EDA : 100 H_2O. Thus prepared mother gel was transferred into a Teflon-lined autoclave (20 mL) and crystallized in an oven at 170 ^oC for 7 days with tumbling at 20 rpm. The solid product was recovered by filtration, washing with distilled water and drying overnight at 100 ^oC. Thus obtained Na-type as-synthesized samples were calcined in air at 550 ^oC for 6 h to remove organic moieties. The RTH-type zeolites synthesized with PMP, MP and PY were designated as PMP-RTH, MP-RTH and PY-RTH, respectively.

5.2.2.2 OSDA-free RTH-type zeolites (TTZ-1)

Al- and B- containing TTZ-1 zeolites were synthesized via the OSDAs-free synthesis route with the aid of seed [11]. In a typical synthesis, H_3BO_3 (0.054 g) and $Al_2(SO_3)_3$ (0.003 g) were dissolved in an aqueous solution of NaOH (0.028 g) with stirring at ambient temperature. The fumed silica (0.21 g) was added to the mixture. The molar composition of the resulting mixture was 1 SiO_2 : 0.0025 $Al_2(SO_4)_3$: 0.25 H_3BO_3 : 0.2 NaOH : 200 H_2O. Finally, the calcined B-containing RTH-type zeolite

synthesized with PMP and EDA as seed (5 wt%) was added to the mixture. Thus prepared mother gel was crystallized under the same conditions as those for the OSDAs-directed synthesis. The following procedures were similar to those for the OSDAs-directed synthesis.

5.2.2.3 Ion-exchange

The Na-type calcined samples were converted to the H-type ones as follows. The calcined samples were treated with 1 M NH_4NO_3 aq. at 80 ^oC for 3 h twice followed by calcination at 550 ^oC for 10 h to exchange Na^+ ions for protons.

5.2.3 Characterizations

5.2.3.1 Structural characterization

Powder X-ray diffraction (XRD) patterns were collected on a Rigaku Ultima III using a Cu Kα X-ray source (40 kV, 20 mA). FE-SEM images of the samples were obtained on a Hitachi S-5200 microscope operated at 1 kV. The samples on a carbon tape were observed without any metal coating. Elemental analyses of the samples (Si/Al ratio) were performed on an inductively coupled plasma-atomic emission (ICP) spectrometer (ICP-AES, Shimadzu ICPE-9000). The Na content was determined by atomic absorption (AA) spectrometry (Shimadzu AA-6200). Solid-state ^{11}B, ^{27}Al, and ^{29}Si NMR spectra were obtained on a JEOL ECA-400 spectrometer at 9.4 T. The samples were spun at 7 kHz by using a 6 mm ZrO_2 rotor.

The amount of OSDAs in the as-synthesized samples was determined from the weight loss from 200-700 ^oC in each thermogravimetric (TG) profile, which was performed on a thermogravimetric - differential thermal analyzer (TG-DTA, Rigaku Thermo plus EVO II).

5.2.3.2 Estimation of acid amount by NH_3-TPD

Temperature-programmed desorption of ammonia (NH_3-TPD) spectra were recorded on a multitrack TPD instrument (Japan BEL). Typically, 25 mg catalyst was pretreated at 500 ^oC in He (50 mL min^{-1}) for 1 h and then was cooled to adsorption temperature of 100 ^oC. Prior to the adsorption of NH_3, the sample was evacuated at 100 ^oC. Approximately 2500 Pa of NH_3 was allowed to make contact with the sample for 10 min. Subsequently, the sample was evacuated to remove weakly adsorbed NH_3

for 30 min. Finally, the sample was heated from 100 to 600 ^{o}C at a ramping rate of 10 ^{o}C per minute with the He flow (50 mL min^{-1}) passed through the reactor. A quadrupole mass spectrometer was used to monitor desorbed NH_3 (m/e = 16). The amount of acid sites was determined by using the area of the so-called ''*h*-peak'' in the profiles [34].

5.2.3.3 Detailed characterizations of Al species by high-resolution ^{27}Al MAS NMR and ^{27}Al 3Q MQMAS NMR spectroscopies

The high-resolution ^{27}Al MAS NMR and ^{27}Al 3Q MQMAS NMR spectra were obtained on a JEOL ECA-600 spectrometer (14.1 T) equipped with an additional 1 kW power amplifier. For ^{27}Al 3Q MQMAS NMR spectra, pulse durations were 5.5 μs, 2.1 μs and 0.2 ms for the 3Q excitation pulse, the 3Q-1Q conversion pulse and z-filter, respectively. The relaxation delay time was 10 ms. The ^{27}Al chemical shift (δ) was referenced to $AlNH_4(SO_4)_2 \cdot 12H_2O$ at -0.54 ppm and samples were spun at 17 kHz by using a 4 mm ZrO_2 rotor. For high-resolution ^{27}Al MAS NMR spectra at 14.1 T, which were recorded using a single pulse, the pulse width was set at 0.1 μs and 10000 scans were accumulated at a sample spinning rate of 17 kHz. A 10 ms relaxation delay was determined so as to be long enough to permit quantitative analysis of zeolite samples. $AlNH_4(SO_4)_2 \cdot 12H_2O$ was also used as a reference for the ^{27}Al chemical shift.

5.2.3.4 Evalution of aicd property by in-situ FT-IR using CO as probe molecule

In-situ FT-IR spectroscopy was also applied to the evaluation of the acid property by using CO as probe molecule [33]. FT-IR spectra were obtained by use of a Jasco FT-IR 7000 spectrometer equipped with an MCT detector at a 4 cm^{-1} resolution; 64 scans were collected to obtain each spectrum. About 30 mg of each sample was pressed into a self-supporting disk of 20 mm diameter, and placed in a quartz cell connected to a conventional closed gas-circulation system. The sample disk was pretreated at 500 ^{o}C for 1 h under evacuation. Temperature was then decreased to -120 ^{o}C under evacuation. FT-IR spectra of clean samples before adsorption experiments were measured under evacuation at -120 ^{o}C and were used as background spectra. Then, 0.85 μmol of CO was introduced to the sample. IR spectra were measured with the CO dosage increased up to 24 μmol; the CO pressure was changed

from 0.008 to 0.225 kPa. The IR spectra resulting from the subtraction of the background spectra from those with CO adsorbed are shown unless otherwise mentioned.

5.2.4 Methanol to olefins (MTO) reaction

The MTO reaction was carried out in a fixed bed reactor. The reaction was performed at 400 ^{o}C at the time factor W/F (MeOH) of 34 g/mmol h^{-1}. The weight hourly space velocity of methanol (WHSV) was 0.9 h^{-1}. Typically, 100 mg catalyst was centered at a quartz reactor in a furnace and 5 % methanol diluted with helium was used as reactant. The catalyst was calcined prior to the reaction at 500 ^{o}C for 1 h, and then the reactor was cooled to the desired reaction temperatures. The methanol conversion was defined as methanol consumed divided by methanol fed to the reactor. The selectivities of the products, including methane (C1), ethane (C2), ethene (C2=), propane (C3), propene (C3=), C4-C6 paraffins and dimethyl ether (DME) were based on a carbon mass balance.

5.3 Results and discussion

The XRD patterns of the as-synthesized products are shown in Figure 1 (a), indicating that all the products exhibited the pure **RTH** phase irrespective of the preparation methods. This **RTH** structure was completely retained after the calcination to remove the OSDAs and the following ion-exchange processes (Figure 1 (b)). The particle morphology of the products was assessed by FE-SEM observations (Figure 2). All the products were uniform plank-like crystals and they were 100-200 nm in thickness, 0.5-1 μm in width and 1-10 μm in length. In TTZ-1, tiny plank-like crystals 50 nm in thickness and 50-100 nm in length were formed on the main plank-like crystals (Figures 2 (d) and (e)).

The ^{29}Si MAS NMR spectra of the H-type products are shown in Figure 3 (a), indicating that all products exhibited two peaks at –112 and –106 ppm. The first main peak at -112 ppm is assigned to $Si(OSi)_4$ units. The second at -106 ppm is due to $\equiv Si(OSi)_3(OM)$, where M = B or Al [9]. The proportion of the peak area at -112 ppm to the total peak area is over 70 % in all the products; it was computed at 74, 77, 81 and 71 % for the PMP-RTH, MP-RTH, PY-RTH and TTZ-1 samples, respectively. The ^{11}B MAS NMR spectra of all the H-type products showed a large peak observed at -2.5 ppmand also a small peak observed at -3.2 ppm. Both peaks are assigned to tetrahedrally coordinated B atoms in the framework (Figure 3 (b)). Figure 3 (c) shows the ^{27}Al MAS NMR spectra (9.4 T), which exhibit a sharp peak at 58 ppm that is assigned to tetrahedrally coordinated aluminum atoms in the framework, irrespective of the preparation routes. No remarkable peak at 0 ppm assigned to octahedrally coordinated aluminum was observed in all the products. These NMR results suggest that the local structures of the **RTH**-type zeolites are similar, irrespective of the preparation methods.

Table 1 summarizes the data obtained by elemental analyses and NH_3-TPD measurements. The Si/Al atomic ratios of PMP-RTH, MP-RTH, PY-RTH and TTZ-1 were close to those of the gel (200). On the other hand, the Si/B atomic ratio of the as-synthesized product was found to be 20-26, while that of the gel was set at 4. The Si/Al and Si/B ratios were unchanged after the ion-exchange process.

The content of the organics derived from PMP, MP, or PY with EDA in the as-synthesized samples was investigated based on the weight loss of TG curve ranging from 200 - 700 ^{o}C. There is no marked difference in the weight loss among the

samples; it was estimated at 14.3, 13.0, and 13.6 wt.% for the as-synthesized PMP-RTH, MP-RTH and PY-RTH samples, respectively. We have found that the PMP molecule was formed irrespective of the type of OSDA used after the crystallization process [12]; the formation of PMP was confirmed by the ^{1}H and ^{13}C NMR and MS spectra even when only EDA was used. If the organics in the as-synthesized samples are the PMP molecule, its content was calculated to be 0.84 - 0.90 mmol/g.

To use as solid an acid catalyst, the Na-type samples were converted to the H-type ones by the ion-exchange. The Na/Al atomic ratios before and after the ion-exchange are listed in Table 1. For the Na-type samples, the Na/Al ratios of the OSDAs-directed products were 0.22-0.33, while that of TTZ-1 was 1.03. When one Al^{3+} is incorporated into the silica framework, it must be accompanied by one cation to match the charge balance. In the OSDAs-directed route, the lack of charge was compensated with the OSDAs cations as well as Na^{+} ions, while, in the OSDAs-free route, it was compensated with only Na^{+} ion. After the ion-exchange, the Na/Al ratios of the OSDAs-directed products were 0.05-0.07, while that of TTZ-1 was 0.18; about 22-28 and 40% of Na^{+} ions still remained in the OSDAs-directed products and TTZ-1, respectively. Although, in general, Na^{+} species in 8-MR pores could not completely be exchanged for H^{+}, this difference would be related to the difference in the Al distribution in the framework

Figure 4 shows the NH_3-TPD curves of the ion-exchanged products. The temperature of the peak top in the range of 250 to 400 ^{o}C is 331, 333, 338 and 328 ^{o}C for PMP-RTH, MP-RTH, PY-RTH and TTZ-1, respectively; there is no remarkable difference in the acid strength. The acid amount estimated by the NH_3-TPD results was 0.050, 0.045, 0.048 and 0.037 mmol·g^{-1}, respectively. Assuming that all Al species in the solid work as acid sites, the acid amount based on the ICP results should be 0.081, 0.088, 0.089 and 0.078 mmol·g^{-1} for PMP-RTH, MP-RTH, PY-RTH and TTZ-1, respectively. The proportion of the Al species that can work as acid site to the total Al species in the solid is estimated at 61, 51, 54 and 47%, respectively. A part of the framework Al species cannot work as acid site because of the limited degree of the ion-exchange of Na^{+} for H^{+}. Another possible reason is that acid sites derived from the framework Al species might be located at T3 site, which is not facing to either 8-MR pores where NH_3 molecules can access.

To evaluate performance as a solid acid catalyst, the MTO reaction was conducted over thus prepared **RTH**-type zeolites at 400 ºC. Conversion of methanol reached to 100% over the PMP- MP- and PY-RTH samples at the initial stage of the reaction, and deactivation gradually progressed along with the reaction time (Figure 5). For TTZ-1, methanol conversion was below 100% even at the initial stage and deactivation occurred quickly. The amounts of coke formed during the reaction for 6 h were not significantly different depending on the samples; they were found to be 0.06, 0.09, 0.07 and 0.09 mg per 1 g of PMP-RTH, MP-RTH, PY-RTH and TTZ-1, respectively.

The product distributions are shown in Figure 6, indicating that all the catalysts produced propene as a main product with the selectivity over 40 % at the initial time of the catalytic run. For the PMP- and MP-RTH samples, high conversion of methanol was kept for 90 min, and after that methanol conversion became below 100 % and DME gradually appeared. However, the selectivity to propene was almost unchanged (*ca.* ~ 44 %). For PY-RTH, the selectivity to propene was gradually decreased along with the reaction time and DME became a main product after deactivation started. For TTZ-1, the selectivity to propene was almost unchanged (*ca.* ~ 41 %).

In conclusion, in terms of the life and the selectivity to propene, PMP- and MP-RTH samples gave higher catalytic performance for the MTO reaction than PY-RTH and TTZ-1. The fact that different preparation methods resulted in the different performance of the catalysts of the same structure leads us to consider that the distribution of Al in the **RTH**-framework might be dependent on the preparation methods.

Solid-state NMR techniques with a high magnetic field (600 MHz, 14.1 T) were utilized to investigate the environment of Al species in detail. All the samples exhibited only one sharp peak at 56 ppm in the ^{27}Al MAS NMR spectra under 9.4 T. Therefore, the region of tetrahedrally coordinated Al species was characterized in detail by measuring the solid-state NMR spectra in the high magnetic field.

The ^{27}Al 3Q MQMAS NMR spectra of the H-type samples are shown in Figure 7, indicating that two cross-sections were clearly observed in all the spectra. The axis F1 in the MQMAS NMR spectra after an appropriate shearing consists of isotropic lines accompanied by second-order quadrupolar shifts for the central transition

with their respective anisotropic quadrupolar features on the axis F2 [17]. The spectra on the axis F1 suggest that all the samples have at least two crystallographically distinct Al sites in the **RTH** framework; the peaks at 57 and 61 ppm were designated as $Al(IV)_a$ and $Al(IV)_b$, respectively.

Figure 8 shows the high-resolution ^{27}Al MAS NMR spectra of the H-type samples. A peak around 56-57 ppm, which is designated as Al^F_A, was observed for all the samples. Note that another peak around 60-61 ppm, which is designated as Al^F_B, was clearly observed for TTZ-1 and PY-RTH while PMP-RTH and MP-RTH showed this peak only as a shoulder. The intensity ratio of the two peaks is dependent on the preparation methods; the intensity ratio of Al^F_A to Al^F_B was estimated at 13.0, 13.5, 7.1 and 3.3 for PMP-RTH, MP-RTH, PY-RTH and TTZ-1, respectively; Al^F_A is predominant for all the samples, while Al^F_B is present in PY-RTH and TTZ-1 with a relatively higher proportion. There is no marked difference in the intensity ratio of the two peaks between ^{27}Al MQMAS NMR spectra and the projection lines on the axis F1 of the ^{27}Al 3Q MQMAS NMR ones; the intensity ratio of $Al(IV)_a$ to $Al(IV)_b$ on the axis F1 of the ^{27}Al 3Q MQMAS NMR spectra were also estimated at 11.5, 11.0, 5.1 and 3.0 for PMP-RTH, MP-RTH, PY-RTH and TTZ-1, respectively. We have proved that the proportion of Al occupying each of the 4 different T-sites in the **RTH**-type zeolite is dependent on the preparation methods, *i.e.* the kind of SDA.

The high resolution ^{27}Al MAS NMR spectra in the strong magnetic field suggest that the coordination environment of the Al species in the framework depends on the preparation method. Therefore, in order to more clarify the difference in the state of the Al species, *in-situ* FT-IR spectroscopy was applied to the evaluation of acid property by using CO as probe molecule. Figure 9 shows the FT-IR spectra of the CO adsorbed PMP-RTH, MP-RTH, PY-RTH and TTZ-1 samples with the CO pressure varied. Besides the band at 2140 cm^{-1}, which is attributed to physically adsorbed CO species, all samples show a band at 2154 cm^{-1}, which is attributed to the CO species adsorbed on the BASs derived from framework B species [31, 33]. The PMP- and MP-RTH samples show a band at 2172 cm^{-1}, which is attributed to the CO species adsorbed on the BASs derived from framework Al species, while the PY-RTH and TTZ-1 samples give this band at 2174 cm^{-1}. Furthermore, in the PY-RTH and TTZ-1 samples, this band was shifted to a lower wavelength with increasing CO pressure; the peak positions were changed from 2174 to 2172 cm^{-1}. On the other hand, such a shift

was not observed in the spectra of the PMP- and MP-RTH samples. In the FT-IR spectrum of a CO-adsorbed sample, a band at higher wavelength is attributed to the CO species adsorbed on stronger BASs and vice versa [33]. Although the observed difference in the wavelength is not prominent, it is concluded that there are at least two types of weak and strong BASs derived from the framework Al species in the PY-RTH and TTZ-1 samples but that PMP-RTH and MP-RTH have virtually one type of the weak BASs. These considerations are almost in accordance with those based on the findings of the high resolution ^{27}Al MAS NMR spectra. Based on the intensity ratio of Al^{F}_{A} to Al^{F}_{B} in the ^{27}Al MAS NMR spectra (Figure 9), the order of the proportion of the stronger acid sites in the total acid sites should be TTZ-1 > PY-RTH > PMP-RTH ≈ MP-RTH. Thus we conclude that BASs due to the bands at 2174 and 2172 cm^{-1} corresponds to Al^{F}_{A} and Al^{F}_{B}, respectively.

To date, high-resolution ^{27}Al MAS NMR and ^{27}Al MQ/MAS NMR techniques have been extensively applied to ZSM-5 [35-38], MCM-22 [39, 40], USY [41] and Beta [42] to obtain information about the acid property as well as Al distribution in T sites. It is considered that the framework Al sites at lower magnetic field has narrower T-O-T angle and such Al species provide stronger "Brønsted acid site (BAS)" [43].

Here, it is assumed that this correlation of chemical shift with T-O-T angle is applicable to the **RTH**-zeolites. Considering that the mean values of T-O-T angle for T1, T2, T3 and T4 sites are 151.8, 150.5, 150.3 and 145.0° [9], it can be estimated that Al^{F}_{A} is at T1, T2 and/or T3 and Al^{F}_{B} is at T4 and also that the acid strength derived from T4 is higher than that from T1, T2 and T3.

Why Al species preferentially occupied Al^{F}_{A} (T1, T2 and/or T3) sites when PMP and MP were used as OSDAs? It is considered that Al species are located near OSDAs as well as Na^{+} ions to balance the charge. Large OSDA molecules such as PMP and MP might be more preferentially located in the larger pore, *i.e.* the non-distorted 8-MR pore rather than the distorted 8-MR one. Consequently, Al species would be preferentially incorporated into T1 and T2 sites of Al^{F}_{A} species; the possibility for the T3 site is excluded because it is not facing to any 8-MR pores. On the other hand, in the OSDAs-free synthesis, Al species could be uniformly distributed on the T1, T2 and T4 as well as T3 sites as they are accompanied by only Na^{+} ions. The use of PY, which is smaller than PMP and MP, would also lead to the uniform distribution. Consequently, the more Al atoms would be incorporated into the T4 site

located at distorted 8-MR pore for PY-RTH and TTZ-1 than for PMP-RTH and MP-RTH. However, T4 site did not effectively work as the active site for the MTO reaction despite of stronger BAS. This is probably because the Na^+ ions in the distorted 8-MR pore are not completely exchanged with H^+ by the ion-exchange process. Another reason is that, even if the Na^+ ions against T4 site Al is exchanged for H^+, the accessibility of methanol to T4 site might be retarded, considering that the kinetic diameter of methanol is computed at 0.38 nm.[44] Consequently, PY-RTH and TTZ-1 exhibited a slightly lower catalytic performance. More details on the influence of the Al distribution on the acid properties and the catalytic performance are under investigation.

4.4 Conclusions

The **RTH**-type aluminosilicate zeolites were successfully synthesized by using 1,2,2,6,6-pentamethylpiperidine, *N*-methylpiperidine or pyridine in combination with ethylenediamine as OSDAs and without using any OSDAs. All the prepared **RTH**-type zeolites produced propene selectively on the MTO reaction. However, the catalytic properties significantly depended on the type of OSDA used for the zeolite synthesis. The high-resolution ^{27}Al MAS NMR and ^{27}Al MQMAS NMR techniques revealed that the Al distribution over framework T sites was clearly dependent on the type of OSDA. The use of bulky OSDAs such as PMP and MP would lead to the preferential incorporation of Al species at T1, T2 and/or T3 sites. On the other hand, in the OSDAs-free synthesis, Al species were uniformly distributed on the T1, T2 and T4 as well as T3 sites as they are accompanied by only Na^+ ions. We first revealed that the acid properties as well as Al distribution in the RTH framework are strongly dependent on the preparation methods, the type of SDA, in particular. Our findings will contribute to the development of the zeolite catalysts with acid sites in the pores properly controlled.

References

1 C. S. Cundy, P. A. Cox, *Chem. Rev.* 2003, **103**, 663-702

2 Corma, A. *J. Catal.* 2003, **216**, 298-312

3 Q. Zhu, J. N. Kondo, R. Ohnuma, Y. Kubota, M. Yamaguchi, T. Tatsumi, *Microporous Mesoporous Mater.* 2008, **112**, 153-161

4 Q. Zhu, M. Hinode, T. Yokoi, J. N. Kondo, Y. Kubota, T. Tatsumi, *Microporous Mesoporous Mater.* 2008, **116**, 253-257

5 J. Liang, H. Li, S. Zhao, W. Guo, R. Wang, M. Ying, Applied Catalysis 1990, **64**, 31-40.

6 Q. Zhu, J. N. Kondo, T. Tatsumi, S. Inagaki, R. Ohnuma, Y. Kubota, Y. Shimodaira, K. Domen, *J. Phys. Chem. C* 2007, **111**, 5409-5415.

7 J. W. Park, J. Y. Lee, K. S. Kim, S. B. Hong, G. Seo, *Appl. Catal. A* 2008, **339**, 36-44.

8 http://www.iza-structure.org/

9 S. Vortmann, B. Marler, H.Gies, P. Daniels, *Microporous Mater.* 1995, **4**, 111-121.

10 G. S. Lee, S. I. Zones, *J. Solid State Chem.* 2002, **167**, 289-298.

11 T. Yokoi, M. Yoshioka, H. Imai, T. Tatsumi, *Angew. Chem. Int. Ed.* 2009, **48**, 9884-9887.

12 M. Yoshioka, T. Yokoi, H. Imai, S. Inagaki, T. Tatsumi, *Microporous Mesoporous Mater.*, 2012, **153**, 70-78 .

13 J. Klinowski, *Chem. Rev.* 1991, **91**, 1459-1479.

14 E. Lippmaa, A. Samoson, M. Magi, *J. Am. Chem. Soc.* 1986, **108**, 1730-1735.

15 W. Kolodziejski, C. Zicovich-Wilson, C. Corell, J. Perez-Pariente, A. Corma, *J. Phys. Chem.* 1995, **99***,* 7002-7008.

16 C. A. Fyfe, Y. Feng, H. Grondey, G. T. Kokotailo, H. Gies, *Chem. Rev.* 1991, **91**, 1525-1543.

17 Medek, J. S. Harwood, L. Frydman, *J. Am. Chem. Soc.*, 1995, **117**, 12779-12787.

18 S.-J. Hwang, C. Fernandez, J. P. Amoureux, J.-W. Han, J. Cho, S. W. Martin, M. Pruski, *J. Am. Chem. Soc.*, 1998, **120**, 7337–7346.

19 S. E. Ashbrook, L. Le Pollès, R. Gautier, C. J. Pickard, R. I. Walton, *Phys. Chem. Chem. Phys.*, 2006, **8**, 3423-3431.

20 K. H. Lim, C. P. Grey *J. Am. Chem. Soc.*, 2000, **122**, 9768-9780.

21 K. Shimoda, Y. Tobu, Y. Shimoikeda, T. Nemoto, K. Saito, *J. Magnetic Resonance*

2007, *186*, 156-159.

22 K. Shimoda, Y. Tobu, K. Kanehashi, T. Nemoto, K. Saito, *J. Non-Crystalline Solids*, 2008, **354**, 1036-1043.

23 H. G. Karge, V. Dondur and J. Weitkamp, *J. Phys. Chem.* 1991, **95**, 283-288.

24 N. Katada and M. Niwa, *Catal. Surv. Asia* 2004, **8**, 161-170.

25 R. B. Borade, A. Adnot and S. Kaliaguine, *J. Chem. Soc., Faraday Trans*., 1990, **86**, 3949-3956.

26 J. W. Ward, in Zeolite Chemistry and Catalysis, ed. J. A. Rabo, ACS Monograph 171, American Chemical Society, Washington, DC, 1976, pp. 118-284.

27 Jentys and J. A. Lercher, *Stud. Surf. Sci. Catal.* 2001, *137*, 345-386, and the references therein.

28 L. M. Kustov, V. B. Kazansky, S. Beran, L. Kuvelkova, P. Jiru, *J. Phys. Chem.* 1987, **91**, 5247-5251.

29 N. Echoufi and P. Gelin, *J. Chem. Soc., Faraday Trans.* 1992, **88**, 1067-1073.

30 Zecchina, S. Bordiga, G. Spoto, D. Scarano, G. Petrini, G. Leofanti, M. Padovan and C. O. Arean, *J. Chem. Soc., Faraday Trans.*, 1992, **88**, 2959-2969.

31 S. Bordiga, E. E. Platero, C. O. M. Arean, C. Lamberti and A. Zecchina, *J. Catal.* 1992, **137**, 179-185.

32 L. Mirojew, S. Ernst, J. Weitkamp and H. Knozinger, Catal. Lett., 1994, **24**, 235-248.

33 J. N. Kondo, R. Nishitani, E. Yoda, T. Yokoi, T. Tatsumia, K. Domenc, *Phys. Chem. Chem. Phys.* 2010, **12**, 11576-11586.

34 M. Niwa, K. Katada, *Catal. Surv. Jpn.* 1997, **1**, 215-226.

35 P. M. Kentgens, D. Iuga, M. Kalwei, H. Koller, *J. Am. Chem. Soc.* 2001, **123***,* 2925-2926.

36 P. Sarv, C. Fernandez, J.-P. Amoureux, K. Keskinen, *J. Phys. Chem.*, 1996, **100**, 19223-19226.

37 H. Han, C.-S. Kim, S. B. Hong, *Angew. Chem. Int. Ed.*, 2002, **41**, 469-472.

38 S. Sklenak, J. Dedecek, C. Li, B. Wichterlová, V. Gábová, M. Sierka, J. Sauer, *Angew. Chem. Int. Ed.*, 2007, **46**, 7286-7289.

39 D. Ma, X. Han., S. Xie, X. Bao, H. Hu, S. C. F. Au-Yeung, *Chem. Eur. J.*, 2002, **8**, 162-170.

40 Zheng, L. Chen, J. Yang, M. Zhang, Y. Su, Y. Yue, C. Ye, F. Deng *J. Phys. Chem. B* 2005, **109***,* 24273-24279.

41 N. Katada, S. Nakata, S. Kato, K. Kanehashi, K. Saito, M. Niwa, *J. Mol. Catal. A*, 2005, **236**, 239-245.

42 J. A. van Bokhoven, D. C. Koningsberger, P. Kunkeler, H. van Bekkum, A. P. M. Kentgens, *J. Am. Chem. Soc.*, 2000, **122**, 12842-12847.

43 N. Katada, K. Suzuki, T. Noda, G. Sastre, M. Niwa, *J. Phys. Chem. C,* 2009, **113**, 19208-19217

44 B. Tokay, J. L. Falconer, R. D. Noble, *J. Membrane Sci.*, 2009, **334**, 23-29.

Table 1 Physicochemical properties of Al containing **RTH**-type zeolites via various synthesis routes

	Si/Al[*1]	Si/B[*1]	Na/Al[*2]		Acid amount [mmol·g^{-1}]	
			Na-type	H-type	by ICP[*3]	by NH_3-TPD[*4]
PMP-RTH	207	24	0.33	0.05	0.081	0.050
MP-RTH	190	20	0.22	0.08	0.088	0.045
PY-RTH	187	25	0.24	0.07	0.089	0.048
TTZ-1	213	26	1.03	0.18	0.078	0.037

[*1] estimated by ICP. [*2] estimated by AA. [*3] Based on the Al content. [*4] Based on the h-peak area in the NH_3-TPD curve.

Table 2 The results of the MTO reactions for the reaction time of 90 min at 400ºC

	Si/Al	Conv.	Selectivity / %					
		/ %	C1	C2=	C3=	C2 + C3	C4 – C6	DME
PMP-RTH	207	93.3	0	26.6	44.6	0.9	24.1	3.8
MP-RTH	190	93.4	0	24.2	44.0	1.4	28.1	2.3
PY-RTH	187	91.3	0	19.3	32.7	0.8	25.4	21.8
TTZ-1	213	47.9	0	19.6	42.8	1.2	32.1	4.3

Reaction conditions: catalyst, 100 mg; temperature, 400 ^{o}C; W/F, 34 g-cat h/(mol-MeOH); WHSV, 1.0 h^{-1}; partial pressure of MeOH, 5.0 kPa.

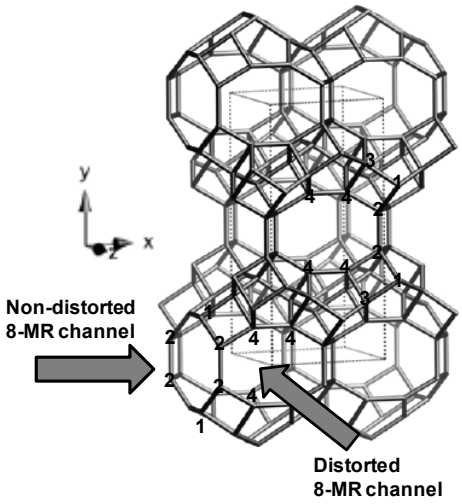

Scheme 1

Framework of the RTH-type zeolite viewed along [001]

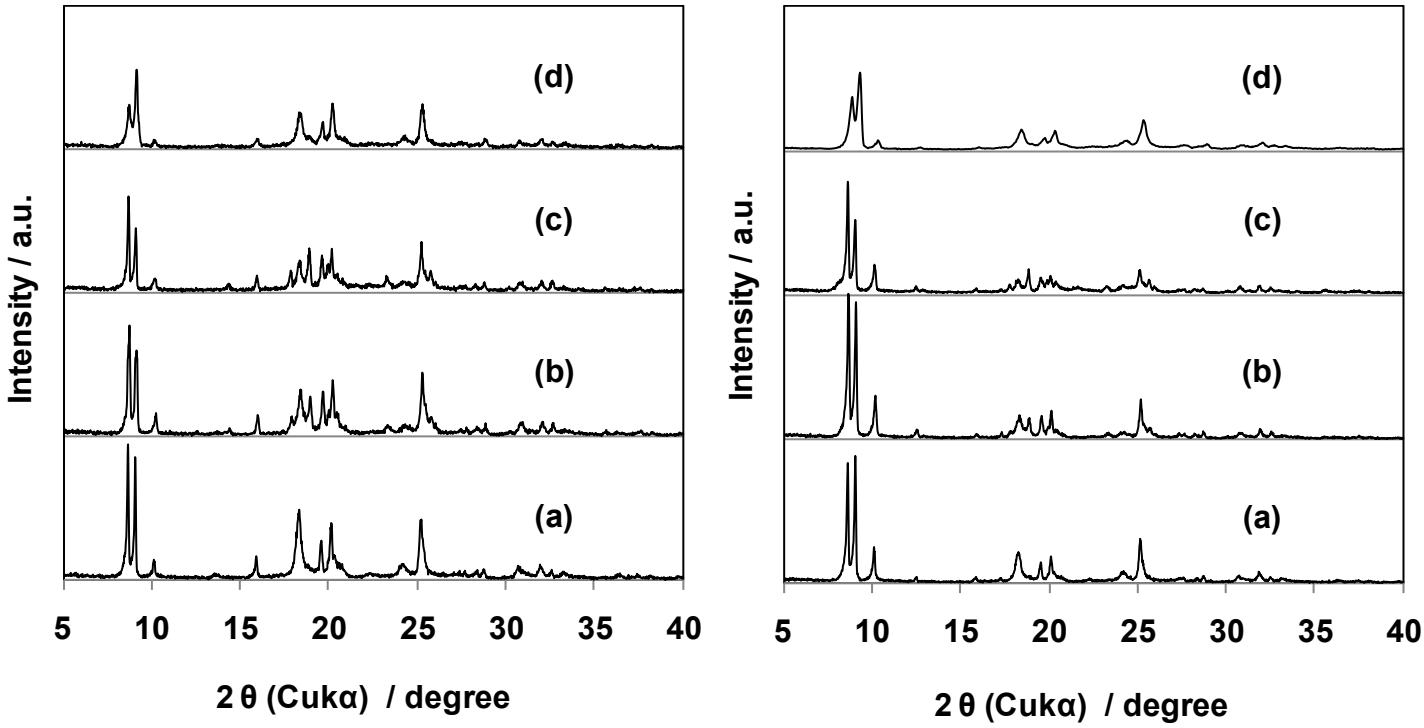

Fig. 1

XRD patterns (2θ = 5 - 40º) of the as-synthesized (left) and ion-exchanged (right): (a) PMP-RTH, (b) MP-RTH (c) PY-RTH and (d) TTZ-1.

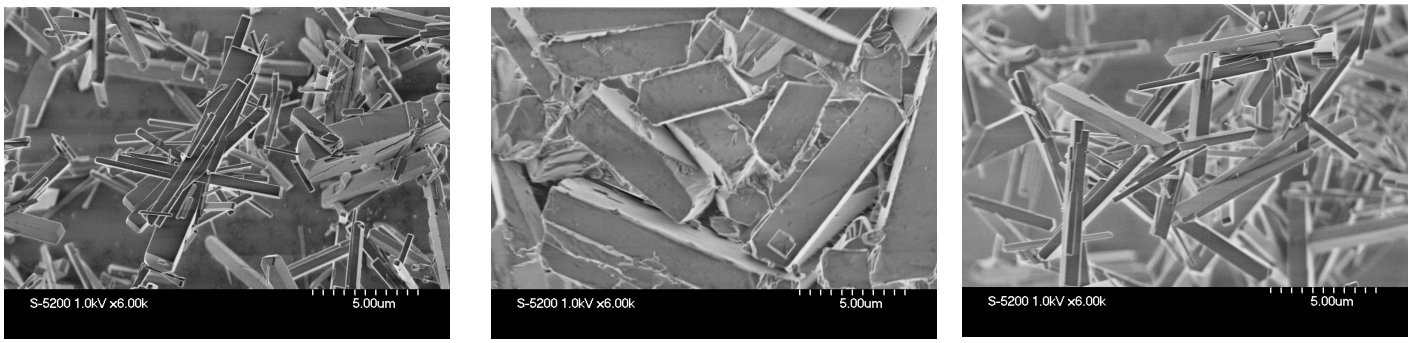

(a) PMP-RTH **(b) MP-RTH** **(c) PY-RTH**

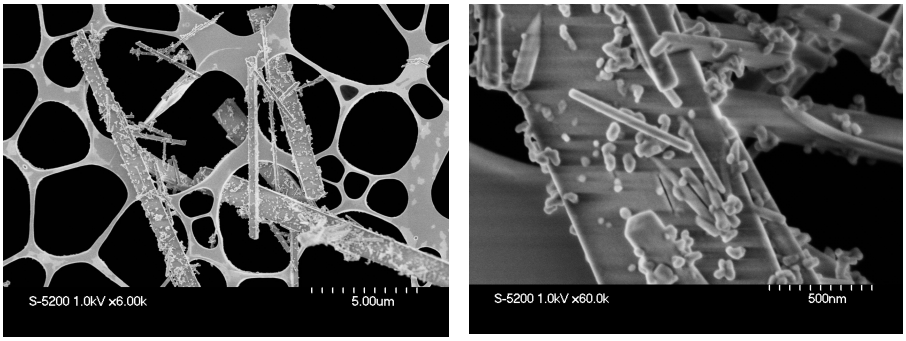

(d) TTZ-1 **(e) TTZ-1**

Fig. 2

SEM images of the ion-exchanged products: (a) PMP-RTH, (b) MP-RTH (c) PY-RTH, (d) TTZ-1 (low magnification) and (e) TTZ-1 (high magnification)

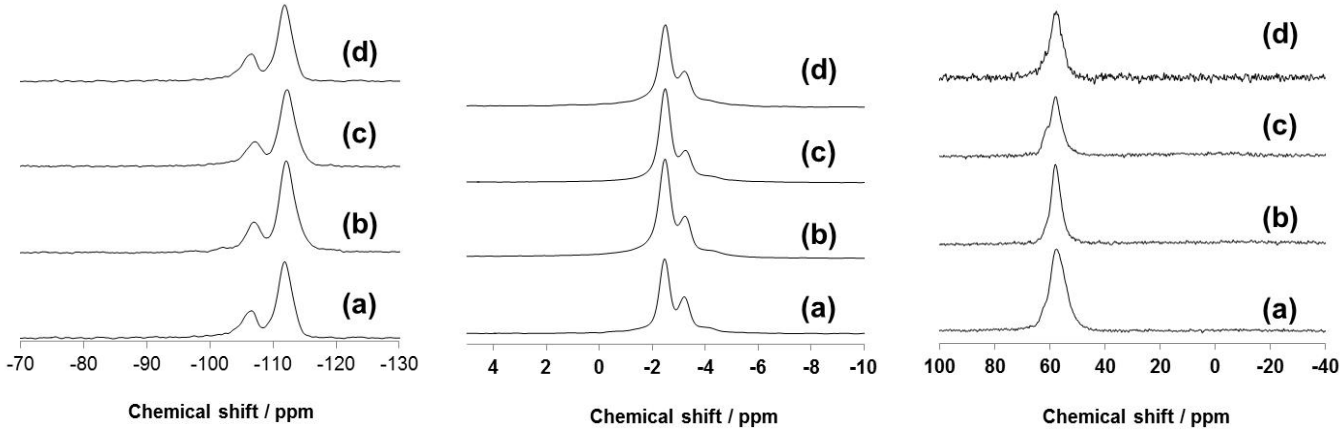

(A) ^{29}Si MAS NMR spectra (B) ^{11}B MAS NMR spectra (C) ^{27}Al MAS NMR spectra

Fig. 3

(A) 29Si, (B) 11B and (C) 27Al MAS NMR spectra (9.4T) of the ion-exchanged products, (a) PMP-RTH, (b) MP-RTH (c) PY-RTH and (d) TTZ-1.

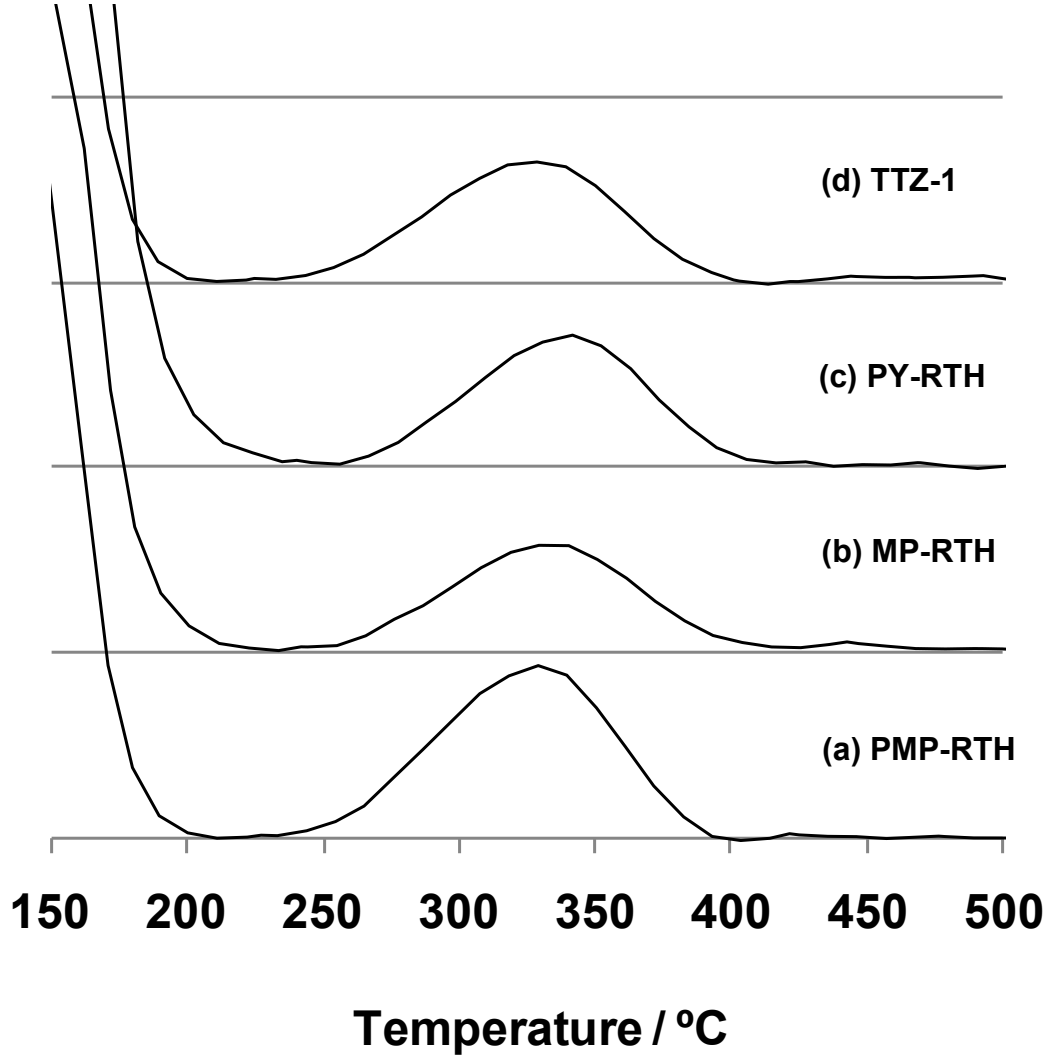

Fig. 4

NH_3-TPD profiles of the ion-exchanged products: (a) PMP-RTH, (b) MP-RTH (c) PY-RTH and (d) TTZ-1.

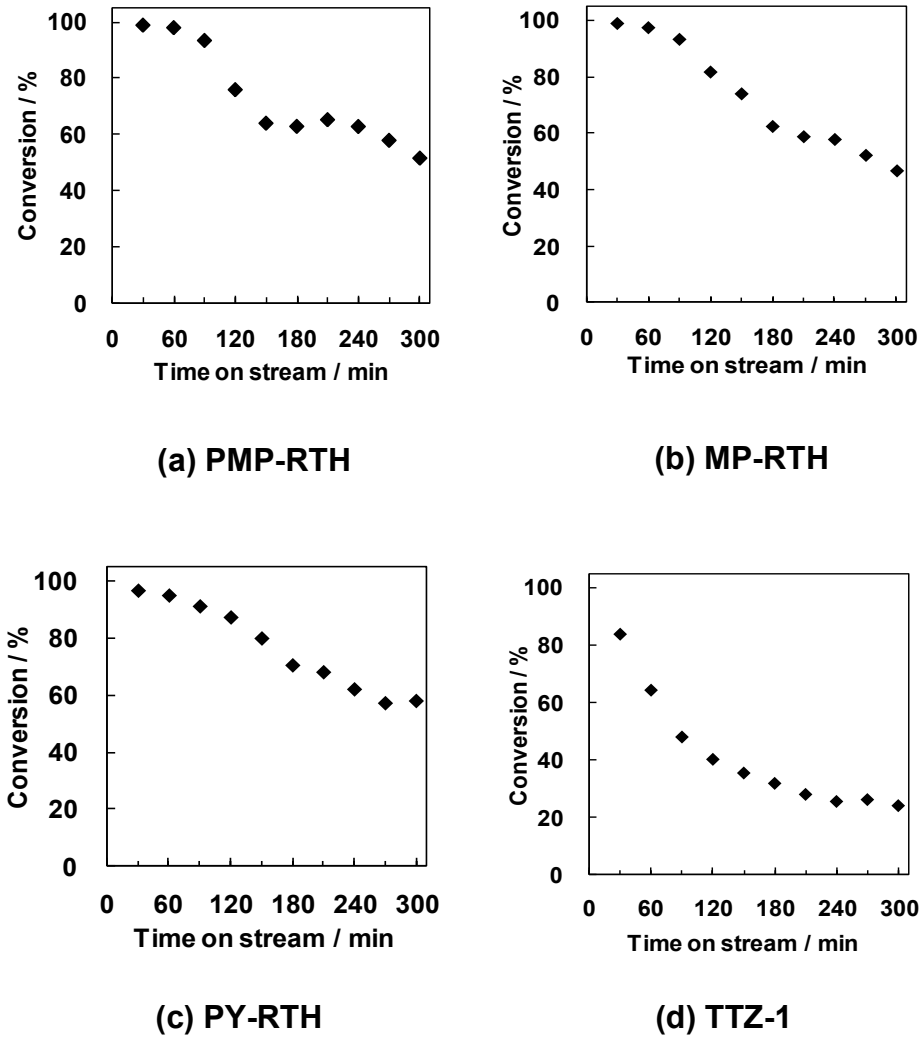

Fig. 5

Conversion profiles of the MTO reaction over (a) PMP-RTH, (b) MP-RTH (c) PY-RTH and (d) TTZ-1.

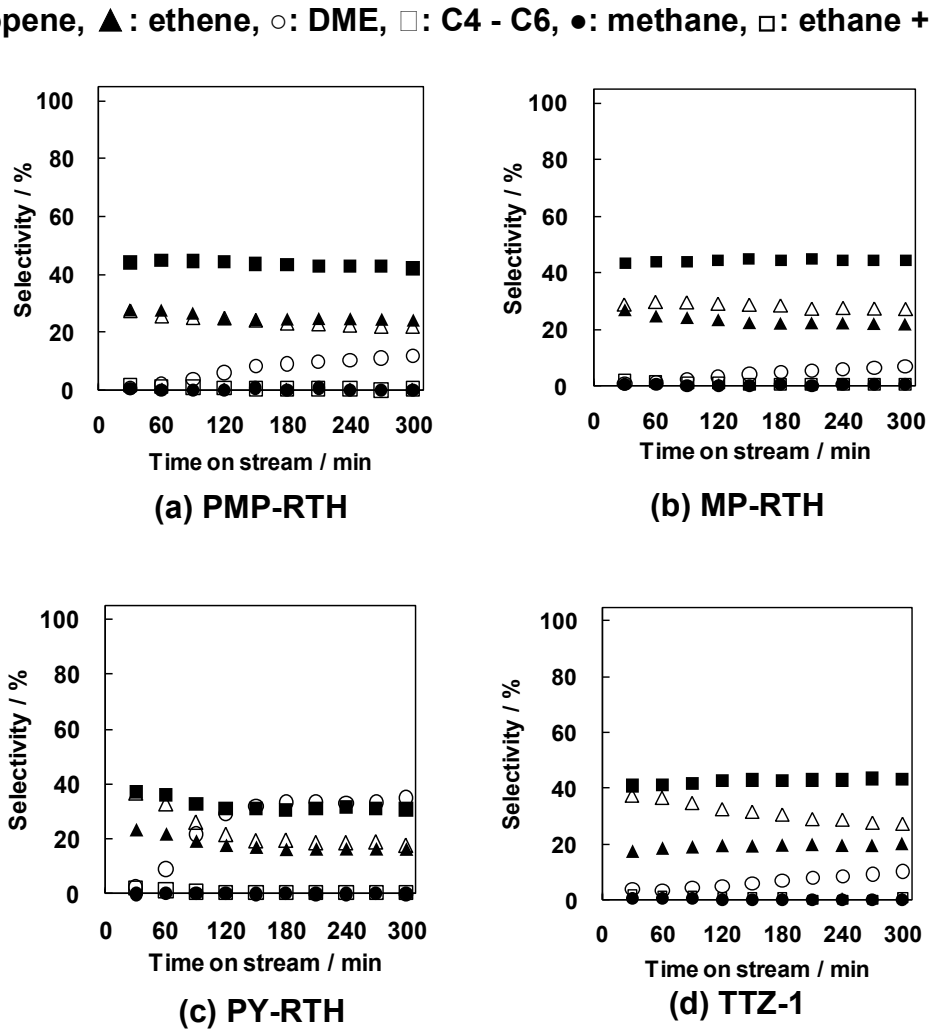

Fig. 6

Product selectivity profiles of the MTO reaction over (a) PMP-RTH, (b) MP-RTH (c) PY-RTH and (d) TTZ-1.

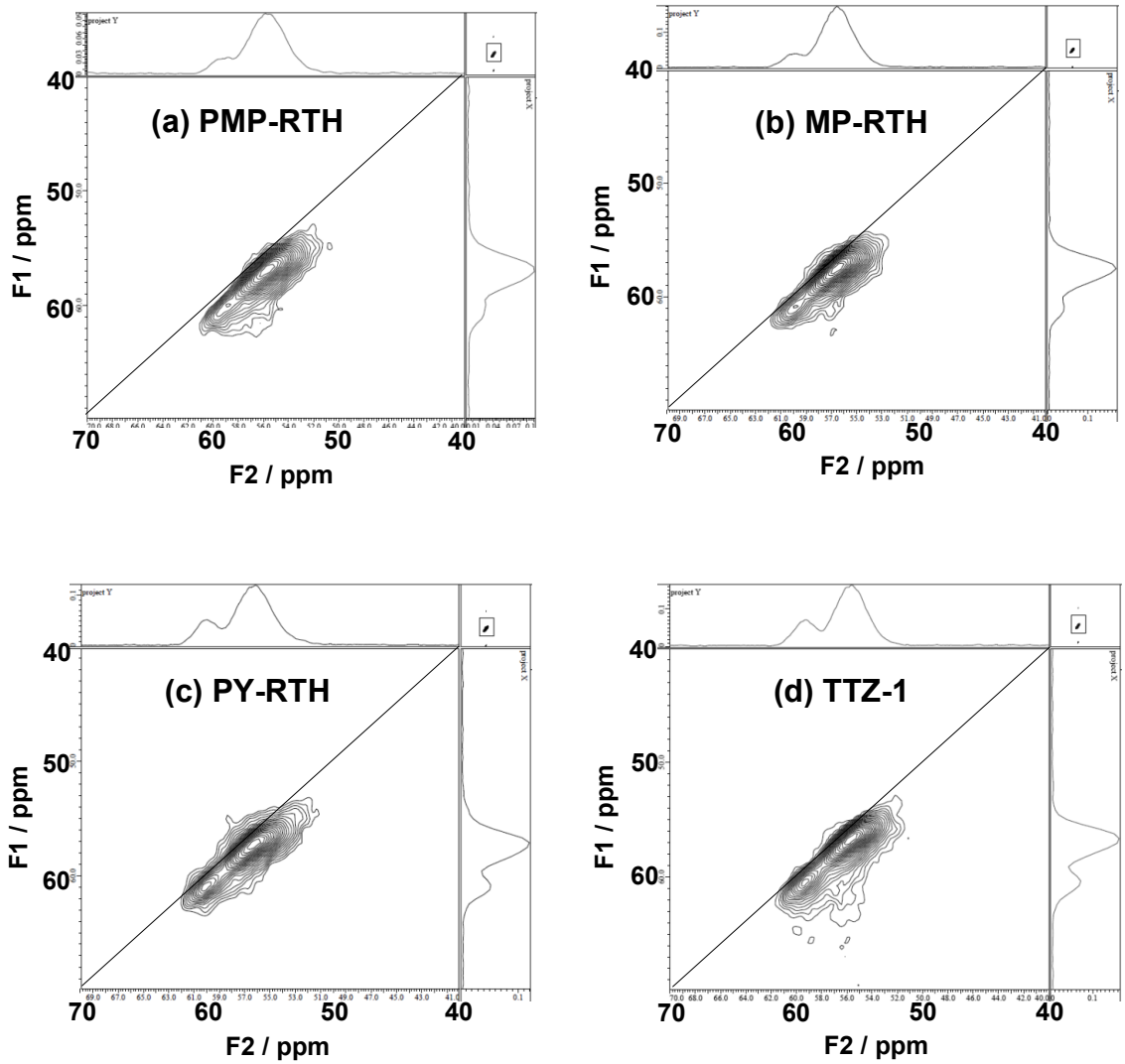

Fig. 7

27Al MQMAS NMR spectra (14.1T) of the ion-exchanged products: (a) PMP-RTH, (b) MP-RTH (c) PY-RTH and (d) TTZ-1.

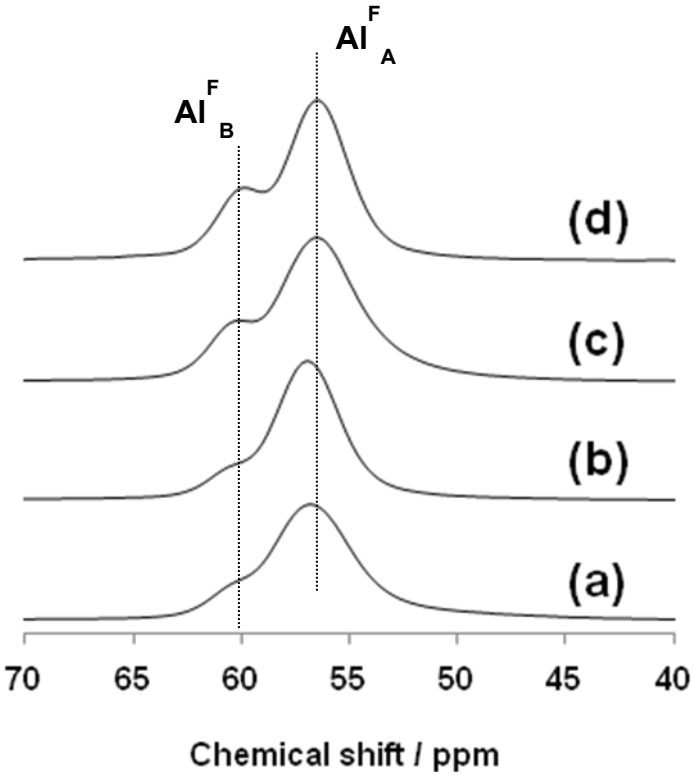

Fig. 8

High-resolution ^{27}Al MAS NMR spectra (14.1T) of the ion-exchanged products: (a) PMP-RTH, (b) MP-RTH (c) PY-RTH and (d) TTZ-1.

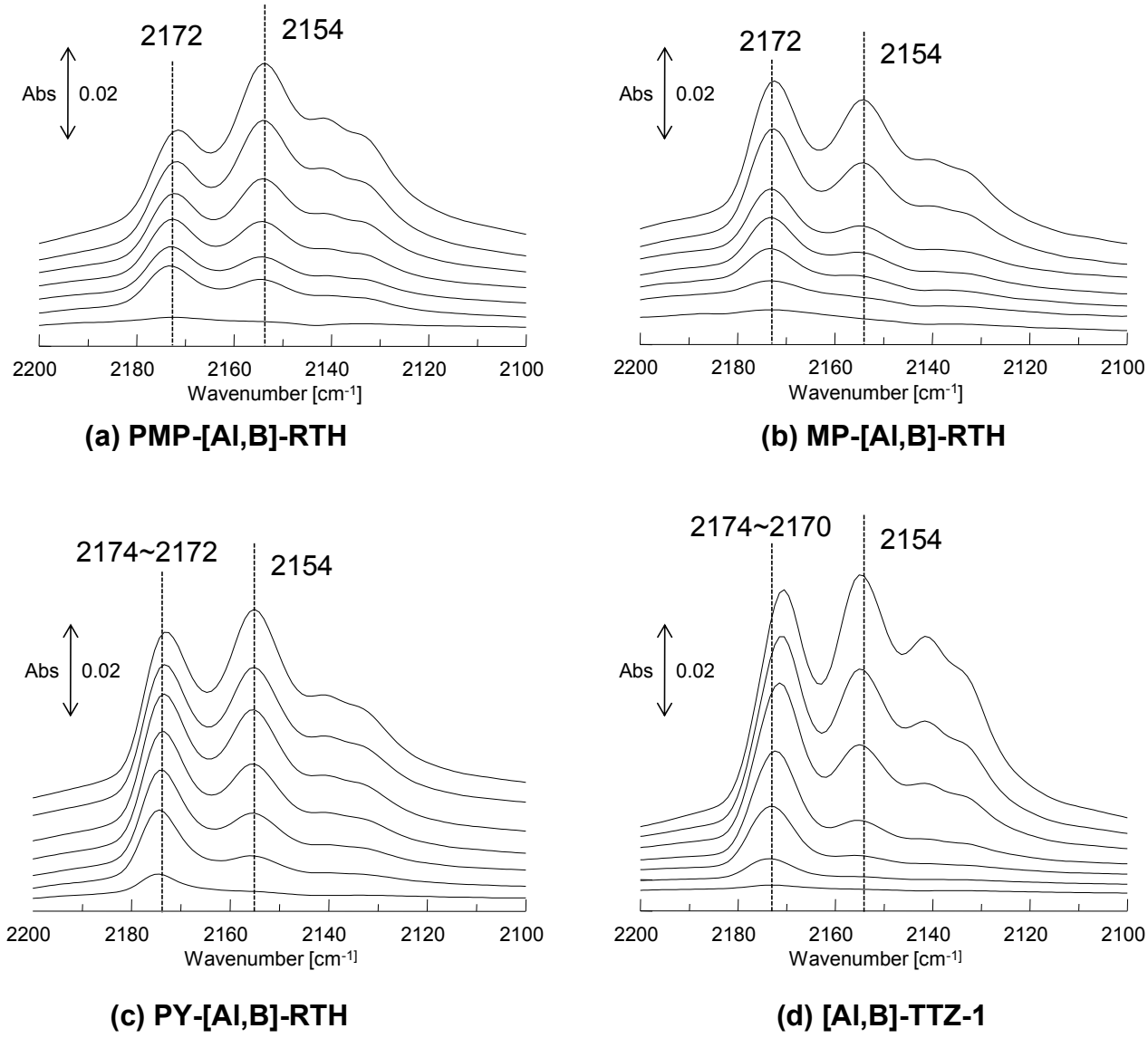

Fig. 9

CO adsorbed FT-IR spectra of the ion-exchanged products, (a) PMP-RTH, (b) MP-RTH (c) PY-RTH and (d) TTZ-1.

Chapter 6

Summary

Chapter 2

The **SFH**-type aluminosilicate zeolites were successfully synthesized by direct- and post-synthesis methods. The ^{27}Al MAS and ^{27}Al MQMAS NMR reveals that most Al species of the samples are located in the framework but there is a marked difference in the distribution of Al atoms in the framework between direct- and post-synthesis methods; at least five kinds of framework Al species are formed in the zeolites prepared by the direct-synthesis method. [Al,B]-SFH-D exhibited a higher catalytic performance in the acylation compared to [Al,B]-SFH-P. The differences in the catalytic performance as well as acid property are due to the difference in the distribution of Al atoms in the framework, and the distribution of Al atoms is strongly dependent on the preparation route.

Chapter 3

According to the synthesis results of **SFH**-type zeolite in chapter 2, the direct-synthesis method for preparing the **SFN**-type aluminosilicate zeolites, designated as [Al,B]-SFN-D, was successfully improved by increasing the SDA/SiO_2 ratio to 0.3 and adding 10 wt% seeds. However, high Al content containing **SFN**-type zeolite could not be synthesized by direct-synthesis method like **SFN**-type zeolite. Similar to the results of chapter 2, the ^{27}Al MAS NMR reveals that most Al species of the samples are located in the framework but there is a marked difference in the distribution of Al atoms in the framework between direct- and post-synthesis methods. [Al,B]-SFN-D exhibited a higher catalytic performance in the acylation compared to [Al,B]-SFN-P.

Chapter 4

14 membered ring extra-large-pore zeolite, CIT-5 (California Institute of Technology Number 5), was synthesized by direct-synthesis method according to the literature reported previously. Thus prepared CIT-5 (**CFI**-type) zeolite was characterized in details. Finally, Al containing CIT-5, SSZ-53 and SSZ-59 synthesized by

direct-synthesis method were utilized as catalysts for acylation of 2-methoxynaphthalene under same reaction condition in order to compare the catalytic performace. Commercial 12 membered ring zeolites Beta and Mordenite were also used in the same reaction in order to compare the catalytic performance with 14 membered ring zeolites. Al containing CIT-5 was successfully synthesized by direct-synthesis method under hydrothermal conditions. According to the results of NH_3-TPD, the acid strength of [Al]-CIT-5 was considered to be the weakest of the five zeolites. [Al.B]-SSZ-53 showed the highest catalytic performance due to its extra-large-pore and medium degree of acid strength.

Chapter 5

The **RTH**-type aluminosilicates were synthesized with different types of OSDA or without using any OSDAs. Thus obtained zeolite synthesized with different preparation methods were characterized by using various techniques, especially, high-resolution ^{27}Al MAS NMR and CO-adsorbed in-situ FT-IR techniques. All the prepared **RTH**-type zeolites produced propene selectively on the MTO reaction. However, the catalytic properties significantly depended on the type of OSDA used for the zeolite synthesis. The high-resolution ^{27}Al MAS NMR and ^{27}Al MQMAS NMR techniques revealed that the Al distribution over framework T sites was clearly dependent on the type of OSDA.

Acknowledgement

The present thesis is collection of the studies which have been carried out at Chemical Resources Laboratory, Tokyo institute of Technology during 2009-2014 under supervision of Prof. Takshi Tatsumi. First of all, I would like to express my greatest gratitude to Prof. Takashi Tatsumi for giving me the opportunity to do this research. I am really grateful for his constructive guidance, valuable suggestion, insightful comments and considerable encouragement.

I would like to express my sincere gratitude to Assoc. prof. Dr. Junko N. Kondo and Assist. Prof. Dr. Toshiyuki Yokoi for their insightful and valuable advice, detailed comments, concrete suggestions and hearty encouragement. I would also like to express my gratitude to Assoc. Prof. Dr. Hiroyuki Imai (The University of Kitakyushu) for his constructive suggestions and advice.

I would like to express my thanks to all the staffs and members of Tatsumi Nomura laboratry, especially Mr. Ryoichi Otomo, Mr. Hiroshi Yamazaki and Mr. Hiroshi Mochiduki who are my contemporaries at laboratory for their cooperation and help.

Finally, I would like to express my best thanks to my family, especially my parent (Baoqing Liu and Yueling Wang) for their support, understanding and encouragement.

December,2013

Ming Liu

List of publications

Papers:

1. Differences in Al distribution and acidic property between RTH-type zeolites synthesized with OSDAs and without OSDAs
   Ming Liu, Toshiyuki Yokoi, Masato Yoshioka, Hiroyuki Imai, Junko N. Kondo and Takashi Tatsumi
   Phys. Chem. Chem. Phys., **2013**, **DOI:** 10.1039/C3CP54297A

2. Synthesis of SFH-type aluminosilicate zeolite with 14-membered ring and its applications as solid acid catalyst
   Ming Liu, Toshiyuki Yokoi, Junko N. Kondo, Takashi Tatsumi
   Microporous Mesoporous Mater., **2013**, submitted

3. Preparation of RTH-type zeolites with the amount and/or kind of organic structure-directing agents (OSDA): Are OSDAs indispensable for the crystallization?
   Masato Yoshioka , Toshiyuki Yokoi , Ming Liu , Hiroyuki Imai , Satoshi Inagaki , Takashi Tatsumi
   Microporous Mesoporous Mater., 153 (**2012**) 70-78